(AlGa)As Semiconductor Lasers and Integrated Optoelectronics

Thesis by

Daniel Paul Wilt

In Partial Fulfillment of the Requirements

for the degree of

Doctor of Philosophy

California Institute of Technology

Pasadena, California

1981

(Submitted May 12, 1981)

Acknowledgements

I would like to express my sincere gratitude and appreciation to my advisor, Dr. Amnon Yariv, for his support and encouragement throughout my stay in his quantum electronics group. I owe a great deal to his efforts and kindness in constructing and encouraging this group of highly talented individuals.

I would like to thank also Dr. Nadav Bar-Chaim, Dr. Hussein Izadpanah, Dr. Schlomo Margalit, and Dr. Moshe Yust for their aid and advice throughout the course of the work presented in this thesis. Without their collective expertise much of the work presented in this thesis could not have been undertaken. In addition, I would like to thank Mr. Desmond Armstrong for his expert technical assistance in construction and maintainance of experimental apparatus.

I would also like to express my appreciation to my fellow graduate students for their help and discussions. In particular, I would like to thank Dr. C. P. Lee, Dr. Israel Ury, Mr. P. C. Chen, Mr. Josef Katz, Mr. Kam Lau and Mr. Christoph Harder for their participation in this work.

My wife Pamela and our parents also deserve my deepest thanks for their love, support, and patience.

My special thanks go to the group of people who introduced me to scientific research. In particular, I would like to express my thanks to my advisor during my first two years at Caltech, Dr. James Mercereau, for his support and encouragement. I would also like to thank Dr. Harris Notarys for his enlightening discussions. Mr. Edward Boud also deserves my appreciation for his unselfish aid throughout the course of my research.

The financial support of the National Science Foundation and the Office of Naval Research is gratefully acknowledged.

Abstract

Five subjects related to monolithic integration of electronic and optical devices in the (AlGa)As material system are treated in this thesis. They are:

1. The Integrated Optoelectronic Repeater

The design, fabrication, and testing of the first monolithic integrated optical repeater is described. This device consists of an optical detector, electronic gain stage, and current modulated semiconductor laser transmitter integrated in a single crystal chip to perform the function of regenerating an optical signal as might be found in an optical communication system. The device has a measured optical gain (light out to light in) of 10 dB.

2. Ion Implanted Lasers and Schottky Gate Field Effect Transistors

The use of ion implantation as a technique to fabricate both lasers and field effect transistors is described. Devices fabricated include a beryllium implanted laser diode on N type GaAs substrate, a beryllium implanted laser diode on semi-insulating Cr doped GaAs substrate integrated with a field effect transistor driver, and sulfur implanted GaAs field effect transistors.

3. A Steady State Lateral Model of the Double Heterostructure Laser

A theoretical model of the double heterostructure laser is described which treats the p-n junction in the device correctly by using fundamental semiconductor relationships and reasonable assumptions about the device heterointerfaces. The model treats both the electronic and optical properties self consistently, making the model valid above lasing threshold. Finite element formalism is adopted as a solution technique to enable the treatment of complicated diode geometries. An example is treated and theoretical and experimental

results are compared.

4. The Effect of Lateral Carrier Diffusion

on the Modulation Response of a Semiconductor Laser

The effect of lateral carrier diffusion upon the modulation characteristics of the semiconductor laser is investigated. A self consistent analysis of the spatially dependent rate equations is performed using a finite element model. The transverse junction stripe laser is treated as an example and a comparison is made between lateral carrier diffusion and spontaneous emission as damping mechanisms for the resonance peak. Experimental results bear out the conclusion that the relaxation resonance in this device is damped mainly by lateral carrier diffusion. In addition, a simple analytic result is presented which illustrates qualitatively the effect of lateral carrier diffusion upon such devices. The conclusion from this result is that lateral carrier diffusion serves to damp the relaxation resonance in the semiconductor laser quite well, but probably will not serve to improve the upper limit on modulation frequency as might have been suspected.

5. Effective Permittivity Formalism

and the Design of Buried Heterostructure Lasers

An approach to effective permittivity formalism is presented which clarifies and extends the use of this technique particularly in the treatment of waveguiding in the semiconductor laser. The scalar wave equation is posed in a variational form, and the effective permittivity formalism is treated as a variational approximation technique. This approach shows clearly the nature and limits of the approximation involved. The formalism is applied to the case of the buried heterostructure laser and the results differ considerably from the conventional application of effective permittivity formalism to this device when a reasonable form is assumed for the variational modal profile.

Contents

Chapter I Introduction

I.1	Integrated Optoelectronics	1
I.2	Outline of Thesis	6
I.3	References for Chapter I	10

Chapter II The Integrated Optoelectronic Repeater

II.1	Introduction	12
II.2	Design Considerations for the Repeater	12
II.3	Fabrication of the Repeater	19
II.4	Results	21
II.5	Conclusions	27
II.6	References for Chapter II	28

Chapter III Ion Implanted Lasers and Schottky Gate Field Effect Transistors

III.1	Introduction	29
III.2	Sulfur Implanted GaAs Schottky Gate Field Effect Transistors	31
III.3	Beryllium Implanted (AlGa)As Double Heterostructure Lasers	32
III.4	Conclusions	47
III.5	References for Chapter III	51

Chapter IV A Steady State Lateral Model of the Double Heterostructure Laser

IV.1	Introduction	53
IV.2	Simplifying Assumptions used in the Model	56
IV.3	The Electrical Model	60

IV.4 The Optical Model 69

IV.5 Solution Technique 76

IV.6 Sample Case and Comparison with Experiment 80

IV.7 Summary and Conclusions 94

IV.8 References for Chapter IV 96

Chapter V The Effect of Lateral Carrier Diffusion on the Modulation Response of a Semiconductor Laser

V.1 Introduction 98

V.2 The Spatially Dependent Rate Equations 99

V.3 Analytic Treatment of Lateral Carrier Diffusion Effects 101

V.4 Modulation Response of the TJS Laser 108

V.5 References for Chapter V 117

Chapter VI Effective Permittivity Formalism and the Design of Buried Heterostructure Lasers

VI.1 Introduction 118

VI.2 Effective Permittivity Formalism 119

VI.3 Design of the Buried Heterostructure Laser 123

VI.4 References for Chapter VI 139

Chapter I

Introduction

I.1 Integrated Optoelectronics

Optical communication has become a subject of intense interest and research recently. This is in large part due to the extremely large bandwidths available and the small dimensions involved in the generation and guiding of light waves as compared with conventional microwave transmission systems.

Of particular interest at present are systems based upon fused silica fibers as the transmission medium, and semiconductor light sources and detectors. These systems have a large number of advantages compared with other transmission systems. Fused silica fibers are small, light weight, heat and radiation resistant, free from electronic cross talk, have low losses, and large transmission bandwidths [1]. The semiconductor laser light sources and detectors used in these systems are small, high speed, easy to control (being solid state devices) and highly efficient.

A communications system based on these components will serve as an interface between purely electronic media: high speed computers, television and voice transmission systems, and analog microwave systems such as phased array radars. In this case, the optical communications link derives and delivers its signals to and from electronic devices such as silicon based integrated circuits in an electronic environment. One can envision then that in the interest of low cost and circuit simplicity the terminal sources and recievers in the optical link may take on electronic processing involved with the communication link. As an example, the source might include with its laser transmitter an active device to serve as an interface between standardized signal transmission levels and impedances in the system and the drive requirements of the laser. On the other end of the optical link, again active devices may be included with the receiver

detector to interface its characteristics to the requirements of the system, and might also include some signal conditioning such as level detection. This is an advantage unique to the use of semiconductor light sources and detectors, where a monolithic single crystal chip can contain both electronic and optical devices in an integrated design.

A particular advantage of this concept is that simple optical and electronic processing can be performed in a single chip, highly simplifying some of the potential applications of such devices. A good example of this is in repeater links for a long distance optical communication system, where detection, amplification of the resulting electrical signal, and retransmission can all be performed by the same integrated circuit.

These devices fall under the general classification of optoelectronic integrated circuits, or OEICs. The integration of semiconductor optical and electronic components in the OEIC was first suggested by Yariv [2]. A block diagram of the OEIC is shown in Figure 1.1. In general, this device consists of three sections; a detector section, an electronic processing section, and a transmission section. The detector section consists of detectors, preamps, and any other components for signal preconditioning, and it feeds an electronic input to the following electronic processing section which may also accept external electronic inputs. The processing section performs analog or digital processing of these signals, and feeds electronic signals to both the external environment and internally to a source section consisting of lasers which feed output optical fibers and their associated driver electronics.

At present, the OEIC is envisioned to serve mainly as an interface between electronic media and optical fiber communication links. However, there is no fundamental reason why one cannot envision the OEIC eventually assuming a role of its own, for example, as the fundamental component of a computer

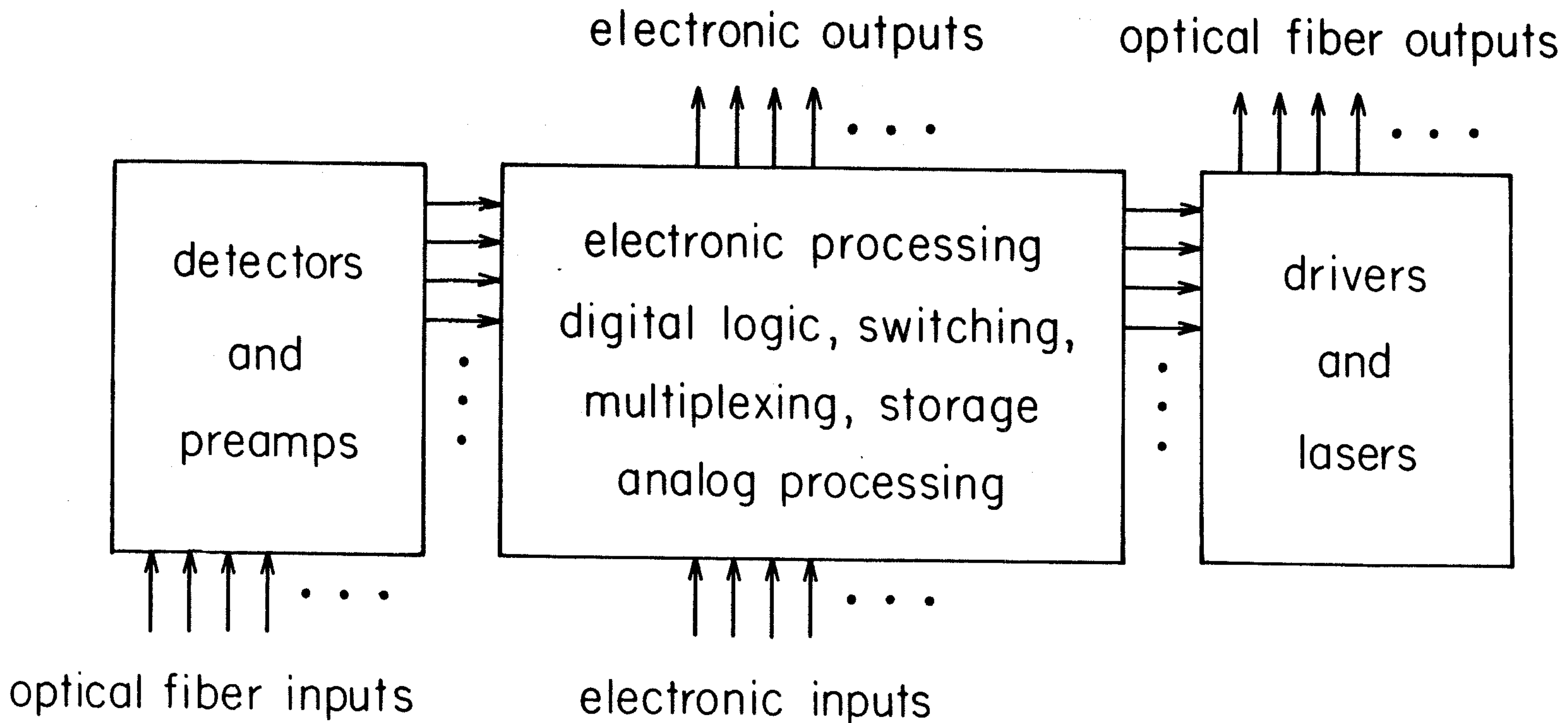

Figure 1.1 **Block diagram of an optoelectronic integrated circuit (OEIC).**

based upon optical data bussing.

The fundamental requirement for the OEIC is a material system and processing technology capable of producing light sources, detectors, and electronic components on the same single crystal chip. Unfortunately the most well understood semiconductor material, silicon, is incapable at present of meeting this requirement. This is because it is an indirect bandgap material and does not generate light efficiently. At present, the optimum material system for the production of OEICs is the ternary, (AlGa)As. The use of this material as the basis for the OEIC was first suggested by Yariv[2]. This material has the following properies:

1. The ternary (AlGa)As is well lattice matched to the binary substrate GaAs for the entire alloy composition range. This means that layered heterostructures can be grown with high quality material interfaces where a minimal amount of recombination takes place, a requirement for efficient lasers and detectors.

2. By varying the alloy composition, the bandgap energy of the material may be varied over the range from 1.43 eV (GaAs) to 1.95 eV ($Al_{0.45}Ga_{0.55}As$) in the direct bandgap region, and from 1.95 eV to 2.17 eV (AlAs) in the indirect bandgap region. This allows the construction of efficient light emitting devices over the wavelength range from 0.9 μm to 0.7 μm and matching detectors for these emitters.

3. Semi-insulating (Cr doped) substrates of GaAs are readily available. This allows the fabrication of electronic devices such as Schottky gate field effect transistors (MESFETS) with low parasitic capacitances and therefore good high frequency characteristics.

4. There is a large number of epitaxial techniques available to produce high quality layered heterostructures of (AlGa)As. Foremost among these is the technique of liquid phase epitaxy (LPE). However, interest is growing in molecular beam epitaxy (MBE) and metallorganic chemical vapor deposition (MOCVD) as important future technologies.

5. Well developed technologies exist for the fabrication of electronic and optical devices separately in this material system. GaAs Schottky gate field effect transistors are widely accepted microwave components, and a high speed integrated circuit family utilizing this component as the active device is developing [3,4,5]. Semiconductor lasers using (AlGa)As are also in commercial production, and state of the art devices are displaying single mode operation and threshold currents below 10 mA [6].

The problem to be overcome in the construction of the OEIC in (AlGa)As, then, is that of blending together these two separate technologies in a manner so that the best features of each may be retained. This is a nontrivial problem, for the two technologies have developed essentially independently. Field effect transistor technology has been developed upon semi-insulating Cr doped substrates with strict control upon epilayer dimensions and dopings to obtain reproducible device characteristics. However, little attention has been paid to the growth of high quality (AlGa)As ternary material which is considerably more difficult due to the reactivity of aluminum. On the other hand, laser and detector technology has developed with primary attention to the growth of high quality ternary material and secondary attention paid to the reproducibility of epilayer thicknesses and dopings. In addition, lasers were developed first on conductive substrates due to the high power dissipations and temperature sensitivity which required the mounting of the devices with the epitaxial side embedded in high thermal conductivity material such as indium solder for heat sinking.

The first design choice to be made is that of substrate material. Based upon the choice of the MESFET as an active device, which needs semi-insulating substrate to operate at high frequencies, semi-insulating Cr doped GaAs has been chosen. However, this choice requires the operation of the laser light sources far away from the heat sink in a device-up configuration. In addition, GaAs has a poor thermal conductivity at room temperature. To realize a practical OEIC with a continuously operating laser requires careful attention to the power dissipation requirement and particular attention to the development of low power dissipation lasers on semi-insulating substrates.

From the standpoint of electronic component technology, the barriers to be overcome in OEIC technology are similar to those encountered in GaAs integrated circuit technology. Reproducibility of device characteristics, and particularly the subject of substrate behavior under thermal cycling are important subjects. During high temperature processing, semi-insulating Cr doped GaAs has a tendency for the deep acceptor Cr atoms to redistribute leaving behind conducting layers in the material[7]. This is a disaster for many device processes, and this problem is receiving a great deal of attention from workers in the integrated circuit field. It should be noted that from the standpoint of OEIC fabrication low temperature processing is to be considered a very important feature of new technology.

I.2 Outline of Thesis

Throughout this thesis, a familiarity with both semiconductor devices and double heterostructure lasers is assumed. For background information, the interested reader is referred to the standard texts[8,9,10,11,12,13].

Five subjects in the field of integrated optoelectronics will be presented and discussed in this thesis. Chapter II will present a prototype OEIC fabricated from (AlGa)As[14]. This circuit, a prototype of a repeater chip as might be found in an

optical communication system, detects optical signals, amplifies the resulting electrical signals, and retransmits them through current modulation of a semiconductor laser. Some aspects of the design of this integrated circuit will be discussed, especially with regard to the expected performance. The fabrication and testing of the device will then be described.

Chapter III will be concerned with ion implantation techniques and their use in fabricating low threshold, well behaved lasers as well as reproducible GaAs MESFETs for use in OEICs. The characteristics of beryllium ions implanted into (AlGa)As as well as the fabrication and testing of beryllium implanted laser diodes will be presented. Both a beryllium implanted laser on n type GaAs substrate [15] and a beryllium implanted laser on semi-insulating Cr doped GaAs substrate integrated with a field effect transistor driver [16] are described. These devices are very simple and easy to fabricate, and have very attractive characteristics for integrated optoelectronics, such as single lateral mode operation and low threshold currents which allow CW operation at room temperature.

Chapters IV, V, and VI are concerned with theoretical modelling of double heterostructure laser diodes.

In Chapter IV a steady state model of the double heterostructure laser is presented [17] which is fully consistent with the master equations for semiconductor materials, a significant departure from models popular in this field. In particular, it treats the diode junction of the device by using the continuity of quasi-fermi levels across the heterojunction interfaces instead of the usual diode equation. This introduces naturally into the theory the saturation of carrier quasi-fermi levels above lasing threshold, as has been measured experimentally [18]. This model is also valid above the lasing threshold, and shows quantitatively the behavior of the diode as it is driven into the regime where spatial holeburning in the gain profile causes shifts between optical modes. The model

is formulated and solved using the finite element method as a solution technique so that it offers a large degree of flexibility in the choice of diode geometry. A specific example is analyzed, and the results of the model are compared with experiment.

Chapter V treats the effects of lateral carrier diffusion upon the modulation characteristics of the laser diode [19]. Here lateral diffusion is taken to mean diffusion parallel to the heterointerfaces on either side of the active region, a direction in which the injected carriers are quite often not tightly confined.

The relaxation oscillation resonance in the semiconductor laser represents a major obstacle to the use of this device in communications systems. This resonance has a typical magnitude of 10 dB over the low frequency value in the small signal response of the laser, and degrades seriously the high frequency modulation response of the laser. Several techniques have evolved to control and damp this resonance, including the use of lateral carrier diffusion. The diffusion of inverted carriers into and out of the optical mode region of the laser represents a considerable damping to the exchange of power between the carriers and the cavity photons. In addition, one might suspect that lateral carrier diffusion would serve to improve the upper modulation frequency limit of the laser. This follows from the fact that in a device with a highly confined optical mode, the inverted carriers may be considered to have a shorter effective lifetime based upon their diffusion away from the optical mode region.

In Chapter V, a simple general model of the effect of lateral carrier diffusion upon the modulation characteristics of the diode laser is presented and solved. To aid the calculation, simplified spatial rate equations are used. A finite element model is used to determine both the steady state and small signal modulation characteristics of the device. The model is applied to the case of a laser where lateral carrier diffusion is known to affect the modulation response, the

TJS (transverse junction stripe) laser, and the calculation is compared with an experimental measurement of the modulation response for this device. In addition, an analytic relationship is derived which describes the maximum contribution of lateral carrier diffusion to the modulation response of the laser.

The essential result of this calculation is that lateral carrier diffusion can serve to damp the relaxation oscillations in the semiconductor laser quite well. However, there is little improvement in the upper modulation frequency limitation from this technique.

Chapter VI presents a treatment of waveguiding in the semiconductor laser that refines and extends the technique described as effective index formalism[20]. This technique involves the solution of a two dimensional waveguiding eigenvalue problem through the use of one dimensional solutions and averaging techniques to form effective refractive index profiles. This technique is often presented as an approximate solution to the scalar wave equation, and the approximations involved are rarely quantified. As a result, this technique is quite often used in an incorrect manner. In this chapter, the effective index method is derived as a variational technique for the solution of the two dimensional eigenvalue problem, and the limits of the technique indicated. The refined technique is applied to the problem of waveguiding in the buried heterostructure laser[6]. The usual approach to this problem is shown to be a poor approximation and a more accurate approach is treated as an example.

I.3 References for Chapter I

1. W. G. French, J. B. McChesney, P. B. O'Connor and G. W. Tasker, "Optical Waveguides with Very Low Losses," Bell Syst. Tech. J. **53**, 951 (1974).

2. A. Yariv, "Active Integrated Optics," Proc. Esfahan Symposium on Fundamental and Applied Laser Physics, M. S. Feld, A. Javan, and N. A. Kurnit, eds., Wiley-Interscience, New York (1973).

3. C. A. Liechti, "Microwave Field-Effect Transistors - 1976," IEEE Trans. Microwave Theory and Techniques **MTT-24**, 279 (1976).

4. C. A. Liechti, "GaAs Fet Logic," Proc. 6th International Symp. on GaAs and Related Compounds, Pt. I, Edinburgh, Scotland, 1976, Inst. Phys., London (1977).

5. R. C. Eden, B. M. Welch, R. Zucca, and S. I. Long, "The Prospects for Ultrahigh Speed VLSI GaAs Digital Logic," IEEE Trans. Electron Devices **ED-26**, 299 (1979).

6. K. Saito and R. Ito, "Buried-Heterostructure AlGaAs Injection Lasers," IEEE J. Quant. Electron. **QE-16**, 205 (1980).

7. C. A. Evans, V. R. DeLine, T. W. Sigmon, and A. Lidow, "Redistribution of Cr During Annealing of ^{80}Se-Implanted GaAs," Appl. Phys. Lett. **35**, 291 (1979).

8. A. Yariv, **Quantum Electronics,** 2nd edition, John Wiley and Sons, Inc., New York (1975).

9. A. Yariv, **Introduction to Optical Electronics,** 2nd edition, Holt, Rinehart, and Winston, New York (1976).

10. H. C. Casey, Jr., and M. B. Panish, **Heterostructure Lasers: Part A, Fundamental Principles; Part B, Materials and Operating Characteristics,** Academic Press, New York (1978).

11. H. Kressel and J. K. Butler, **Semiconductor Lasers and Heterojunction LEDs,** Academic Press, New York (1977).

12. G. H. B. Thompson, **Physics of Semiconductor Laser Devices,** John Wiley & Sons, Inc., New York (1980).

13. S. M. Sze, **Physics of Semiconductor Devices,** Wiley-Interscience, New York (1969).

14. M. Yust, N. Bar-Chaim, S. H. Izadpanah, S. Margalit, I. Ury, D. Wilt, and A. Yariv, "A Monolithically Integrated Optical Repeater," Appl. Phys. Lett. **35,** 795 (1979).

15. N. Bar-Chaim, M. Lanir, S. Margalit, I. Ury, D. Wilt, M. Yust, and A. Yariv, "Be-Implanted (GaAl)As Stripe Geometry Lasers," Appl. Phys. Lett. **36,** 233 (1980).

16. D. Wilt, N. Bar-Chaim, S. Margalit, I. Ury, M. Yust, and A. Yariv, "Low Threshold Be Implanted (GaAl)As Laser on Semi-Insulating Substrate," IEEE J. Quant. Electron. **QE-16,** 390 (1980).

17. D. Wilt and A. Yariv, submitted for publication.

18. T. L. Paoli and P. A. Barnes, "Saturation of the Junction Voltage in Stripe Geometry (AlGa)As Double-Heterostructure Junction Lasers," Appl. Phys. Lett. **28,** 714 (1976).

19. D. Wilt, K. Y. Lau, and A. Yariv, submitted for publication.

20. D. Wilt and A. Yariv, submitted for publication.

Chapter II

The Integrated Optoelectronic Repeater

II.1 Introduction

Early integration experiments carried out by Lee et al. and Ury et al. involved the integration of single electronic devices with lasers. The first such experiment involved the integration of a GaAs bulk effect device, a Gunn device, electrically in series with a laser diode [1]. High speed modulation of the laser diode was demonstrated through the spontaneous transit time mode oscillations of the series connected Gunn device. The second such experiment involved the integration of a single GaAs MESFET in series with a laser diode [2] and demonstrated modulation of the laser diode by varying the gate bias on the series connected FET. These were demonstrations concerned with the compatibility of the device fabrication procedures.

As the next step in the development of OEIC technology, a working integrated circuit was designed and fabricated [3]. This OEIC is fashioned as an optoelectronic repeater, a monolithic chip that will detect, amplify, and retransmit signals such as those that might be found in an operating fiber optic communications link.

II.2 Design Considerations for the Repeater

The schematic of the circuit chosen for the repeater is shown in Figure 2.1. This configuration was chosen as a compromise between simplicity and gain. The device as shown consists of an optical detector, the MESFET labelled Q2, an active load MESFET labelled Q1, a driver MESFET labelled Q3, and a laser diode. In operation, the drain current of the active load transistor is trimmed by adjusting its gate - source voltage so that it matches the drain current on the detector transistor. This is the point where the pair has maximum voltage gain. The load line diagram for this configuration is shown in Figure 2.2.

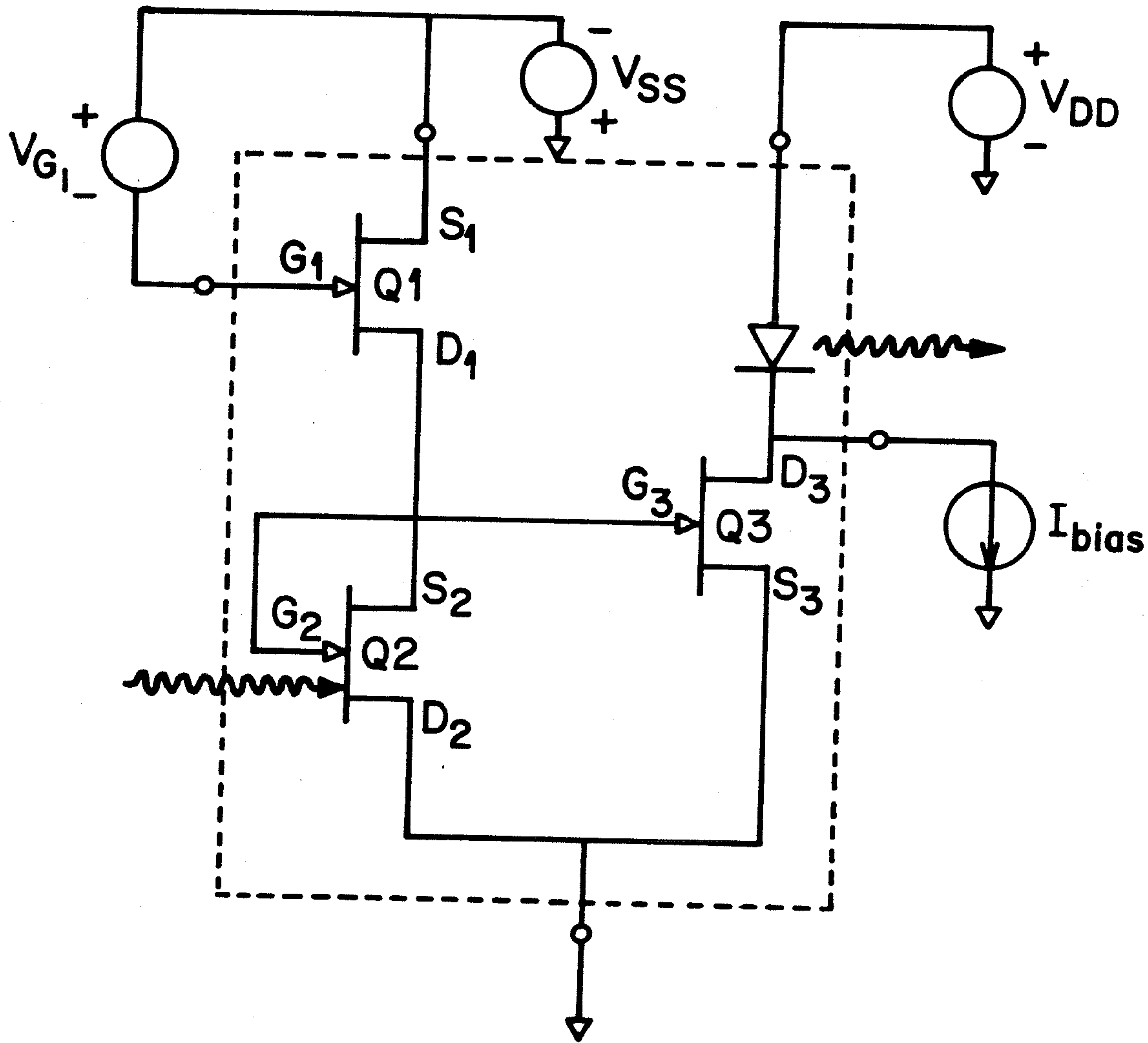

Figure 2.1 Schematic diagram of the repeater integrated circuit.

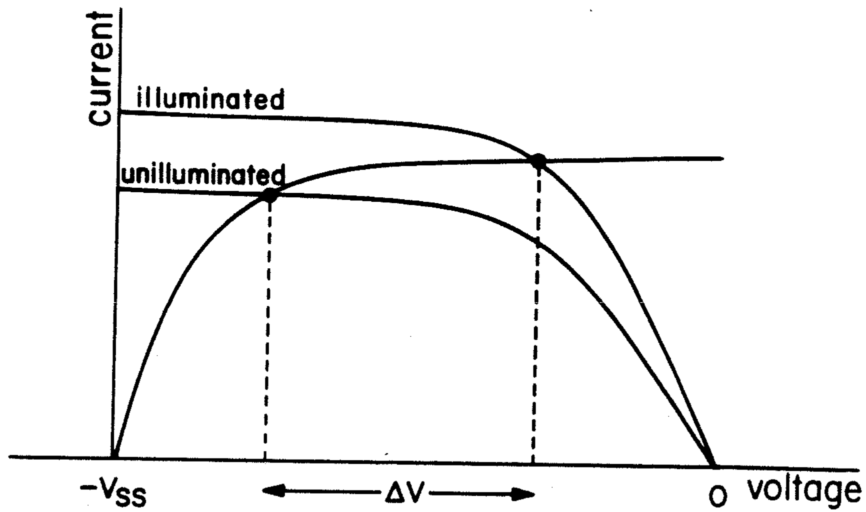

Figure 2.2 Load line diagram for the detector - active load MESFET pair. The voltage here appears on the gate of the driver transistor, Q3.

The operation of the repeater may be described as follows. When light falls on the detector, Q2, the saturated drain current of the transistor increases, causing the voltage at the gate of the driver transistor Q3 to rise in accordance with the load line for the detector - active load pair. This causes the drain current of the driver transistor to increase, increasing the current flow through the laser diode in series with its drain. Thus the light output from the laser diode increases. The repeater circuit can be seen to operate in a noninverting mode, then, as is desired. Note that a current bias source external to the chip is used to hold the laser near its threshold current. This bias current represents a large power dissipation which is both wasteful and unnecessary to pass through the driver transistor, Q3.

The gain of this simple circuit may be calculated in a straightforward manner. When a flux of N photons per second falls on the detector MESFET, its drain current increases by some amount ΔI_d. We can define a detector quantum efficiency by the formula

$$\eta_d = \frac{\Delta I_d}{eN} \tag{2.1}$$

where e is the electronic charge. This represents the number of additional channel carriers flowing per second due to the irradiation. The use of the MESFET as an optical detector was first described and demonstrated by Gammel and Ballantyne[4]. The device is believed to operate as a photoconductor in a source follower configuration. This definition of a quantum efficiency is somewhat misleading, then, since it can be greater than one and has been measured to be as large as five. The response characteristics for this detector are quite good as well, with response times on the order of 50 ps having been reported.

With the definition of quantum efficiency as above, the gain of the repeater

can be calculated as

$$G = \eta_{ci}\, \eta_d\, R_d\, g_m\, \eta_l\, \eta_{co} \qquad (2.2)$$

where η_{ci} represents a coupling efficiency of the input light to the detector, η_d is the quantum efficiency of the detector as defined above, R_d is the detector - active load pair dynamic load impedance, g_m is the driver transistor transconductance, η_l is the laser quantum efficiency, and η_{co} is the output light collection efficiency.

With regard to the operating speed of this IC, the major limitation is represented in the circuit design. The MESFET transistors, if fabricated properly on semi-insulating substrate, should respond well into the gigahertz regime. This includes the operation of the detector MESFET. The laser can be expected to operate at speeds up to approximately one gigahertz, based both upon measurements and theoretical modelling of the dynamic response of the laser diode. With this circuit design, the limitation on the speed of the IC is based upon the charging of the gate capacitance of the driver transistor, Q3, through the dynamic impedance of the detector - active load pair. The time constant for this mechanism is

$$\tau = R_d\, C_g \qquad (2.3)$$

where R_d is the dynamic load impedance, and C_g is the equivalent gate capacitance of the driver transistor, which should include the gate capacitance of the detector and all stray capacitances in the device which must be charged through R_d.

There is a design tradeoff to be made in the circuit, then, based on a compromise between high speed and high gain. The parameters to be varied are the load impedance, R_d, and the driver transconductance, g_m, which is related to the gate capacitance.

To get an idea of what sort of limitation this represents, we will assume a detector with $\eta_{ci}\,\eta_d = 1$, a load characteristic $R_d = 10\ k\Omega$, a driver MESFET with transconductance and gate capacitance $g_m = 10$ mmho , $C_g = 0.3$ pF , and a laser with $\eta_l\,\eta_{co} = 0.5$. This gives as the gain 50 or 17 dB, and as the gate charging delay time 3 ns. Thus the 3 dB cutoff frequency is expected to be approximately 50 MHz, and the gain - bandwidth product of the device 2.5 GHz. On the other hand, with $R_d = 1\ k\Omega$, we get 7 dB of gain and a cutoff frequency of 500 MHz. High speeds are possible, but with a necessary reduction in gain.

The configuration of the repeater is shown in Figure 2.3. The laser in the device was chosen to be the crowding effect laser of Lee et al.[5,6] for simplicity. This laser configuration makes use of the base crowding effect to confine injected current in the active layer to a narrow region near the edge of the etched mesa. Thus the carrier density and optical gain are high in this region, and the lasing filament forms there. The crowding is accomplished by making the sheet resistivity of the lower n type layers as high as possible (consistent with making good MESFETs). The lateral voltage drop in this layer along with the exponential current - voltage distributed diode characteristics cause the injected current to crowd to the mesa edge. This type of laser is extremely simple to fabricate but has a number of drawbacks. It places the optical gain region near the etched mesa edge which serves both as a nonradiative recombination center for injected carriers as well as a light scattering center for the optical mode. These cause the device to have a high threshold current, and it is for this reason that such a crowding effect laser has never been operated continuously at room temperature.

The MESFETS forming the electronic portion of the repeater are fabricated on the bottom n GaAs layer which also serves to connect the laser diode with the driver transistor. The MESFET gate pads are placed in an etched recess on the semi-insulating substrate to minimize the gate capacitances. The gate width on

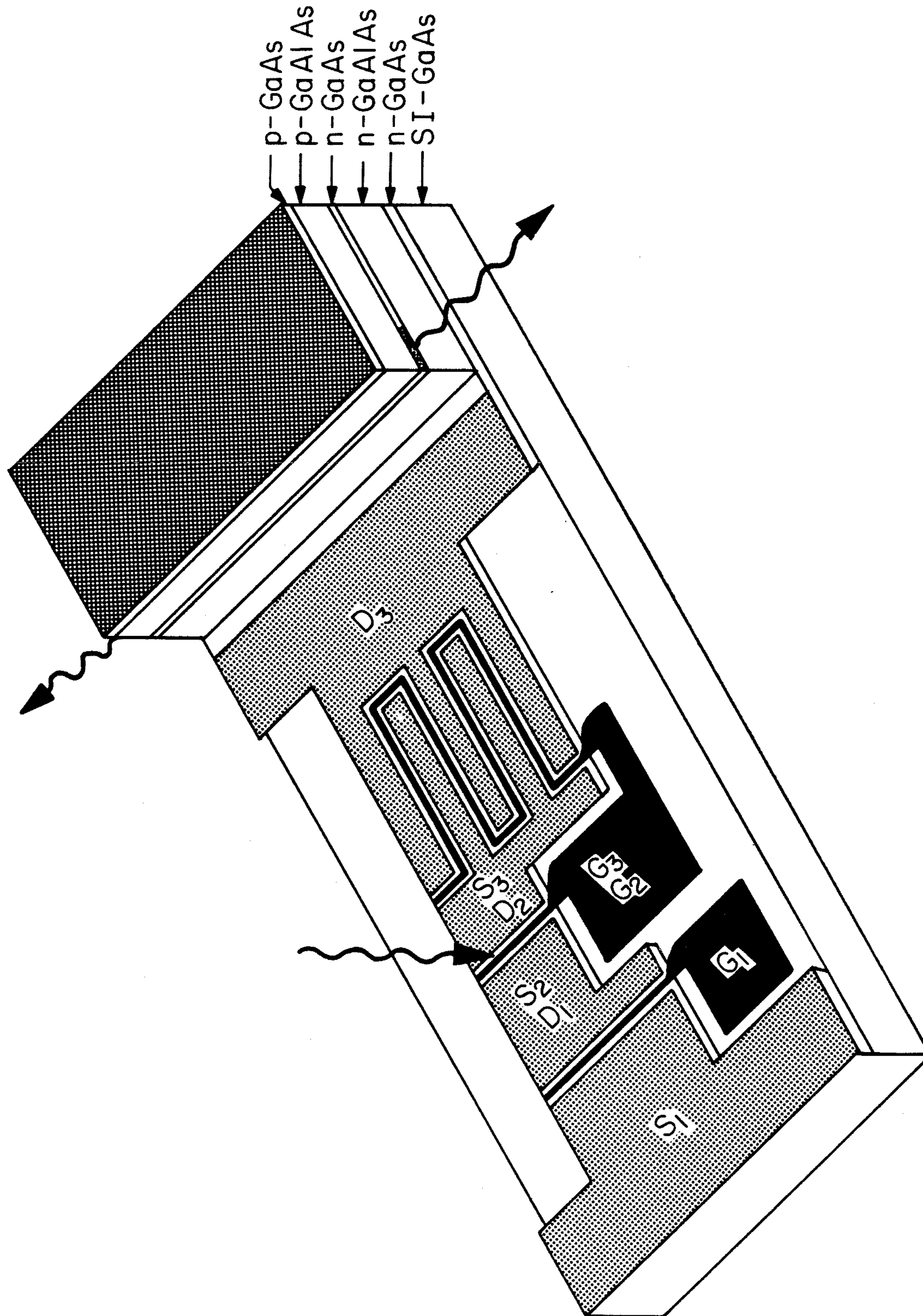

Figure 2.3 Schematic drawing of the repeater integrated circuit.

the driver MESFET is made large to increase its transconductance, and the gate width of Q1 is made slightly larger than that of Q2 so that their drain currents can be matched easily by applying negative bias to the gate of Q1 with respect to its source. The transitions from the recessed semi-insulating island to the FET channels are all oriented in the same direction so that the gates of the FETs can be made continuous over the slanted edge by performing an angled vacuum evaporation of the gate metal. Note that the gates of transistors Q2 and Q3 share a common bonding pad, which must be externally connected to the common $S_2 - D_1$ metallization.

II.3 Fabrication of the repeater

The fabrication of the repeater begins with the LPE growth of five epilayers on an (001) oriented Cr doped semi-insulating GaAs substrate approximately 300 μm thick. The approximate layer dopings and thicknesses are given in Table 2.1. After growth, the wafer is cleaned of any excess gallium and the Cr-Au p contact is evaporated over the top surface. The laser mesa is then defined photolithographically and etching is performed. The contact metal is etched by conventional Cr and Au etchants, and the underlying epilayers by using 1:8:8 ($H_2SO_4 : H_2O_2 : H_2O$) as a nonselective etchant and HF as a selective etchant for (AlGa)As. This leaves the bottom GaAs MESFET layer exposed. This layer is then further etched with the nonselective 1:8:8 etchant to obtain the desired transistor characteristics. The n side metallization, AuGe eutectic alloy and Au, is then shadow evaporated over the laser mesa to form the transistor source and drain contact pads. Another lithographic step, etching of the n contact metal, and nonselective etch is performed to define the gate pad semi-insulating recess. The wafer must have been oriented as mentioned earlier so that the slope of this etch allows the gate metal to be continuous over the step. The transistor channels and gate contact pads are defined photolithographically and the underlying

Table 2.1 **Epilayer characteristics for the repeater.**

Layer	Composition	Doping	Thickness
1	n−GaAs	$2 \cdot 10^{16}$ cm^{-3}	1.4 μm
2	n−$Ga_{0.5}Al_{0.5}As$	10^{17}	2.1
3	n−GaAs	10^{17}	0.3
4	p−$Ga_{0.5}Al_{0.5}As$	10^{17}	2.1
5	p−GaAs	10^{19}	1.0

n contact metal etched. The aluminum gate metal is then evaporated and the gates formed by lifting off the unused metal with the underlying photoresist. This self aligned process produces gates typically 5 μm in length. The n metallization is then alloyed at a temperature of 380 °C and the wafer lapped and cleaved into individual devices.

II.4 Results

In the device reported, shown in Figure 2.4, the final thickness of the MESFET layer was 0.6 μm, and the measured transconductance of the driver FET was 12 mmho. Pinchoff voltages on the FETs were 5 V. The drain characteristics of the three transistors in this device are shown in Figures 2.5, 2.6, and 2.7. The laser, whose length was 480 μm, had a threshold current of 400 mA and a differential quantum efficiency of 10 percent.

The repeater was tested under pulsed conditions due to the high threshold current of the laser diode which made continuous operation impossible. The light source was an external (AlGa)As laser coupled to a fiber, which was oriented so that the light would fall on the detector MESFET. A silicon VMOS transistor was used as an external current source to bias the laser near threshold. The V_{dd} contact of the chip was connected to an external pulse source, which supplied a synchronization signal to the external light source. Tested under these conditions, the repeater chip showed a gain (light output to light input) of 10 dB. The operation of the repeater is shown in Figure 2.8. The upper trace in these photographs shows the current passing through the external laser light source, and the lower trace shows the light output from one facet of the repeater laser diode. The scale on the lower trace is approximately 350 μW per division. The measured power coupled into the detector was 140 μW.

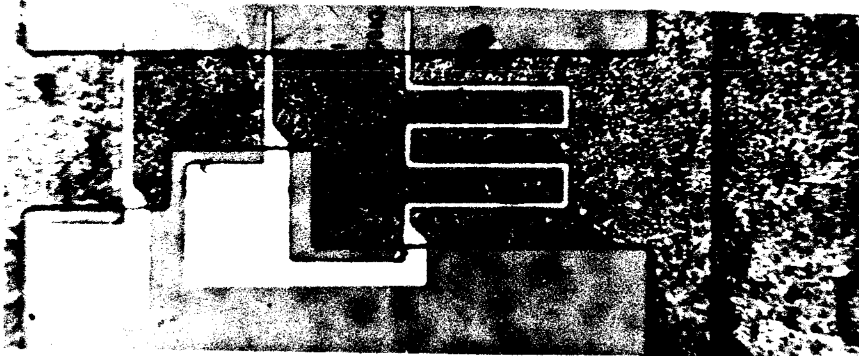

Figure 2.4 Photograph of the completed repeater integrated circuit. The dimensions of the integrated circuit are approximately 1200 μm by 480 μm.

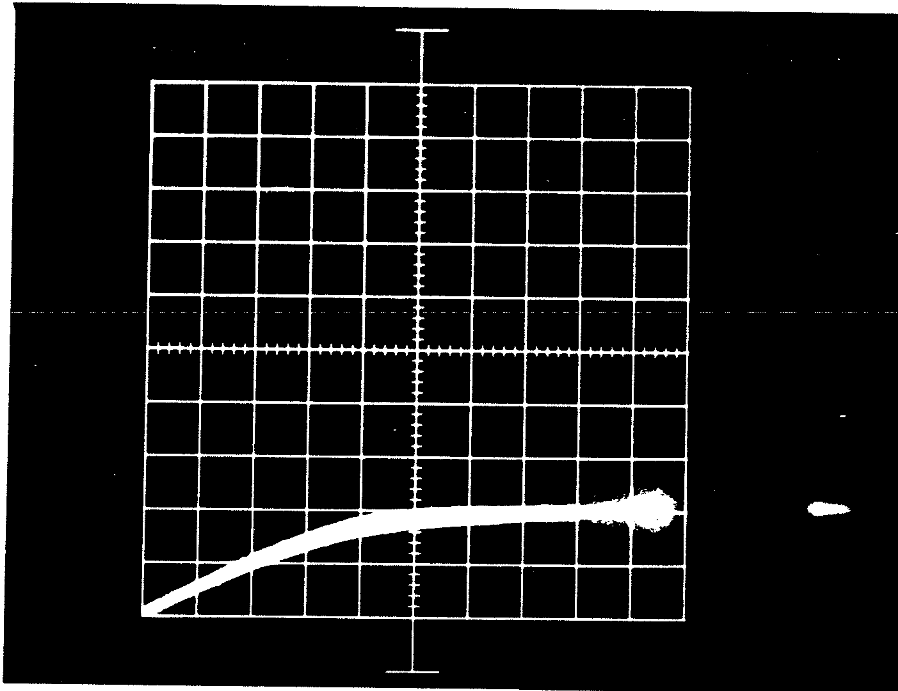

Figure 2.5 Drain current versus voltage characteristics of the detector MESFET in the repeater. The gate of the device is shorted to its source. The horizontal scale is 1V/div and the vertical scale is 2 mA/div.

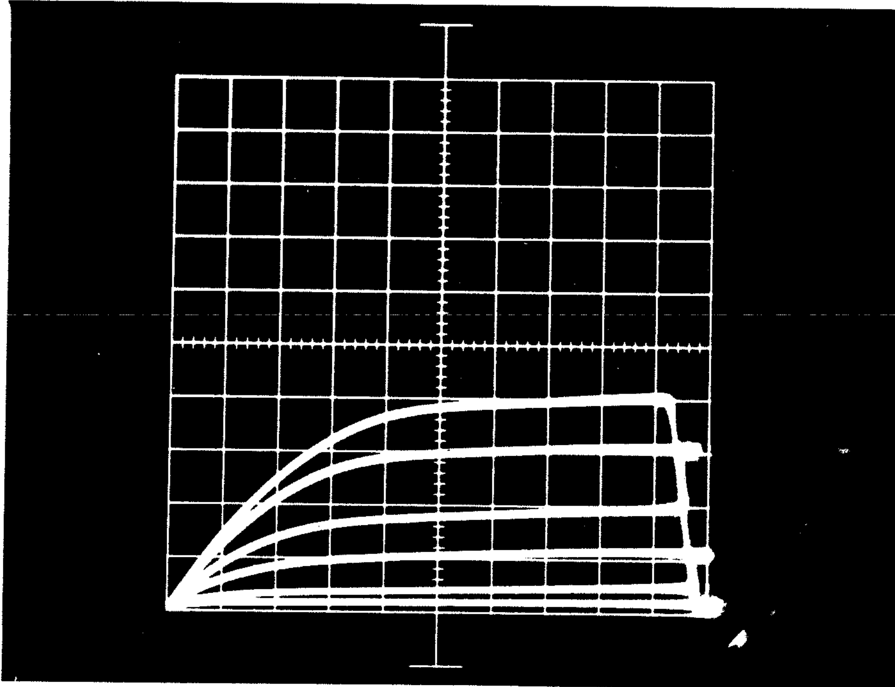

Figure 2.6 Drain current versus voltage characteristics of the active load MESFET in the repeater. Gate voltage is incremented at 1V/step from 0 to -6V. The horizontal scale is 1V/div and the vertical scale is 2 mA/div.

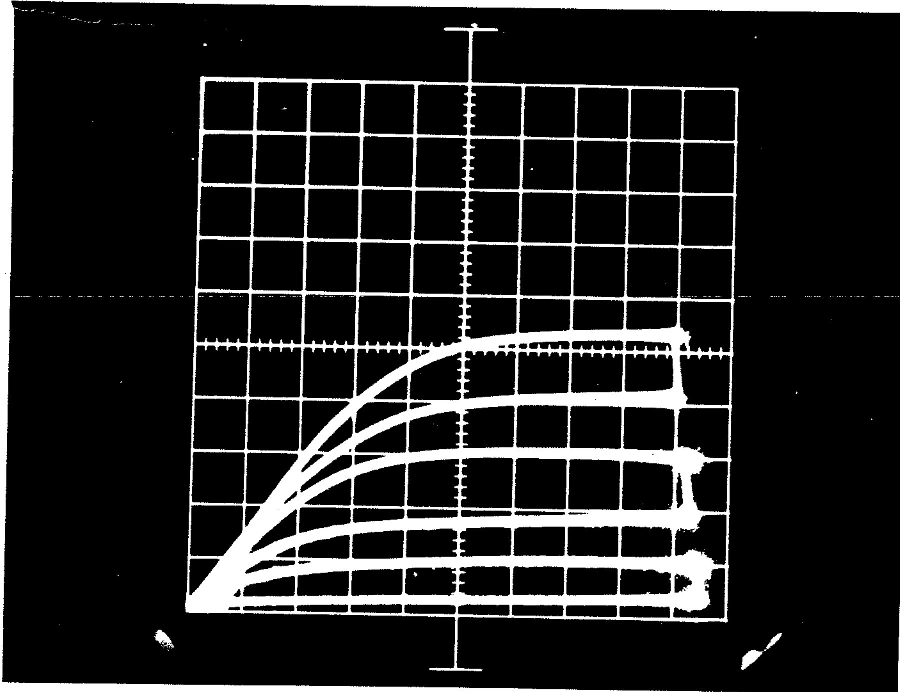

Figure 2.7 Drain current versus voltage characteristics of the driver MESFET in the repeater. Gate voltage is incremented at 1V/step from 0 to -6V. The horizontal scale is 1V/div and the vertical scale is 10 mA/div.

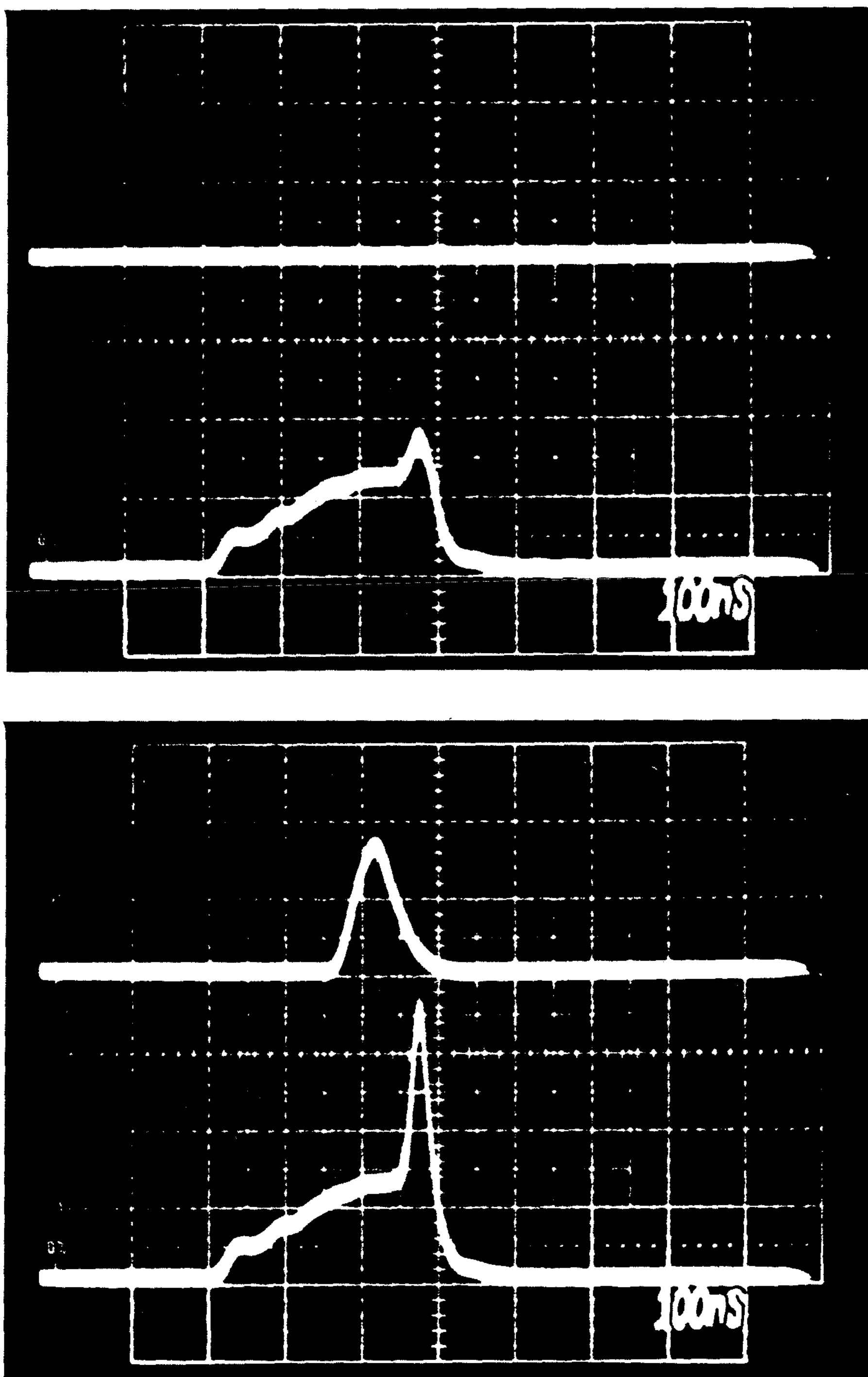

Figure 2.8 Operation of the repeater integrated circuit. The top trace in each photograph is the current through the external laser light source, and the bottom is the light output from the repeater laser. The scale on the lower traces is 350 μW/div. The horizontal time scale is 100 nS/div.

II.5 Conclusions

In this chapter we describe an investigation which demonstrates the feasibility of (AlGa)As based optoelectronic integrated circuits. The limitations due to fabrication problems, but not fundamental, of this first device are the poor performance of the laser diode and the nonreproducible characteristics of the MESFET layers. The laser that would go into a production OEIC should be capable of at least 10 times lower threshold current and 5 times higher quantum efficiency. One example of such an improved laser is the TJS laser on semi-insulating substrate, first demonstrated by Lee et al. [7]. This laser structure has been reported to operate CW at heat sink temperatures as high as 110 °C [8] and in addition has been reported to have extremely long lifetimes of 10^6 hours at room temperature [9]. Another example of an improved laser and an improved technique of making reproducible MESFET characteristics is reported in the next chapter, where ion implanted lasers and MESFETs are described.

II.6 References for Chapter II

1. C. P. Lee, S. Margalit, I. Ury, and A. Yariv, "Integration of an Injection Laser with a Gunn Oscillator on a Semi-Insulating GaAs Substrate," Appl. Phys. Lett. **32,** 806 (1978).

2. I. Ury, S. Margalit, M. Yust, and A. Yariv, "Monolithic Integration of an Injection Laser and a Metal-Semiconductor Field Effect Transistor," Appl. Phys. Lett. **34,** 430 (1979).

3. M. Yust, N. Bar-Chaim, S. H. Izadpanah, S. Margalit, I. Ury, D. Wilt, and A. Yariv, "A Monolithically Integrated Optical Repeater," Appl. Phys. Lett. **35,** 795 (1979).

4. J. C. Gammel and J. M. Ballantyne, "The OPFET: A New High Speed Optical Detector," Proc. IEDM, 120 (1978).

5. C. P. Lee, S. Margalit, and A. Yariv, "Double Heterostructure GaAs-GaAlAs Lasers on Semi-Insulating Substrates Using Carrier Crowding," Appl. Phys. Lett. **31,** 281 (1977).

6. C. P. Lee, S. Margalit, and A. Yariv, "Waveguiding in an Exponentially Decaying Gain Medium," Optics Commun. **25,** 1 (1978).

7. C. P. Lee, S. Margalit, I. Ury, and A. Yariv, "GaAs-GaAlAs Injection Lasers on Semi-Insulating Substrates Using Laterally Diffused Junctions," Appl. Phys. Lett. **32,** 410 (1978).

8. H. Kumabe, T. Tanaka, H. Namizaki, M. Ishii, and W. Susaki, "High Temperature Single Mode CW Operation with a Junction-Up TJS Laser," Appl. Phys. Lett. **33,** 38 (1978).

9. S. Nita, H. Namizaki, S. Takamiya, and W. Susaki, "Single-Mode Junction-Up TJS Lasers with Estimated Lifetime of 10^6 Hours," IEEE J. Quant. Electron. **QE-15,** 1208 (1979).

Chapter III

Ion Implanted Lasers and Schottky Gate Field Effect Transistors

III.1 Introduction

One of the major problems associated with the development of GaAs and other III-V semiconductor materials for device applications is that of selective doping. In particular, the attempted adaptation of diffusion masking and diffusion processes from the silicon technology has failed to achieve satisfactory results for many potential applications. The difficulty lies in two aspects of GaAs technology: the lack of an easily grown thermally matched diffusion mask, and the fact that one of the two components of the compound, arsenic, has a high vapor pressure at normal diffusion temperatures (600 - 1000 °C). This high vapor pressure requires that diffusions in this system be performed under partial pressures of arsenic vapor sufficient to prevent decomposition of the wafer surface, or with a cap on the wafer to prevent the escape of the arsenic from the surface. Either choice results in the introduction of further problems. The diffusion coefficients of most dopants have some dependence on arsenic partial pressure which represents additional control problems, and capping the wafer with a poorly thermally matched dielectric layer leads to stress induced defects and stress enhanced diffusion of the desired dopant, making pattern definition more difficult. In addition, some desirable dopants (e.g. beryllium, a p type dopant) have no compounds with sufficient vapor pressure to realize a satisfactory vapor phase diffusion process.

One of the techniques developed to alleviate some of the problems outlined above is that of ion implantation of dopant atoms selectively into the semiconductor wafer. With this technique, an ion beam of atoms at moderate kinetic energies (up to several hundred keV) is directed at the wafer and the atoms penetrate the surface to a shallow depth (on the order of one μm). Usually the

wafer is oriented along a high index crystal direction or coated with an amorphous material such as Si_3N_4 to minimize the effects of channeling, where high energy atoms travel long distances along low index crystal directions. This process introduces the dopant atoms into the host crystal, but at the same time introduces some lattice damage. A short duration high temperature anneal after the implant repairs this damage and in addition incorporates the implanted atoms into the host lattice, activating their electrical properties. These ion implantations are usually done at low temperatures relative to diffusion processes (up to a few hundred degrees Celsius) and can be masked with little difficulty using conventional photolithographic techniques and non-thermally matched dielectric films. The anneal step usually requires that the wafer be under arsenic vapor pressure or capped, but the short times involved and the facts that dose has already been determined in the implant and the cap does not have to serve as a diffusion mask make this a much easier process to control.

To minimize the damage created in the implanting step, one usually prefers to implant light atoms. However, light atoms diffuse faster and are associated with faster degradation rates for some device applications. Other criteria are also applied to ion implanted dopants, such as annealing requirements, dose activation percentage, and solid solubility limits. These are of course in addition to such considerations as electrical behavior in the host lattice and the difficulty of getting a good ion beam to implant.

At present, the most desirable p dopant for GaAs appears to be beryllium. It has quite low mass and is easily implanted, and shows essentially complete activation after anneals as low as 15 minutes at 800 °C. It has in addition interesting diffusion behavior which will be discussed later. An important consideration, however, is its extreme toxicity. Another important question remains as well, regarding the degradation of beryllium implanted devices.

A host of elements are available for n type implanted dopants. Sulfur, silicon, and selenium have all seen use in ion implanted devices; in particular, for MESFET applications. All have shown quite high activations and good mobility in the resulting layers, a requirement for high speed devices. This is a fortunate coincidence, for while zinc is considered an acceptable p diffusant for GaAs, the n diffusants are in comparison much less controlled. This work has been spurred mainly by the development of GaAs MESFET integrated circuits, and most of this work has involved the direct implantation of the selected dopant into Cr doped semi-insulating substrates. The simplicity of the process for producing large numbers of MESFETs on a common substrate is a prime consideration in the development of OEIC technology.

In this chapter, the use of ion implantation as a technique in the fabrication of OEICs is presented. A laser structure using beryllium as an ion implanted dopant and sulfur implanted MESFETs are described. The resulting devices are easier to fabricate and more reproducible in their characteristics than their corresponding zinc diffused and LPE grown counterparts. In addition, they have some advantages in dimensional control associated with the simpler masking techniques used for ion implanted dopants.

III.2 Sulfur Implanted GaAs Schottky Gate Field Effect Transistors

Other researchers have already reported the use of sulfur implantation as a method of forming MESFET layers in Cr doped semi-insulating substrates [1,2]. This method has been adopted to make MESFETs suitable for OEIC fabrication. The process begins with a sulfur ion implantation at an energy of 200 keV and a dose of $5 \cdot 10^{12}\ cm^{-2}$ into Cr doped semi-insulating GaAs substrate. At this implanting energy, a projected range of 0.15 μm with a standard deviation of 0.06 μm is predicted for sulfur in GaAs using the theory of Lindhard, Scharf, and Schiott [3]. The wafer is then capped with approximately 2500 Å of CVD SiO_2, and

annealed at 850 °C for 30 minutes. The resulting MESFET layers have mobilities of approximately 3500 $\frac{cm^2}{Vs}$ and sheet resistivities of approximately 1000 $\frac{\Omega}{\square}$. These layers have been used to fabricate MESFETs with characteristics suitable for OEICs.

This process is compatible with the other processes used, for instance, in the production of semiconductor lasers. After the epitaxial step and etching required to form the laser structures, a deep etch can be done to reveal the surface of the semi-insulating wafer where it is desired to form MESFETs. Then a selective implant can be done using the same mask that is used to perform the etching, and the wafer capped and annealed. The remaining metallization steps are easily performed together on both the MESFETs and the lasers.

III.3 Beryllium Implanted (AlGa)As Double Heterostructure Lasers

Beryllium ion implantation has gained a great deal of interest lately as a method of fabricating p type layers in GaAs. Beryllium is an extremely light ion which can be implanted at low energy, and annealed easily at relatively low temperatures.

The characteristics of beryllium as an ion implanted dopant in GaAs have been researched by a number of investigators [4,5,6,7,8]. Annealing studies [6,7,8] have shown that full electrical activation can be achieved with as low as 700 °C annealing temperature at large doses (corresponding to beryllium concentrations greater than 10^{18} cm^{-3}), and have revealed an interesting diffusion characteristic for beryllium implanted in GaAs. This is that at beryllium concentrations greater than approximately 10^{18} cm^{-3} in GaAs, beryllium diffuses very quickly. This allows the use of beryllium ion implantation as a predeposition step for beryllium diffusion to form high quality p layers with relatively uniform concentrations near 10^{18} cm^{-3}. The great advantage of this technique is that the junction depth depends most strongly upon the predeposited dose, which can be

controlled very precisely. No information about beryllium implantation into the ternary alloy (AlGa)As had appeared yet, an important consideration in the production of optoelectronic devices by ion implantation.

The use of ion implantation as a technique for fabricating semiconductor lasers had been reported by Barnoski et al. in 1974 [9]. This involved a homostructure laser formed by implanting zinc atoms at very low energy into a GaAs substrate and subsequently diffusing the zinc in to form a shallow p-n junction for the laser. Ion implantation is also used routinely as an isolation technique in GaAs technology, utilizing the fact that damaged GaAs has high resistivity. Usually protons are implanted to produce this damage, and an effort is made to keep the damaged region well away from the important recombination regions in the device such as the active layer of a laser.

In this section a double heterostructure laser formed using beryllium ion implantation as a fabrication technique is described [10,11]. It has the desirable features of low threshold current, well behaved modal properties, high quantum efficiency, and easy fabrication that make it an attractive device for OEIC applications.

The lateral cross section of the device is shown in Figure 3.1. This device is fabricated in a stripe geometry which is closed in the sense that the p-n junction in the device has a limited cross sectional area. With this geometry, the current injection into the active layer of the device is limited to the narrow region where the p stripe contacts it. The p-n junction formed in the upper cladding layer draws a negligible current due to the difference in bandgap energy, and the surface leakage in this type of device is negligable.

This geometry has several advantages from the standpoint of laser structure. The typical stripe geometry laser, formed with a broad area p-n junction and current confining insulating stripe, relies upon sheet resistivity in the upper

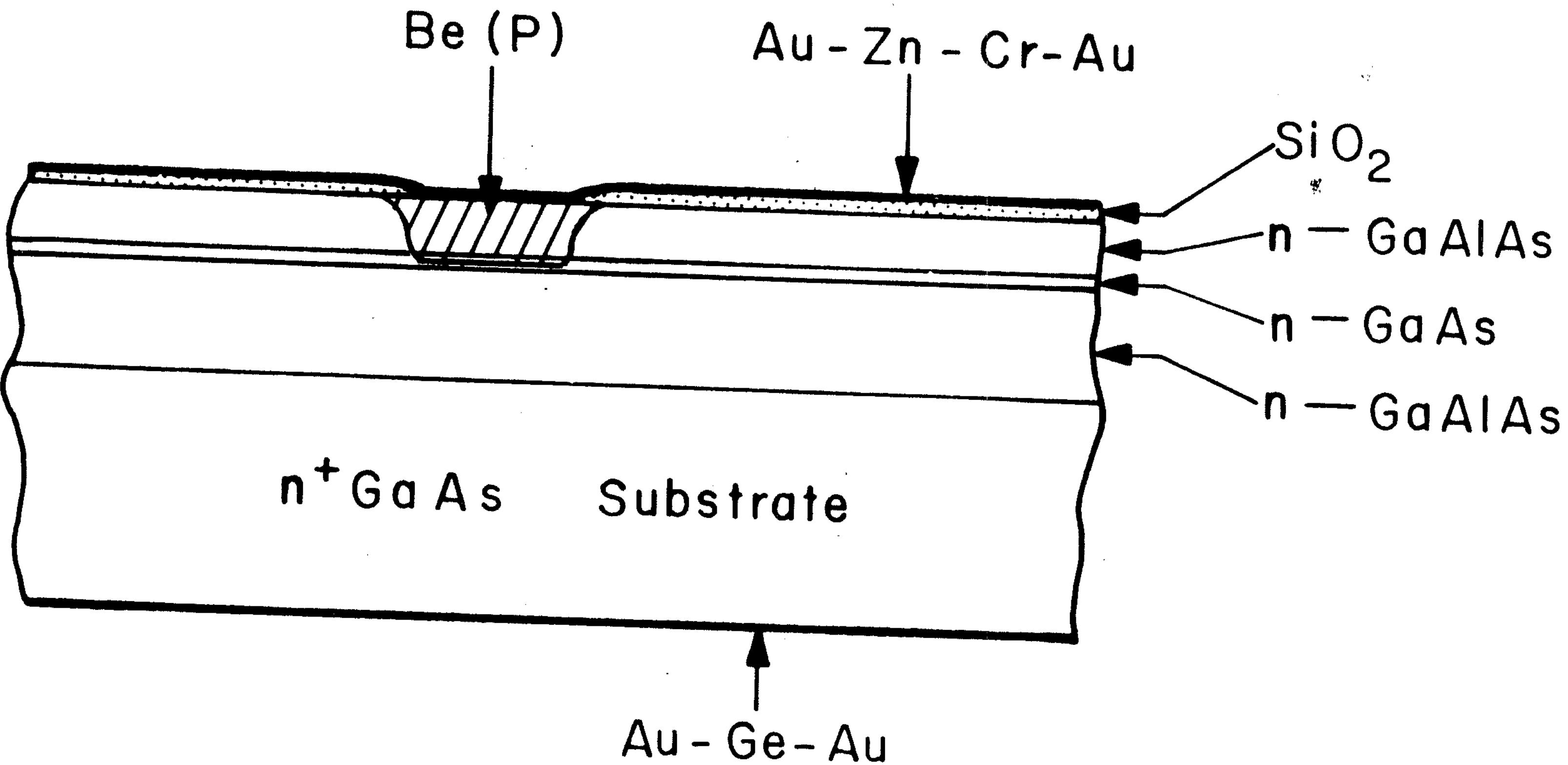

Figure 3.1 Schematic lateral cross section of a beryllium implanted laser.

layers to provide confinement of injected current. This depends strongly upon growth conditions such as background doping and gives a great deal of variation in device behavior. In addition, it is difficult to achieve current confinement tight enough to limit the laser oscillation to a single filament. This results in multimode oscillation and unstable characteristics such as kink formation in the light versus current characteristics. An additional problem is the difficulty of obtaining low threshold currents due to the presence of the two injected current tails on either side of the stripe. This current is essentially lost.

In this closed stripe laser, filament stabilization is much easier to achieve due to the reduction in the width of the p stripe. This results in stable near field patterns and linear light versus current characteristics over a wider range of output power. In addition, the only current lost is that which diffuses away from the gain region of the laser, permitting very low threshold currents to be attained.

The fabrication of the beryllium implanted laser begins with the LPE growth of three layers on an n type GaAs substrate. Typical layer thicknesses and dopings are given in Table 3.1. After the growth, the wafer is cleaned of excess gallium and coated with approximately 2500 Å of CVD SiO_2. The laser stripes are then defined photolithographically in AZ-1350J photoresist using stripe widths of between 2 and 10 μm, and the underlying SiO_2 in these openings etched. A 100 keV beryllium implantation is then performed with a dose of $3 \cdot 10^{15}$ cm^{-2} at room temperature, using the photoresist as a mask. The predicted projected range and standard deviation in $Al_{0.45}Ga_{0.55}As$ at this energy are 0.35 and 0.12 μm, respectively[3]. The photoresist is then stripped and a high temperature anneal performed at 800 °C for 40 minutes. This anneal is uncapped but performed in an H_2 ambient in a semi-sealed graphite holder, so that arsenic loss from the substrate is minimized. The implanted beryllium diffuses down through the structure in this step and contacts the active layer. This is related

Table 3.1 Epilayer characteristics for the beryllium implanted laser.

Layer	Composition	Doping	Thickness
1	n$-Ga_{0.55}Al_{0.45}As$	10^{17} cm^{-3}	3 μm
2	n$-$GaAs	10^{17}	0.25
3	n$-Ga_{0.55}Al_{0.45}As$	10^{16}	1

to the process in GaAs where the high beryllium concentration diffuses very quickly. At this implanted dose, the experimental junction depth was 0.8 μm in GaAs and 1.4 μm in $Al_{0.45}Ga_{0.55}As$. These junction depths are not strongly dependent upon anneal temperature, as is shown in Table 3.2, again illustrating the concentration dependence of the diffusion process, and providing some data on beryllium implantation into (AlGa)As. The junction depth rises monotonically with aluminum content up to an alloy composition of $Al_{0.65}Ga_{0.35}As$, possibly indicating a decrease in the concentration required to initiate the fast diffusion mechanism. The result of this is that the diffusion front will often stop at the heterojunction interface, a process easily controlled by regulating implanted dose.

An SEM photomicrograph showing the cross section of the finished device is shown in Figure 3.2. The lateral diffusion of the Be can be seen to be minimal, and the diffusion touches the active layer of the device, as desired.

An ohmic contact to the p region is formed by a shallow zinc diffusion followed by plating of AuZn alloy, and the evaporation of Cr and Au. The contact is alloyed at 460 °C. The substrate is lapped and the back n contact of AuGe and Au is formed by vacuum evaporation and alloying at 380 °C. The contact resistance of the finished devices is typically 10 Ω.

This technique has the virtue of having high device yields due to the simple processing involved. Typical pulsed threshold currents for a 7.5 μm stripe width were 55 mA for 250 μm cavity length, and 30 mA for 125 μm cavity length. For a 3.5 μm wide stripe, these were 40 mA and 25 mA for 250 μm and 125 μm cavity length, respectively. The lowest pulsed threshold current found was 21 mA. CW operation was established, with the threshold current approximately 30 percent higher than pulsed operation. The stable near field pattern of the device is

Table 3.2 Be diffusion data for $Ga_{1-x}Al_xAs$. Implanted dose = $3 \cdot 10^{15}$ cm^{-2}, energy = 100 keV.

X	Anneal		Junction Depth (μm)	Sheet Resistance ($\frac{\Omega}{\square}$)
	Temperature (°C)	Time (min)		
0.00	800	40	0.8	100
	850	40	0.9	-
0.45	800	40	1.4	370
	850	40	1.6	-
0.65	800	40	1.9	1000
	850	40	2.1	-

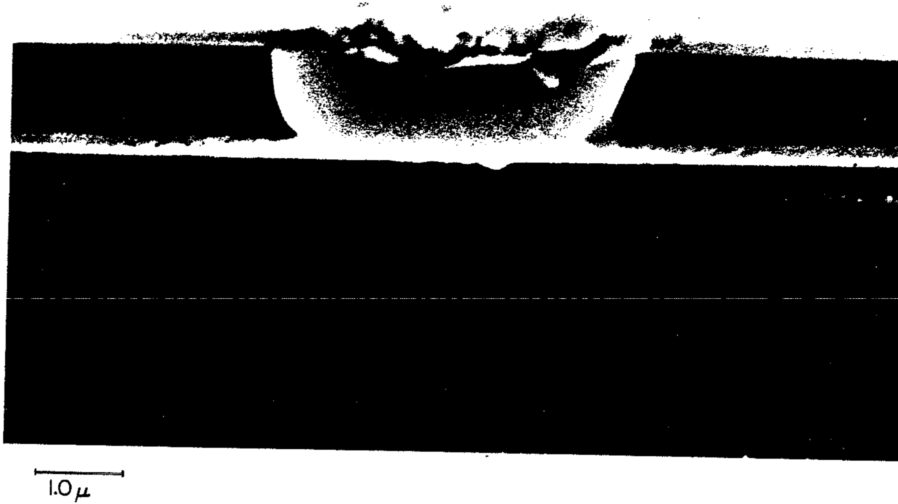

Figure 3.2 SEM photomicrograph of the lateral cross section of a beryllium implanted laser.

shown in Figure 3.3. The light versus current characteristics were linear and kink-free up to 10 mW power output. The measured differential quantum efficiency was 45 percent.

One of the interesting aspects of laser diode operation, and a revealing test of the understanding of these devices, is the guiding mechanism that determines the optical modes of the laser. In a device such as the beryllium implanted laser, it is not obvious whether the optical modes are determined by the gain profile generated by the injected carriers or by a change in the real refractive index of the diffused beryllium doped region. Experimentally, a measurement of the near field and far field patterns of the laser and a comparison of the two shows whether the device is gain or real refractive index guided. To show how this happens, we must look at the wave equation defining the optical modes.

As a starting point, we consider the vector wave equation,

$$(\nabla^2 + k^2 \varepsilon) \vec{E} = 0 \tag{3.1}$$

where k is the vacuum wavevector, $k = \frac{\omega}{c}$, and ε is the complex relative permittivity of the medium. Assuming a waveguide mode with a z dependence of $e^{i\beta z}$ and substituting we obtain

$$(\nabla_t^2 + k^2 \varepsilon - \beta^2) \vec{E} = 0 \tag{3.2}$$

where ∇_t is the transverse gradient operator,

$$\nabla_t = \vec{e}_x \frac{\partial}{\partial x} + \vec{e}_y \frac{\partial}{\partial y} \tag{3.3}$$

The influence of the planar mirrors on the device is to introduce the round trip phase and gain conditions

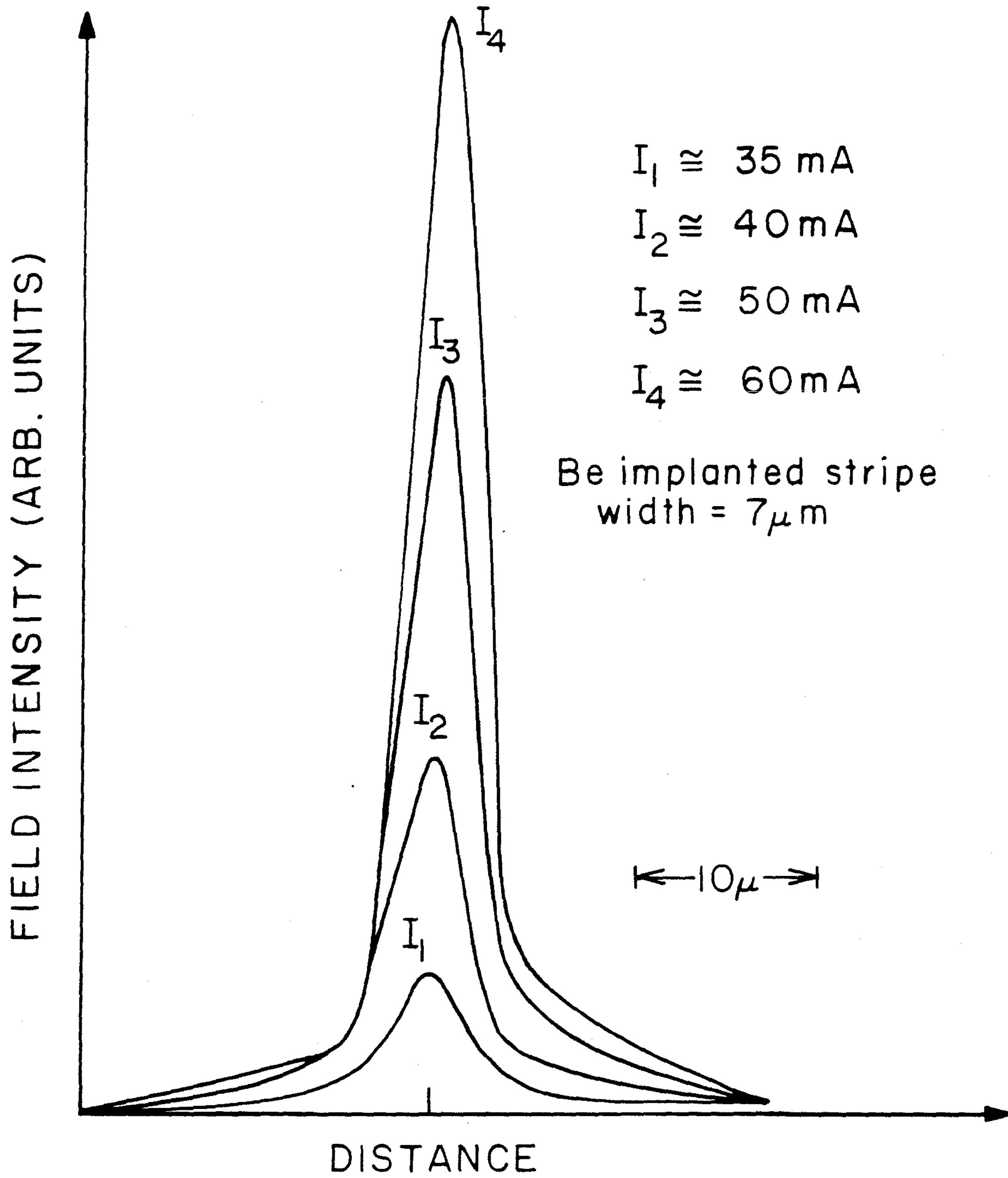

Figure 3.3 The near field pattern of the beryllium implanted laser.

$$\mathrm{Re}(\beta) = \frac{N\pi}{L} \tag{3.4}$$

$$2\,\mathrm{Im}(\beta) = \alpha + \frac{1}{L}\ln\left(\frac{1}{R}\right) \tag{3.5}$$

where L is the length of the laser cavity, N is an integer, α is the distributed loss in the cavity, and R is the mirror reflectivity. These relations, equations (3.2) through (3.5), define the electromagnetic modes of the laser cavity. The manner in which this differs from other types of lasers is that the dominant guiding mechanism in the device is the internal permittivity instead of the mirror geometry.

If the real part of permittivity is the dominant mechanism in determining the laser optical modes, the operator in the eigenequation (3.2) is essentially real or Hermitian. This forces the bound eigensolutions to the equation to have no phase variation in planes of constant z, or in other words to have planar wavefronts. On the other hand, if the imaginary part of the permittivity is important to the waveguide problem, the bound eigensolutions have a phase variation in the planes of constant z or curved wavefronts.

Using the fourier transform relation between the near field distribution at the mirror surface and the far field angular distribution [12] we find the imaginary permittivity ("gain") guided device to have a wider far field intensity distribution than the real permittivity ("index") guided device, given the same near field intensity distribution. This can be quantified for a device with Gaussian field distributions as

$$W\,\Theta \geq \frac{\lambda \ln 4}{\pi} \tag{3.6}$$

where W is the half power width of the near field, Θ is the half power width of the

far field, and λ is the free space wavelength. Equality holds for the real permittivity guided mode.

In the typical semiconductor laser, the waveguide consists of a perturbed dielectric slab. This means that in one direction (normal to the p-n junction) there is a large step in the real part of the permittivity, which essentially determines the modal profile in this direction. This modal profile is index guided. In the perpendicular direction, parallel to the p-n junction, the guiding mechanisms are much weaker and can be either gain or index determined. We wish to determine which controls the behavior of this laser. Accordingly, the near and far field intensity distributions of the device parallel to the p-n junction were measured, and the result of this measurement is shown in Figure 3.4. The measured near field half power beamwidth is 2.3 μm and the far field half power beamwidth is 14°. The intensity distributions closely resemble gaussian distributions, and they are compared with the gaussian beam formula, equation (3.6). For the wavelength of these devices, 0.883 μm, $\frac{\lambda \ln 4}{\pi} = 22$ μm-degrees. The experimental result shows $W\,\theta = 32$ μm-degrees so it is concluded that these devices are gain guided. Equivalently, we can compare the location of the virtual beam waists in the direction normal to the junction plane where it is index guided to that in the plane of the junction using an infrared microscope. Astigmatism in the output beam from the laser diode (different beam waist locations) indicates the presence of a gain guiding mechanism in the lateral direction. This qualitative measurement was performed and the output beam of the laser diode was seen to be highly astigmatic, agreeing with the conclusion that the devices are gain guided in the lateral direction.

This is not a surprising result since these devices have no lateral structure to introduce a lateral perturbation in the real part of the permittivity. What the measurement indicates is that the beryllium implanted region does not have a

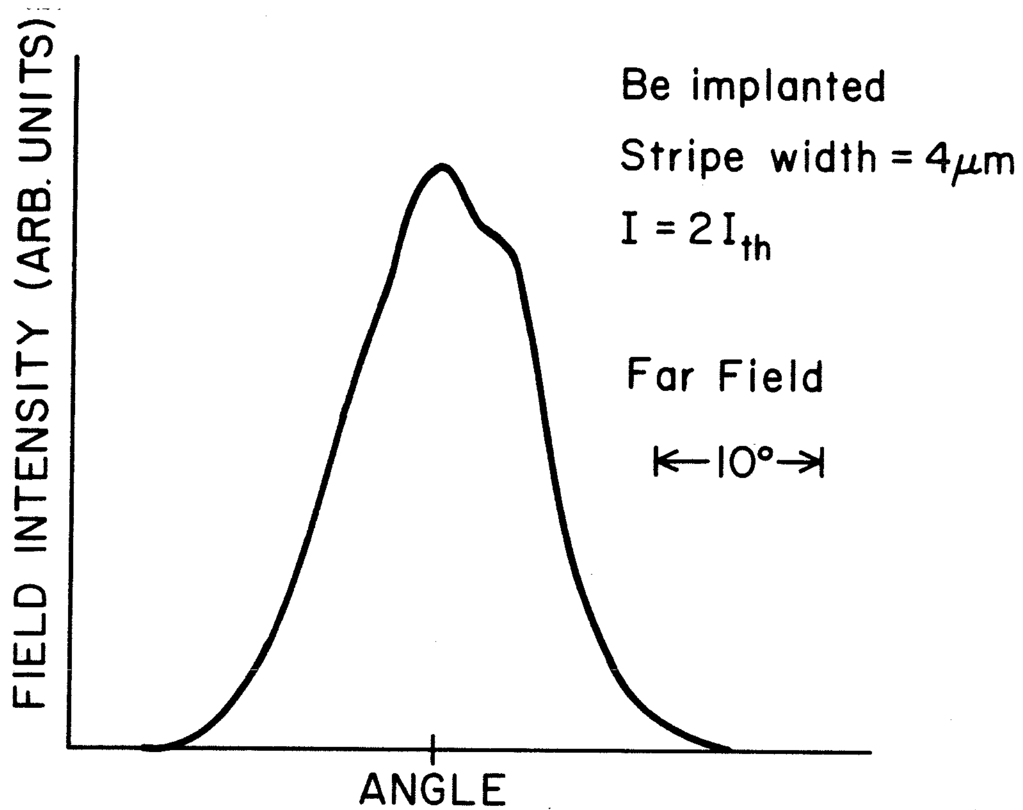

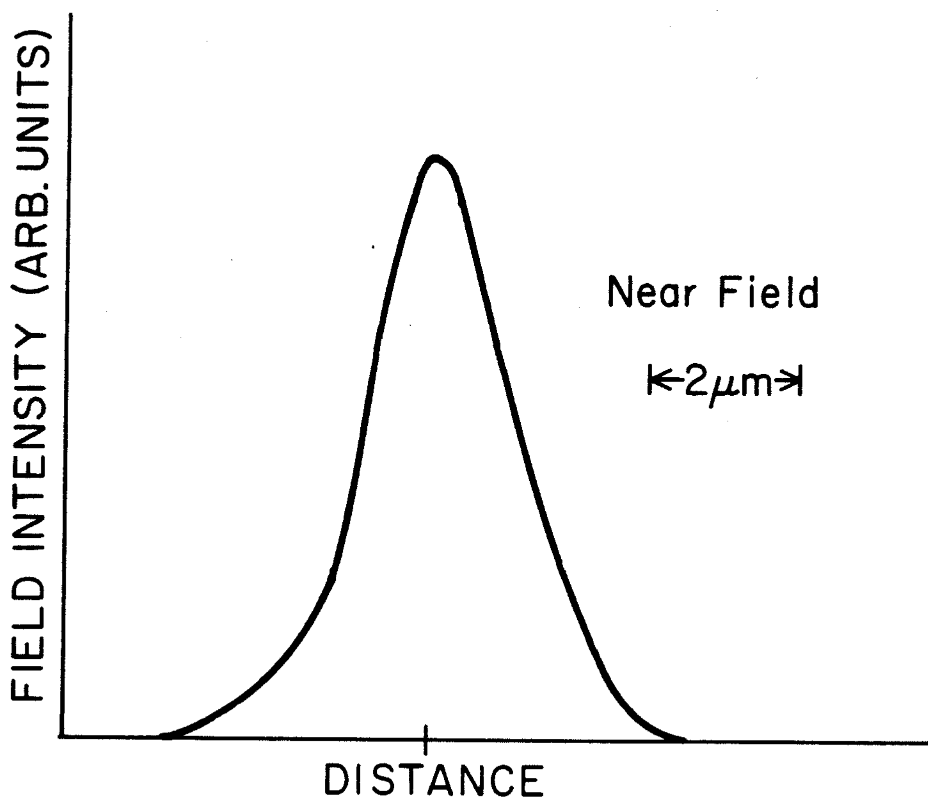

Figure 3.4 A comparison of the near and far field patterns of the beryllium implanted laser.

significantly different real permittivity from the surrounding LPE doped regions.

The active layer doping in the device described here was approximately 10^{17} cm^{-3}. Devices with higher active layer dopings, up to 10^{18} cm^{-3}, had similar behavior. This is characteristic of semiconductor lasers, which operate at carrier densities of approximately 10^{18} cm^{-3}, so that the added dopant atoms play a minor role in the device behavior.

One of the important features of this device is its compatibility with semi-insulating substrates. This is by virtue of the closed structure used. The device can be fabricated on semi-insulating substrate simply by incorporating one more layer of epitaxial growth underneath the laser structure. This layer is n doped GaAs, which is required for good ohmic contact. In addition, by doping this layer properly and controlling its thickness, it can serve as the channel layer for MESFETs. This device has been fabricated and is shown in Figure 3.5. The bottom MESFET layer is doped approximately 10^{16} cm^{-3} and grown approximately 0.8 μm thick.

Fabrication of this device follows the procedure outlined above up to the point where the p contact for the laser is alloyed. At this point, the laser mesa is defined photolithographically and etched with 1:8:8 ($H_2SO_4 : H_2O_2 : H_2O$). The n side contact metal, AuGe and Au, is shadow evaporated onto the wafer, and the MESFET drain and gate formed using the self aligned liftoff process described in connection with the repeater integrated circuit. The n contact is alloyed at 380 °C and the wafer thinned and cleaved into individual devices.

The behavior of these lasers is slightly better than the devices on n type substrate. Pulsed threshold currents for 4 μm stripe width and cavity lengths of 250 and 125 μm were 35 and 20 mA, respectively. The lowest threshold current was 15 mA for a 100 μm long cavity. The stable near field pattern of the device is

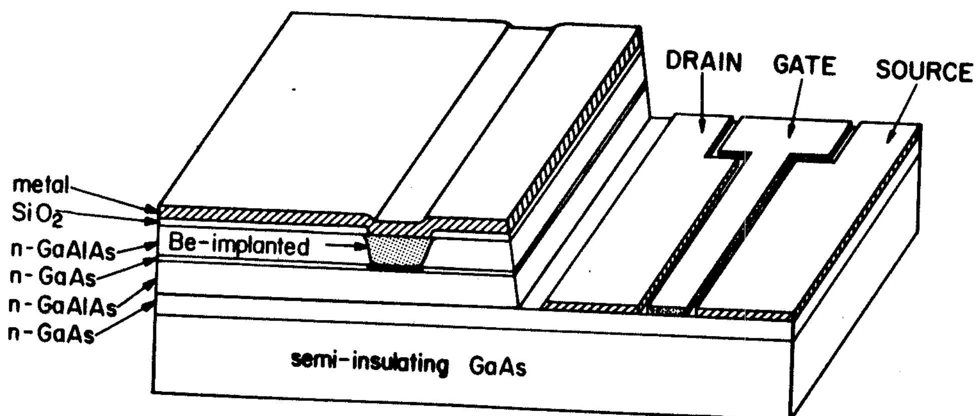

Figure 3.5 The beryllium implanted laser on semi-insulating substrate with an integrated MESFET driver.

shown in Figure 3.6. The near field of this laser shows some asymmetry due to the slight crowding of the injected carriers to the mesa side of the implanted stripe. This occurs because of the sheet resistivity of the lower n type layers. The light versus current characteristics were linear and kink free to 10 mW output power, and the external differential quantum efficiency was measured at 50 percent from both facets. The device was seen to operate in essentially one spectral mode as is shown in Figure 3.7.

The MESFET was used to modulate the light output of the laser by varying its gate bias. This is shown in Figure 3.8.

III.4 Conclusions

Two devices important to the development of the OEIC have been presented which make use of the unique advantages presented by ion implantation as a fabrication technique. Particular attention has been paid to the questions of process compatibility, reproducibility, device yield, and dimensional control. These devices can represent significant improvement over their conventionally fabricated counterparts in these aspects of device evaluation.

It is clear that ion implantation must be seriously considered as an important technique in fabrication of (AlGa)As optoelectronic devices.

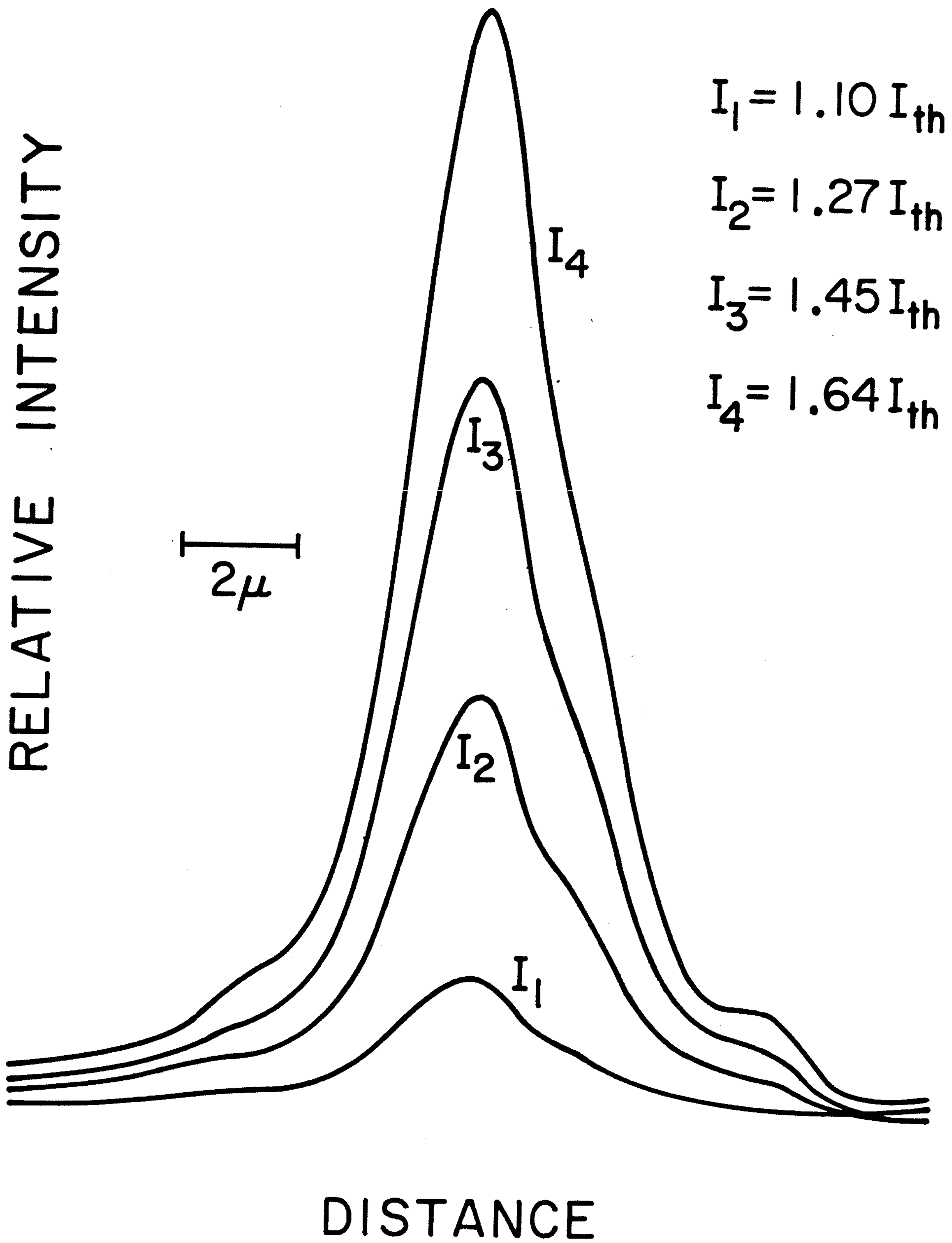

Figure 3.6 The near field pattern of the beryllium implanted laser on semi-insulating substrate.

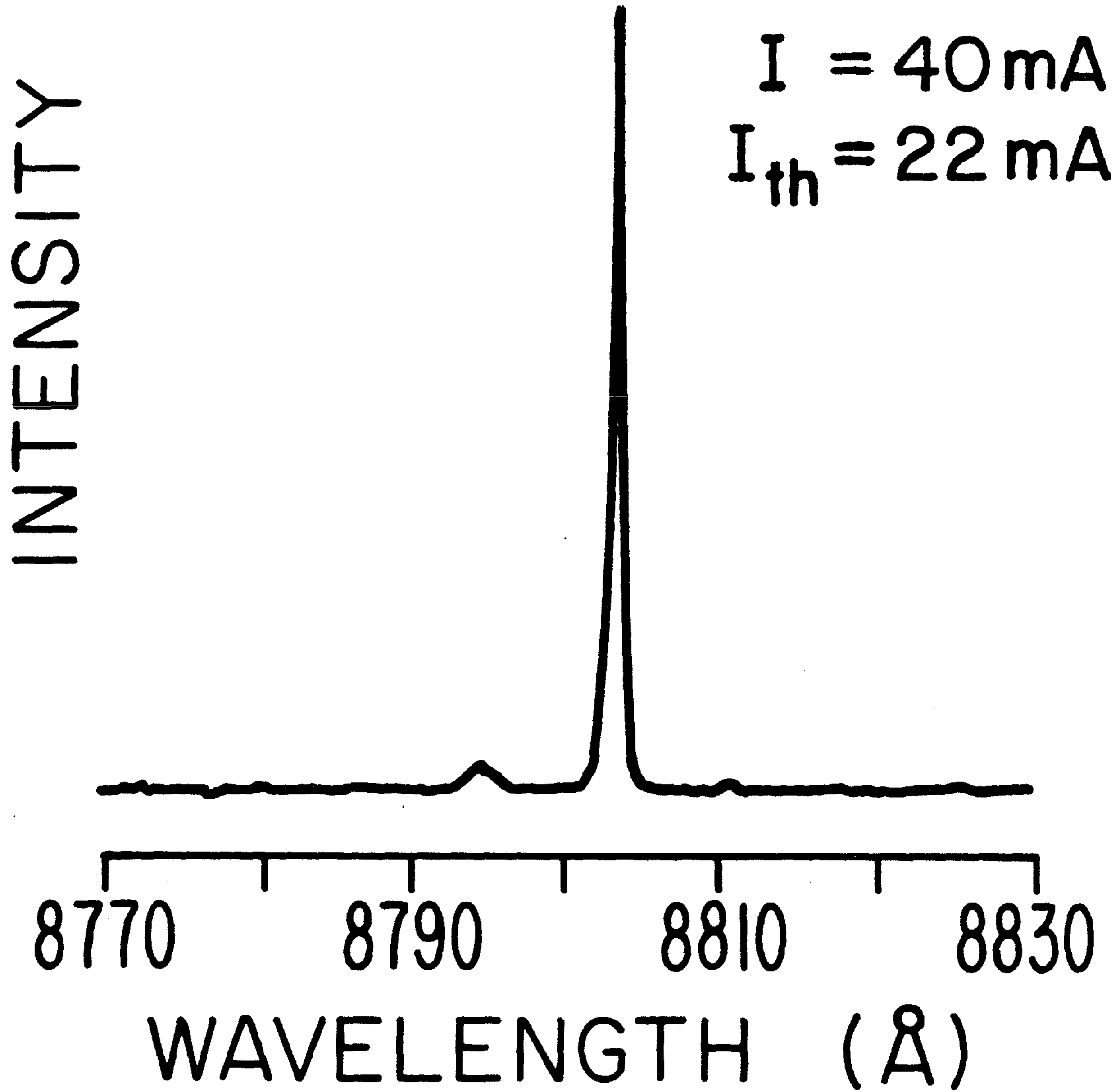

Figure 3.7 Emission spectrum for the beryllium implanted laser on semi-insulating substrate, showing single longitudinal mode operation.

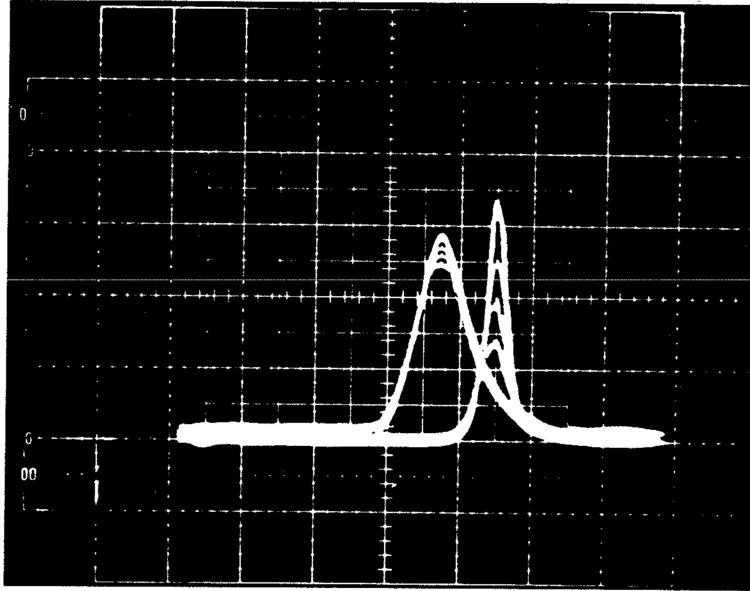

Figure 3.8 Modulation of the beryllium implanted laser on semi-insulating substrate by the integrated MESFET. The laser current is shown on the left side of the scale (10 mA per division) and the light output on the right (arbitrary units) The gate voltage on the MESFET is varied at 0.5 V per step. The horizontal scale is 20 nS per division.

III.5 References for Chapter III

1. R. G. Hunsperger and N. Hirsch, "GaAs Field-Effect Transistors with Ion-Implanted Channels," Electron. Lett. **9**, 577 (1973).

2. T. Mizutani, S. Ishida, and M. Fujimoto, "GaAs Field-Effect Transistors by Sulfur-Ion Implantation," Electron. Lett. **12**, 431 (1976).

3. W. S. Johnson and J. F. Gibbons (unpublished).

4. R. G. Hunsperger, R. G. Wilson, and D. M. Jamba, "Mg and Be Ion Implanted GaAs," J. Appl. Phys. **43**, 1318 (1972).

5. M. J. Helix, K. V. Vaidyanathan, and B. G. Streetman, "Properties of Be-Implanted Planar GaAs p-n Junctions," IEEE J. Solid State Circuits **SC-13**, 426 (1978).

6. J. P. Donnelly, F. J. Leonberger, and C. O. Bozler, "Uniform-Carrier-Concentration p-Type Layers in GaAs by Beryllium Ion Implantation," Appl. Phys. Lett. **28**, 706 (1976).

7. W. V. McLevige, M. J. Helix, K. V. Vaidyanathan, and B. G. Streetman, "Electrical Profiling and Optical Activation Studies of Be-Implanted GaAs," J. Appl. Phys. **48**, 3342 (1977).

8. W. V. McLevige, K. V. Vaidyanathan, and B. G. Streetman, "Diffusion Studies of Be-Implanted GaAs by SIMS and Electrical Profiling," Solid State Commun. **25**, 1003 (1978).

9. M. K. Barnoski, R. G. Hunsperger, and A. Lee, "Ion Implanted GaAs Injection Laser," Appl. Phys. Lett. **24**, 627 (1974).

10. N. Bar-Chaim, M. Lanir, S. Margalit, I. Ury, D. Wilt, M. Yust, and A. Yariv, "Be-Implanted (GaAl)As Stripe Geometry Lasers," Appl. Phys. Lett. **36**, 233 (1980).

11. D. Wilt, N. Bar-Chaim, S. Margalit, I. Ury, M. Yust, and A. Yariv, "Low Threshold Be Implanted (GaAl)As Laser on Semi-Insulating Substrate," IEEE J. Quant. Electron. **QE-16,** 390 (1980).

12. H. C. Casey, Jr., and M. B. Panish, **Heterostructure Lasers: Part A, Fundamental Principles; Part B, Materials and Operating Characteristics,** Academic Press, New York (1978).

Chapter IV

A Steady State Lateral Model of the Double Heterostructure Laser

IV.1 Introduction

It has become clear in recent years that the semiconductor laser has a multitude of practical applications. These include the field of optical communications, but also many others that can make use of the small size, high efficiency, ruggedness, and simplicity of this component. With so many applications and differing requirements for the devices needed, it can be seen that laser diode modelling is potentially a tool of great value. Both the device designer, who tries to optimize a device computationally before entering the laboratory, and the diagnostician, who tries to understand a device he has fabricated, are potential users for laser diode models.

As a comparison, the bipolar transistor, the MESFET, the MOSFET, and a large number of other electronic devices all have complex finite element models available to the interested designer so that he can both optimize and analyze these devices. With these models, an accurate estimation of the effects of geometry, doping, contacts, and many other aspects of devices can be made with extremely large savings in time and effort.

The laser diode has seen, perhaps, more variations in device geometry than any other electronic component. This is because the laser diode has many aspects the designer can interact with. As an electronic component, a great deal of effort has been made to confine the current flow through the device. This results in low threshold current and high quantum efficiency. On the other hand, as an optical component, a great deal of effort has been made to build dielectric waveguiding into the device to define the lateral optical modes. The advantage of this is that the modal characteristics of the laser are well defined, and single lateral mode operation and linear light versus current characteristics

are easier to achieve. In addition, to get a large power output from the laser diode, it is necessary to keep the lateral optical mode spread out to avoid damaging the mirror facets. This calls for the use of weak lateral guiding mechanisms. A final aspect involves the fabrication limitations of the semiconductor material used.

In spite of the need, the status of laser diode modelling is quite primitive. A large number of authors have constructed highly simplified and idealized models of the double heterostructure laser to illustrate qualitatively the effects of various material and structural parameters on device behavior [1]. These models can be quite useful in correlating observed laser threshold currents with experimental results, for instance, but are of little use in understanding the device behavior above lasing threshold. This, however, is perhaps the most important regime of laser diode performance. In addition, these models are not predictive; in practical application, they explain experimental results.

There are at present two general models of the laser diode above lasing threshold [2,3]. However, both of these models make assumptions concerning the electrical characteristics of the diode that are incorrect. Specifically, in each model the diode p-n junction is assumed to behave according to the law

$$j = j_0 \, e^{\frac{q\varphi}{nkT}} \tag{4.1}$$

where j represents the injected electron and hole current densities (which are assumed to be equal), j_0 and n are material parameters, φ is the junction voltage, q is the electronic charge, k is Boltzmann's constant, and T is the absolute temperature. This is not a fundamental relationship. It can be derived for a one dimensional p-n junction from the master equations for semiconductors, and is usually described as the Shockley equation after its discoverer. The use of this relationship to describe the p-n junction in the laser diode, even as an approxi-

mation, neglects two very important effects: first, the effect on the electrical characteristics of lateral carrier drift and diffusion, and second, the saturation of junction voltage (and carrier populations) associated with lasing threshold. This effect, first described and measured by Paoli[4], is associated with the saturation of optical gain at lasing threshold. This causes the carrier populations to clamp, and the separation in carrier quasifermi levels to clamp as well. This causes a clamping of the junction voltage in the laser. A more reasonable condition to apply to the diode junction in the double heterostructure laser is to assume the continuity of the carrier quasifermi levels across the heterojunction interface. This assumption leads naturally to the saturation of the diode voltage as lasing threshold, and is consistent with the physics of the semiconductor. However, the use of this model of the diode junction requires the use of a different model and solution method from that of either of the models already cited.

Another model specifically designed to treat the behavior of a narrow planar stripe laser introduces this type of assumption[5]. However, this model is constructed such a way that it does not lend itself to generalization.

In this chapter, a steady state model of the double heterostructure laser is presented which treats the diode junction in the correct manner as described above[6]. Fundamental relationships that describe the device electrical and optical characteristics are derived and simultaneously solved in a self consistent manner to yield both the electrical and optical behavior of the device. The model is designed for use both above and below lasing threshold. To give as much freedom as possible in the treatment of device geometry, the finite element method is adopted as a solution technique. A number of interesting geometries have been examined and specific results for one such geometry are presented as an example.

IV.2 Simplifying Assumptions used in the Model

In principle, the semiconductor laser is a well understood device. It obeys both the master equations for semiconductors and Maxwell's equations, and if the material parameters for the device are known, its behavior can be calculated.

It is very important, however, to distinguish between understanding in principle and understanding in practice. If the relationships which describe the device cannot be solved in a reasonable amount of calculation time, then in a sense the device cannot be said to be understood. This statement describes the present state of modelling of the semiconductor laser. To model the semiconductor laser fully as both a semiconductor device and optical device would require more calculating ability than is considered reasonable at present.

There are a number of physical approximations that can be made in the equations that describe the semiconductor laser that still allow one to treat a large class of semiconductor laser diodes with good calculating accuracy and retain the desirable aspect of reasonable computational complexity. These approximations are explained in this section.

Again, it is important to distinguish between approximations and ad-hoc assumptions. This is in contrast to many popular laser diode models which begin with such assumptions, leaving unclear the question of their validity or accuracy for the structure analyzed. The advantage of approaching the problem from this standpoint is that the limits of the validity of the model are clearly outlined, and if at some point these limits are crossed, the model can be changed as necessary to remain valid.

The first approximation in this model is to average over longitudinal effects in the laser. Since most semiconductor lasers are fabricated in a stripe geometry with planar mirrors, they depend upon the lateral waveguiding in the device to

define the optical modes. From the longitudinal dimension we get the round trip phase condition which defines the Fabry-Perot longitudinal modes, and the round trip gain condition for stimulated emission, that gain balances loss. For typical cavity lengths of the laser, say 250 μm, the Fabry-Perot modes are quite closely spaced,

$$\Delta\lambda \cong \frac{\lambda^2}{2nL} \cong 5\ \text{Å} \tag{4.2}$$

where λ is the center wavelength, n is the refractive index of the material, and L is the longitudinal length of the device. This distribution may be considered as a continuum compared with the gain bandwidth of the semiconductor material which is on the order of several hundred Å. Thus for this model, the question of longitudinal mode structure is ignored. All longitudinal modes are considered to have the same lateral waveguide mode profile and the laser is assumed to oscillate at the peak of the gain distribution.

Due to the finite reflectivity of the laser mirrors, there is a longitudinal variation in the stimulated power distribution and thus the stimulated recombination rate. These effects are not negligible but represent an uninteresting variation. Therefore, they are averaged over, and only a fictitious average lateral cross section of the device is treated. This immediately turns the three dimensional problem of modelling the laser into a two dimensional problem of modelling the "average" cross section. The only averaging that need actually be done is to determine the relationship between the average power flow in the laser cavity and the emitted power from the laser mirrors. This is done as follows. Assume a mirror reflectivity R for the mirrors and a device length L. The power distribution in the cavity is then

$$P_{cavity} = P_0 \cosh\left(\frac{z}{L} \ln\left(\frac{1}{R} \right) \right) \tag{4.3}$$

where z is the variable representing the longitudinal dimension, and P_0 is an unimportant scaling factor. The average power in the cavity is then

$$P_{avg} = \frac{P_0 (1 - R)}{\sqrt{R} \ln(\frac{1}{R})} \tag{4.4}$$

and the power emitted from the mirror facets is

$$P_{emit} = \frac{P_0 (1 - R)}{\sqrt{R}} \tag{4.5}$$

so that

$$P_{emit} = P_{avg} \ln(\frac{1}{R}) \tag{4.6}$$

With the averaging over the longitudinal direction, the gain condition becomes

$$g_{mode} = \alpha_{mode} + \frac{1}{L} \ln(\frac{1}{R_{mode}}) \tag{4.7}$$

where g_{mode} is the gain experienced by the mode, α_{mode} is the loss for the mode (for example, due to scattering), and R_{mode} is the mirror facet reflectivity for the mode, all evaluated for the average cross section of the laser.

The second approximation is to assume that the active layer of the laser is thin compared to the diffusion lengths of the carriers. Typically this condition is met quite easily, for good practical reasons. To control the optical modal profile in this direction, active layer thicknesses are usually required to be less than 0.5 μm. This is approximately a factor of ten less than a typical diffusion length. With this assumption, the carrier densities in the active region can be assumed to be constant across the active layer thickness. Accordingly, quantities which vary across the active layer thickness, such as the stimulated recombination rate, are averaged in this dimension. This reduces the modelling of the active layer (but not the laser) to a one dimensional problem.

A third approximation is to assume that the cladding layers to the active region which provide the optical and carrier confinement necessary for the double heterostructure laser have bandgap energies large enough so that only the majority carrier conduction current flow in these layers need be considered. A double heterostructure laser that did not meet this requirement would be very poor indeed. Note that this does not prohibit the inclusion of a minority carrier leakage term in the treatment of the active region, it merely says that such leakage is a minor perturbation to the ohmic conduction of majority carriers in the cladding. This reduces the two dimensional lateral cross section modelling to the solution of a linear ohmic conduction problem. Thus in the cladding layers we must solve Laplace's equation

$$\nabla \cdot (\sigma \nabla \varphi) = 0 \tag{4.8}$$

where σ is the conductivity of the material, and φ is the electrostatic potential.

It should be noted that the word "cladding" is taken to mean all regions that surround the active layer and conduct the majority current. This could include, for instance, contact layers and the substrate of the device. The "large bandgap" requirement applies only to the regions of the cladding which come into contact with the active layer.

A fourth assumption used in this model is much harder to quantify without presenting the mathematics of waveguiding in the semiconductor laser. This will be treated in detail later in this chapter. Briefly, however, the method used to find the optical modes of the semiconductor laser, (effective index formalism) involves the solution of the waveguide eigenmode equation by a variational technique. This variational technique solves a reduced modal eigenequation in the direction normal to the active layer, and uses this solution to derive simple modal eigenequation for the direction parallel to the active layer. It is assumed that the tightly confined solution normal to the active layer is only slightly

perturbed by the lateral variation in the optical mode. Qualitatively, this assumes that the lateral variations in refractive index are much less than the normal variations in refractive index.

To treat now the problem of modelling the semiconductor laser, we break it up into two coupled subproblems. The first problem is that of the pumping process in the device, an electrical process involving the injection of electrons and holes (at extremely high densities) into the active layer. This we label the electrical problem. The second problem involves finding the optical modes of the device. This we label the optical problem. These two subproblems are coupled in two ways. The optical modes of the device are in part determined by the injected carriers through their modification of the complex dielectric constant. This includes the effect of optical gain. In addition, the optical modes of the device stimulate carrier recombination, which modifies the carrier density. Both of these subproblems must be treated consistently with the coupling between them.

IV.3 The Electrical Model

The typical geometry of the device we wish to model is shown in Figure 4.1. It consists of two ohmic conduction regions, one p type semiconductor, the other n type semiconductor, and a thin active region which is partially sandwiched between them and partially surrounded by isotype cladding layers (in this case, n type). The only cases that we exclude at this point are those where significant injection occurs across a homojunction in the active layer or from a remote junction in the device. Using the assumptions in the previous section, the electrical modelling problem breaks up into four coupled subproblems: two ohmic conduction problems in the cladding layers, and two continuity relationships in the active layer.

In the cladding layers, we must solve Laplace's equation

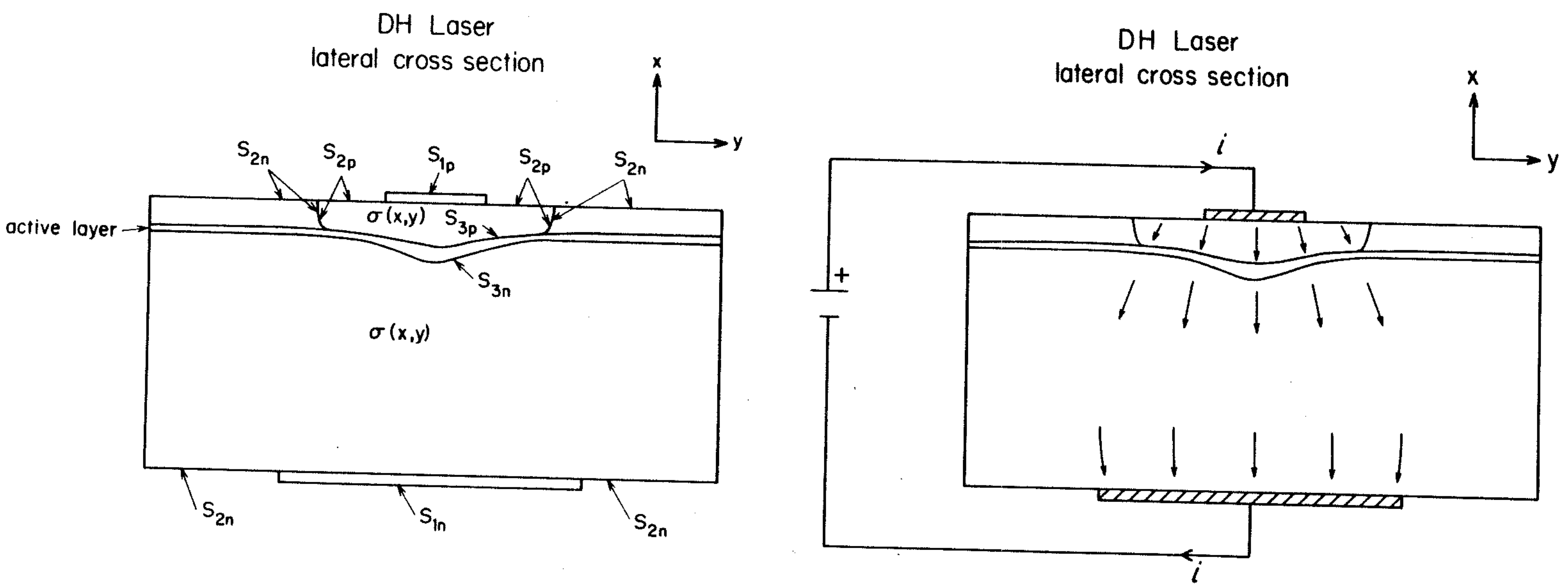

Figure 4.1 **Lateral cross section of the typical double heterostructure laser. The left portion of this figure shows the regions and boundary surfaces defined in the calculation, and the right portion shows the current flow through the device.**

$$\nabla \cdot (\sigma(x,y) \nabla \varphi_p) = 0 \quad (4.9)$$

$$\nabla \cdot (\sigma(x,y) \nabla \varphi_n) = 0 \quad (4.10)$$

where σ is the conductivity of the material, and φ_p and φ_n are the electrostatic potential in the p and n regions, respectively. These equations are subject to the following boundary conditions

$$\varphi_p = \varphi_{p0} \quad \text{on} \quad S_{1p} \quad (4.11)$$

$$\varphi_n = \varphi_{n0} \quad \text{on} \quad S_{1n} \quad (4.12)$$

$$\sigma \vec{n} \cdot \nabla \varphi_p = 0 \quad \text{on} \quad S_{2p} \quad (4.13)$$

$$\sigma \vec{n} \cdot \nabla \varphi_n = 0 \quad \text{on} \quad S_{2n} \quad (4.14)$$

$$\varphi_p = \varphi_p(y) \quad \text{on} \quad S_{3p} \quad (4.15)$$

$$\varphi_n = \varphi_n(y) \quad \text{on} \quad S_{3n} \quad (4.16)$$

S_{1p} and S_{1n} represent equipotential ohmic contacts to the device, S_{2p} and S_{2n} represent surfaces where no normal current is allowed to flow, and S_{3p} and S_{3n} represent the p-n heterojunction surfaces, where the potential is assumed as a function of the lateral coordinate to the interface. The outward pointing normal to the surfaces is represented by $\vec{n}$.

The solution to this problem yields the injected current density into the active layer from each cladding layer

$$j_{p,inj} = -\sigma \vec{n} \cdot \nabla \varphi_p \quad \text{on} \quad S_{3p} \quad (4.17)$$

$$j_{n,inj} = -\sigma \vec{n} \cdot \nabla \varphi_n \quad \text{on} \quad S_{3n} \quad (4.18)$$

as well as the potential distribution inside each of the cladding layers, which for self consistency must be related to the potential distribution along the active layer.

This relationship is provided in this model by the boundary condition on the heterojunction interfaces and the semiconductor continuity relationships. This is in contrast to previous models where the Shockley relationship (4.1) is used for this purpose. In comparison, the resulting relationship used here between injected current and potential difference across the p-n junction is both implicit and nonlocal, making the solution of the relationships comparatively much more difficult even though physically correct.

Referring to Figure 4.2, we have drawn a representative band diagram of the p-n heterojunction interface under forward bias. The detailed spike structure at the interfaces is assumed to be washed out by interfacial mixing as occurs in liquid phase epitaxial material. In this diagram, the carrier quasifermi levels appear as straight lines due to the assumption that the active layer is thin compared to the diffusion length. The actual variation in the quasifermi level in the active region can be shown to be on the order of $\Delta \psi = k T \left(\frac{t_{act}}{L_d} \right)^2$, where t_{act} is the active layer thickness, L_d is the diffusion length, and the high injection assumption has been used, which is negligible in this calculation. Outside the active region, the minority carrier quasifermi levels decay to the majority carrier fermi level in a distance approximately equal to the diffusion length, which is much larger than the scale in this figure. In the case where the active layer is surrounded by isotype cladding, again the continuity of quasifermi levels is assumed.

With this assumption and Poisson's equation for the electrostatic potential in the active layer,

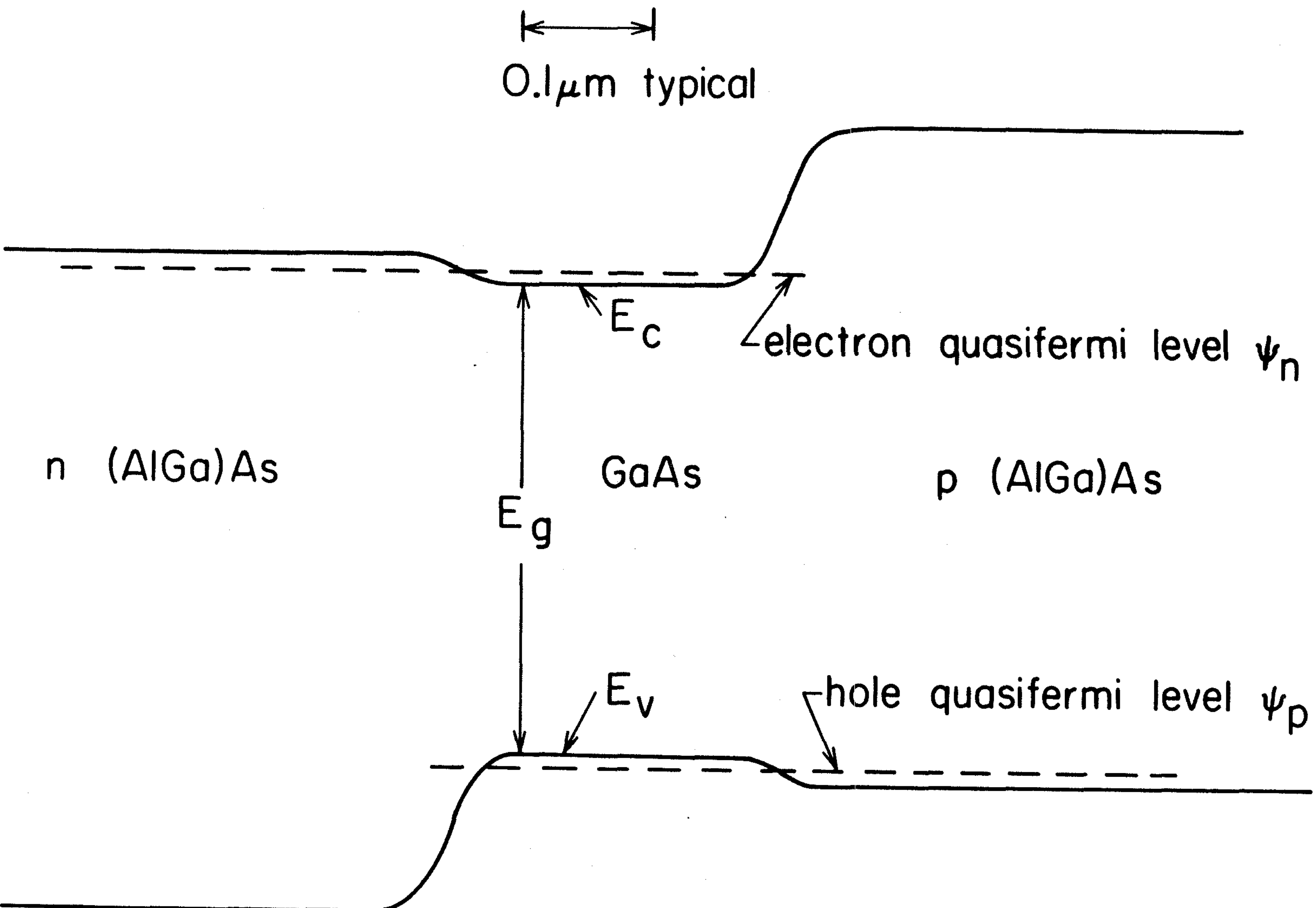

Figure 4.2 Representative band structure diagram for the diode junction in a double heterostructure laser.

$$\nabla^2 \varphi = \frac{\rho}{\varepsilon \varepsilon_0} \tag{4.19}$$

where φ is the electrostatic potential, ρ is the charge density, ε is the relative permittivity, and ε_0 is the permittivity of free space, we can relate the electron and hole densities in the active layer to the potential distribution along the p-n heterojunction. Noting that the typical Debye length for these devices is on the order of 100Å, we will assume quasineutrality and write

$$p + N_d^+ = n + N_a^- \tag{4.20}$$

$$p = \frac{2}{\sqrt{\pi}} N_v F_{1/2}\left(\frac{E_v - \psi_p}{kT} \right) \tag{4.21}$$

$$n = \frac{2}{\sqrt{\pi}} N_c F_{1/2}\left(\frac{\psi_n - E_c}{kT} \right) \tag{4.22}$$

$$E_c - E_v = E_g \tag{4.23}$$

$$\psi_n - \psi_p = e\,(\varphi_p - \varphi_n) \tag{4.24}$$

where n and p are the electron and hole densities, N_d^+ and N_a^- are the ionized donor and acceptor densities, N_c and N_v are the effective densities of states in the conduction and valence bands, $F_{1/2}$ is the fermi function, ψ_n and ψ_p are electron and hole quasifermi levels, E_c and E_v are conduction and valence band edges, E_g is the bandgap of the active layer, and φ_n and φ_p are the electrostatic potential on either side of the p-n heterojunction.

These equations completely define the electron and hole densities as a function of the potential difference across the p-n heterojunction, $\varphi_p - \varphi_n$.

To relate the injected current density to the potential distribution along the active layer, we must consider the continuity relationships

$$\frac{dp}{dt} = G_p - U_p - \frac{1}{e} \nabla \cdot \vec{J}_p = 0 \qquad (4.25)$$

$$\frac{dn}{dt} = G_n - U_n + \frac{1}{e} \nabla \cdot \vec{J}_n = 0 \qquad (4.26)$$

G_n and G_p are electron and hole generation rates, U_n and U_p are electron and hole recombination rates, and $\vec{J}_n$ ($\vec{J}_p$) is the electron (hole) drift plus diffusion current.

Injected current can most easily be included in these equations as a generation term. Thermal generation can be neglected for the laser diode under high forward bias.

$$G_p = \frac{j_{p,inj}}{e\, t_{act}} \qquad (4.27)$$

$$G_n = -\frac{j_{n,inj}}{e\, t_{act}} \qquad (4.28)$$

where $j_{p,inj}$ and $j_{n,inj}$ are the injected current densities, e is the electronic charge, and t_{act} is the active layer thickness.

The recombination terms consist of both nonradiative (trap, surface recombination) and radiative (spontaneous and stimulated) terms. The forms used for these are

$$U_{p,trap} = U_{n,trap} = \frac{p\, n}{p\, \tau_n + n\, \tau_p} \qquad (4.29)$$

$$U_{p,surface} = U_{n,surface} = \frac{S\, \delta(y - y_s)\, p\, n}{p + n} \qquad (4.30)$$

$$U_{p,spont} = U_{n,spont} = B\, p\, n \qquad (4.31)$$

$$U_{p,stim} = U_{n,stim} = \frac{P\, g}{\hbar\omega} \qquad (4.32)$$

where τ_n and τ_p are effective nonradiative minority carrier lifetimes, and may include the effects of leakage over the confining heterojunction barriers. S is a surface recombination velocity, y_s being the location of the surface interface. B is a material constant, P is the optical power density, g is the local optical gain of the medium, and $\hbar\omega$ is the photon energy. In this model, the gain term is assumed to be of the form

$$g = g_0 + g_{1p}\, p + g_{1n}\, n + g_{2pn}\, p\, n \tag{4.33}$$

These relationships are simplified forms of more general relationships [7], making use of the fact that the laser diode operates in the high forward bias regime. Of course, to be consistent with the assumption that the active layer is thin and that the electron and hole densities are uniform across it, the relationship for the stimulated emission recombination rate, (4.32), must be averaged over the direction normal to the active layer.

The drift plus diffusion term that appears in the continuity equations requires more elaboration. Using the degenerate Einstein relations, we have

$$\vec{J}_p = p\, \mu_p \nabla\ \psi_p \tag{4.34}$$

$$\vec{J}_n = n\, \mu_n \nabla\ \psi_n \tag{4.35}$$

where μ_n and μ_p are the electron and hole mobilities. An additional complication that we wish to incorporate into this model is the case where the active layer thickness is allowed to vary. Since we have already separated off the injected current densities from this drift plus diffusion term, to be consistent we must require the latter to be conservative, meaning that no drift plus diffusion current may flow through the heterojunction interfaces, or equivalently to force the drift and diffusion current to flow parallel to the heterojunction interfaces. We will assume that the magnitude of this current is constant across the active

layer, consistent with our assumption that the injected carrier densities are constant across the active layer, but the changing of the active layer thickness introduces an additional term when we take the divergence in the continuity equations (4.25) and (4.26). With the condition that the active layer thickness varies slowly with respect to y and using a local system of cylindrical coordinates, we find for these terms

$$-\frac{1}{e}\nabla\cdot\vec{J}_p = -\frac{1}{e}\left(\frac{1}{t_{act}}\frac{dt_{act}}{dy}+\frac{d}{dy}\right)\left(p\,\mu_p\frac{d\psi_p}{dy}\right) \tag{4.36}$$

$$\frac{1}{e}\nabla\cdot\vec{J}_n = \frac{1}{e}\left(\frac{1}{t_{act}}\frac{dt_{act}}{dy}+\frac{d}{dy}\right)\left(n\,\mu_n\frac{d\psi_n}{dy}\right) \tag{4.37}$$

These terms are seen to be conservative, as is desired. The derivatives of the quasifermi levels that appear in these terms must of course be treated self consistently with the solution to the ohmic conduction problem. The identification is provided by the assumption of continuity of quasifermi levels across the interfaces, as before. Neglecting the contribution of carriers that leak over the confining heterobarriers, this allows us to identify ψ_n with the fermi level in the n cladding, and ψ_p with the fermi level in the p cladding. In the case where the active layer is surrounded by isotype cladding, this identification is performed for the majority carrier, and for the minority carrier we instead demand that injected minority carrier current density be zero.

With these relationships, the electrical behavior of the device is completely defined. It is interesting to note that at no point in the analysis was the assumption of equal injected current densities into the active layer or the assumption of ambipolar diffusion required. These are not necessarily bad assumptions, but cannot be derived from the relationships above. If one could derive the equality of injected current densities, one could also derive ambipolar diffusion and drift coefficients. This stems from the assumption of equal generation and recombi-

nation rates in the derivation of these quantities.

The difficulty lies in the fact that the electron and hole populations are essentially in equilibrium with their isotype cladding layers. An interesting consequence of this is that mirror symmetric devices where p and n type layers are interchanged but resistivities are held constant do not behave identically.

From the standpoint of solving the electrical behavior of the model, the problem is to find an electrostatic potential distribution and quasifermi levels in the active layer which are consistent with all of the relationships set down above.

IV.4 The Optical Model

The optical model presented here is quite similar to that described elsewhere[2,3]. In brief, a two dimensional scalar modal equation for the laser waveguide is derived from the vector wave equation with the assumption of a TE mode and uniformity in the longitudinal (z) direction. This scalar modal equation is approximately solved using a technique known as effective permittivity formalism, presented here in a new variational form which makes clear the approximations involved. If the exact permittivity profile is used, the modal gain is available in the imaginary part of the mode propagation constant. Otherwise, a first order perturbation calculation is used ("modal overlap") to find the modal gain.

In this respect, semiconductor lasers fall into two equivalence classes, those where injected carriers contribute significantly to the waveguiding in the device, and those where injected carriers serve as only a minor perturbation upon the waveguide modes. Roughly speaking, these two classes correspond to devices with geometric structures that define the waveguide modes (e.g. buried heterostructure lasers [8] and channelled substrate lasers[9,10]) and devices that have no built in geometric waveguide structure (e.g. beryllium implanted lasers [11] and oxide stripe lasers [12]). This is a rough division because an important class

of laser diodes utilizes geometric antiguiding as a means of mode control [13]. The optical model presented here, while for convenience limited to TE modes and effective index formalism, is capable of treating both classes of semiconductor lasers.

The vector wave equation, which we take as our starting point, is

$$(\nabla^2 + k^2 \varepsilon) \vec{E} = 0 \tag{4.38}$$

where k is the wavenumber for the frequency of interest ($k = \frac{\omega}{c}$) and ε is the complex relative permittivity for the medium. This wave equation is derived with the assumption that the scale of variation for ε is much larger than a wavelength so that a term involving the gradient of ε can be dropped. $\vec{E}$ is of course the electric field for the mode, assumed to vary as $e^{i\omega t}$.

With the assumption that we are interested in a waveguide mode which varies as $e^{i\beta z}$ where the z axis is chosen to be parallel to the guide, we get

$$(\nabla_t^2 + k^2 \varepsilon - \beta^2) \vec{E} = 0 \tag{4.39}$$

where ∇_t^2 is a transverse Laplacian operator ($\nabla_t^2 = \frac{\partial^2}{\partial x^2} + \frac{\partial^2}{\partial y^2}$).

Semiconductor lasers are most often fabricated with a waveguide that is tightly constricted in one direction and weakly constricted in the other. In the tightly constricted direction, normal to the active layer, the waveguiding is dominated by the discontinuity in permittivity between the active layer and the larger bandgap cladding layers. In order to achieve modal control in this direction, the active layer is made quite thin (on the order of 0.2 μm) so that the lowest modes are much more tightly confined than the higher modes. In the other direction, parallel to the active layer, the waveguiding is usually weak. Thus, the waveguide modes split in a manner similar to the uniform planar waveguide, into pseudo-TE and pseudo-TM modes. The pseudo-TE modes are

known to dominate the behavior of the semiconductor laser. This is because they are more tightly confined to the gain region (the active layer) and also have higher reflectivities off of the cleaved mirrors.

For this reason, we will assume a TE mode for the laser and solve a scalar modal eigenequation

$$(\nabla_t^2 + k^2 \varepsilon - \beta^2) u = 0 \tag{4.40}$$

where u represents the TE electric field, E_y. We have taken the y coordinate, as earlier, to be parallel to the active layer. This eigenequation can be put into variational form as

$$\delta \left(\frac{\int_{-\infty}^{\infty} dx\, dy \left(- \left(\frac{\partial u}{\partial x} \right)^2 - \left(\frac{\partial u}{\partial y} \right)^2 + k^2 \varepsilon u^2 \right)}{\int_{-\infty}^{\infty} dx\, dy\, u^2} \right) = 0 \tag{4.41}$$

To apply effective permittivity formalism to this equation, a variational form will be assumed and this variational principle will be used to derive an Euler equation for the lateral modal field.

Keeping in mind the situation that the mode is tightly confined in one dimension (normal to the active layer) and weakly confined in the other, we might imagine that the profile of the mode in the direction normal to the active layer is quite similar to the profile for a uniform planar guide. Accordingly, we solve the one dimensional eigenequation in the direction normal to the active layer

$$\left(\frac{\partial^2}{\partial x^2} + k^2 \varepsilon(x,y) - \gamma_1^2(y) \right) X(x,y) = 0 \tag{4.42}$$

for an effective variation in the direction normal to the active layer (x). The lateral coordinate y is considered here to be a parameter, and we use the solution with the largest eigenvalue (the lowest mode). Consistent with the use of

complex permittivities, the normalization condition on this field is taken to be

$$\int_{-\infty}^{\infty} dx\, X^2 = 1 \tag{4.43}$$

We would now like to find the best possible approximation to the true modal field using this field X to represent the variation in the perpendicular (x) direction. To do this, we assume a variational form to substitute into the variational equation (4.41)

$$u(x,y) = X(x,y)\, Y(y) \tag{4.44}$$

where Y(y) is the function we will allow to vary. Since we are no longer interested in the variation in the x direction, we may integrate over x in the variational equation and get as a result

$$\delta \left(\frac{\int_{-\infty}^{\infty} dy \left(- \left(\frac{dY}{dy} \right)^2 + \left(\gamma_1^2 + \gamma_2^2 \right) Y^2 \right)}{\int_{-\infty}^{\infty} dy\, Y^2} \right) = 0 \tag{4.45}$$

where

$$\gamma_2^2 = \int_{-\infty}^{\infty} dx \left(- \left(\frac{\partial X}{\partial y} \right)^2 \right) \tag{4.46}$$

The normalization condition (4.43) and the field equation for X(x,y) (4.42) have been used in the simplification of the expression (4.45).

The Euler equation for this variational expression is then

$$\left(\frac{d^2}{dy^2} + k^2\, \varepsilon_{eff} - \beta^2 \right) Y = 0 \tag{4.47}$$

where the effective permittivity is

$$k^2 \varepsilon_{eff} = \gamma_1^2 + \gamma_2^2 \tag{4.48}$$

The second term in this expression, γ_2^2, is usually quite small and is neglected here. However, it is important to keep in mind when the structure to be analyzed has abrupt changes in geometry in the y direction. In this case, it is wiser to use a slightly different variational form than (4.44). This leaves us with the expression

$$k^2 \varepsilon_{eff} = \gamma_1^2 \tag{4.49}$$

for the effective permittivity. The field Y will be assumed to be normalized according to

$$\int_{-\infty}^{\infty} dy\, Y^2 = 1 \tag{4.50}$$

so that the normalization on the field u is then

$$\int_{-\infty}^{\infty} dx\, dy\, u^2 = 1 \tag{4.51}$$

The advantage of approaching the effective permittivity problem from the standpoint of the variational principle, aside from the term (4.46) which we have chosen to neglect, is that it assures in some sense that the best possible approximation to the true modal field has been obtained. If first order perturbation theory is applied to the modal profiles found, (assuming for the moment that the extra term has not been neglected) the lowest nonzero correction to the modal field involve overlaps of the field X with higher order modes in the x direction. This means that corrections associated with overlaps of X with itself are not present. This quantifies the approximation in effective index formalism, in contrast to the literature on this subject where the form for u (4.44) is substituted directly into the modal equation [2,3].

The modal gain is made available as the imaginary part of the propagation constant for the mode.

$$g_{mode} = 2 \text{ Im } \beta_{mode} \tag{4.52}$$

If the proper permittivity is used in the calculation, this result is exact. Otherwise, a first order perturbation calculation gives

$$d (\beta^2) = \int_{-\infty}^{\infty} dx\, dy\, u^2\, k^2\, d\varepsilon \tag{4.53}$$

this simplifies to

$$d\beta = \frac{k^2}{2\,\beta} \int_{-\infty}^{\infty} dx\, dy\, u^2\, d\varepsilon \tag{4.54}$$

To treat a laser, one must of course include the effects of the longitudinal cavity. As mentioned earlier, this amounts to the condition that modal gain is equal to modal losses,

$$g_{mode} = \alpha_{mode} + \frac{1}{L} \ln(\frac{1}{R_{mode}}) \tag{4.55}$$

where g_{mode} is the modal gain, α_{mode} is the modal loss, L is the device length, and R_{mode} is the mode mirror reflectivity. In this model, the loss term α_{mode} and the mirror reflectivity R_{mode} are assumed to be constants. It is important to note that there is a difference between gain and loss. This difference is that the gain term appears in the stimulated emission term in the electrical model. The loss term here represents nonretrievable losses in the optical mode due to such mechanisms as scattering. Assuming that all modes have the same mirror reflectivity is a good approximation since we have taken them all to have the same modal profile in the x direction where the large variation in permittivity is.

The optical power density in the device is

$$P = P_i \frac{|\,u\,|^2}{\int_{-\infty}^{\infty} dx\,dy\,|\,u\,|^2} \tag{4.56}$$

where P_i is the total power flowing in the cavity, the average over the length of the device of the forward and backward travelling waves. As before, this power is related to that emitted from the mirrors by

$$P_o = P_i \ln\left(\frac{1}{R} \right) \tag{4.57}$$

where P_o is the power emitted from both mirrors of the device.

If the device under consideration is judged to be a member of the geometrically guided class, the lateral mode profiles need be calculated only once and perturbation theory can be applied to determine modal gains for any value of the injected carrier populations. If the device is judged to be of the carrier guided class, the lateral mode profiles must be recalculated for every value of the carrier populations, in particular, while the solution to the electrical problem is being iteratively searched for. If the device is carrier guided, the dependence of both the real and imaginary parts of the permittivity on the carrier density must be included in the calculation. This model is capable of treating both types of device, including the more reasonable procedure for the carrier guided device of using a combination of exact and perturbation methods.

It is an unfortunate fact, however, that the dependence of real permittivity upon carrier concentration is not well known. This means that the carrier guided device represents not only a larger investment in computation time, but also throws doubt on the validity of the calculated results, as the mode profiles in this device can depend strongly upon the magnitude of the change in the real part of the permittivity caused by the injected carriers. It is interesting to note

that the geometrically guided devices are not only easier to analyze, they are better behaved in general than the carrier guided devices in terms of their characteristics such as modal behavior. For this reason, the example of the analysis program presented here is an analysis of a geometrically guided device.

IV.5 Solution Technique

As a first step, the functional dependence between junction voltage and injected carrier concentrations in the active layer is solved, equations (4.20) through (4.24). This is done using a nonlinear rootfinding technique. Since this is only dependent upon the material used for the active layer, it need be done only once for a given material and doping density.

The remaining relationships to be solved (the ohmic conduction problems, the continuity relationships in the active layer, the waveguide modal problem) all have spatial dependences which are influenced by the geometry of the laser diode. One of the major goals in the formulation of the laser diode model presented here was to include the effect of diode geometry on performance. With the proliferation of diode geometries, the advantage of using a general modelling technique was obvious. Thus, a very general technique was chosen to model these spatially dependent problems. This technique, known as the finite element method, has been applied to both semiconductor devices and optical waveguides, but never before to the problem of the laser diode.

The finite element method encompasses a large class of approximation methods for the solution of differential equations. In the most general sense, it consists of the use of a class of functions which appear somewhat like "patchwork quilts" to approximate the true solution to the differential equation. To define these patchwork functions, the solution domain is broken up into many smaller subdomains, called elements. Local functions, called interpolation functions, are defined in each element in terms of local parameters. In one dimen-

sion, an element could be a line segment, and the local parameters could be the function values at the endpoints. The interpolation functions could then be functions which interpolate linearly between the endpoint values. A patchwork function of this sort has the obvious advantage of continuity over the domain. A more complex set of parameters (values and slopes at the endpoints) and cubic interpolation functions (the first order Hermite polynomials) would yield a patchwork function with continuity of both the function and its derivative.

In two dimensions, the simplest element one can imagine would be a triangle, with parameters being the function values at the corners. The interpolation functions could again be linear and the function values inside the element would correspond to passing a plane through the three points defined by the corner values. This choice has the advantage of continuity for the resulting patchwork function.

Once we have a class of these patchwork approximation functions which are determined by a finite set of parameters (e.g. the function values at the nodes of the elements) we need only find an error criterion to choose the best approximating function in the class. This can be relatively easy in some cases, and quite hard in others. The easiest case is one where a variational form exists for the equation whose solution is sought. In this case, one need only substitute the patchwork function into the variational form, differentiate it with respect to its parameters, and set the result to zero. Of course, the patchwork functions in this case must have sufficient continuity as demanded by the variational principle. This requirement is usually less strict than the differential equation that the function must satisfy. The result gives exactly as many conditions on the parameters as are needed. In addition, this procedure leads to the best approximating function available in the class.

If, on the other hand, a variational principle does not exist or cannot be

found, one needs to derive enough error criteria in some other fashion to define the solution to the problem. Usually the approach taken to this problem is Galerkin's criterion. Suppose that the patchwork function can be defined as follows:

$$f_{a_1,\ldots,a_n} = \sum_{i=1}^{n} a_i f_i \tag{4.58}$$

where a_i are the parameters, and f_i are the local interpolation functions, defined to be zero outside the element they are associated with. We desire to find the solution of an equation which we will represent by

$$A f - g = 0 \tag{4.59}$$

where A is a general operator, not necessarily linear, and g is a driving function. If a function which is not a solution of this equation is substituted, in general the right hand side of this equation will not be zero. One possible choice of error criteria, then, is to choose n suitable weighting functions w_i , $i = 1,\ldots,n$ and define the errors

$$e_i = \int (A f_{a_1,\ldots,a_n} - g) w_i \tag{4.60}$$

The variational parameters are then chosen by demanding that these errors e_i , $i = 1,\ldots,n$ be zero.

The remaining problem is to choose these weighting functions w_i. Galerkin's method consists of using the variational functions f_i for this purpose. This choice has the benefit of yielding the same finite element equations as the variational principle if it exists and the operator A is linear. However, the continuity requirements in this approach to the problem are usually much more strict than the variational approach.

The finite element method is applied to this model of the laser diode in several ways. For the ohmic conduction problem the equations (4.9) and (4.10) may be converted to a variational form

$$\delta \left(\int\int dx\, dy \frac{\sigma}{2} (\nabla \varphi)^2 + \int d\vec{S} \cdot \vec{j} \varphi \right) = 0 \qquad (4.61)$$

Here the quantity $d\vec{S}$ is an oriented surface element on the boundary of the solution region, in the direction of the outward pointing normal, $\hat{n}$. The current flowing out of the region at any point is just $\hat{n} \cdot \vec{j}$.

For this problem, a system of triangular elements and linear interpolation functions as described earlier is used. The finite element equations take the form of a linear algebraic system. The result of this calculation can be stated in the form of a Green's function for each ohmic conduction region which relates the nodal values of the potential along the active layer to the normal current flow into the active layer,

$$\int dy\, j_{p,inj}\, f_i = \sum_j K^p_{i,j} (\varphi_{p0} - \varphi_{pj}) \qquad (4.62)$$

$$\int dy\, j_{n,inj}\, f_i = \sum_j K^n_{i,j} (\varphi_{n0} - \varphi_{nj}) \qquad (4.63)$$

where the potentials on the contacts are φ_{p0} and φ_{n0} as before, and φ_{pj} and φ_{nj} are the nodal potentials along the heterojunction interface.

For the optical mode profile, the variational form X(x,y) is obtained from the treatment of the slab waveguide in the direction normal to the active layer. The remaining modal equation for Y, which has a variational form appearing in equation (4.45), is formulated as a finite element problem with a one dimensional grid and first order Hermite interpolation functions. The finite element equations take the form of a generalized eigenvalue problem, which is solved by the use of an efficient iterative technique [14].

The remaining continuity relationships in the active layer are also solved using a finite element technique. Again, a one dimensional grid is used and the nodal variables are defined as the electron and hole quasifermi levels. Linear interpolation is used between nodes. These equations are highly nonlinear, and no variational principle could be found to define the finite element equations. Thus Galerkin's criterion was adopted for this problem, and the resulting finite element equations take the form of a system of nonlinear simultaneous equations. This system is solved through the use of a modified Newton's method technique. It should be noted that the mesh in this problem corresponds to the boundary mesh for the ohmic conduction problem. With the use of linear interpolation functions for the continuity relationships, as in the ohmic conduction problem, the results of the calculation in equations (4.62) and (4.63) may be substituted directly.

The solution of the model then reduces to finding the nodal values of the electron and hole quasifermi levels as functions of a global boundary condition, which may be formulated as either the device voltage $\varphi_{p0} - \varphi_{n0}$, or the total device current. With the inclusion of stimulated emission, additional variables (stimulated power in each mode) and additional relationships (modal gain condition, equation (4.55)) must be considered. In this calculation, up to four lateral modes are included for stimulated emission.

IV.6 Sample Case and Comparison with Experiment

Several device structures have been analyzed, including both cases where carriers are treated as a perturbation and where carriers define the lateral mode structure. Lasers of the first type analyzed include both embedded lasers [16] and channelled substrate lasers [9,10]. Only one laser structure of the second type has been analyzed, the beryllium implanted laser of Chapter III [11]. Specific results are presented here for the structure of Burnham et al. [10] which has been

analyzed in simplified form by Streifer et al.[16,17]. Unfortunately, that analysis neglects the effect mentioned in connection with equations (4.36) and (4.37) and as a result the solution of the diffusion equation in this analysis is incorrect, as it does not conserve carriers.

The structure of this device is shown in Figure 4.3. The material and structural parameters assumed for the device are listed in Tables 4.1 and 4.2 respectively. The n GaAs top layer in the structure is used only as a blocking layer which is shorted by the zinc diffused stripe so the electrical model omits the top n layer and considers the zinc diffusion as a 2 μm wide stripe contact. Refractive indices are given instead of permittivities, where $\varepsilon = n^2$. The substrate and contact layer can be omitted from the waveguiding problem, with the result that the effective permittivity is real. Gain and recombination parameters are chosen compatibly with both direct experimental measurements and measurements of broad area lasing threshold current density.

The solution of the equations for electron and hole densities as a function of voltage difference across the heterojunction is shown in Figure 4.4. Note that since the fermi functions appropriate to degenerate semiconductors are used, the curves begin to saturate at high injection levels.

This device has an obvious mirror symmetry, and this will be exploited to ease the calculation. However, it must be remembered that with this simplification, all currents and output powers should be doubled.

The finite element model used for the calculation of the Green's functions (4.62) and (4.63) is shown in Figure 4.5. The use of a large number of elements for the modelling of the substrate is not necessary, but does give the device a reasonable series resistance. In most situations, assuming the substrate - epilayer interface to be equipotential is a good approximation.

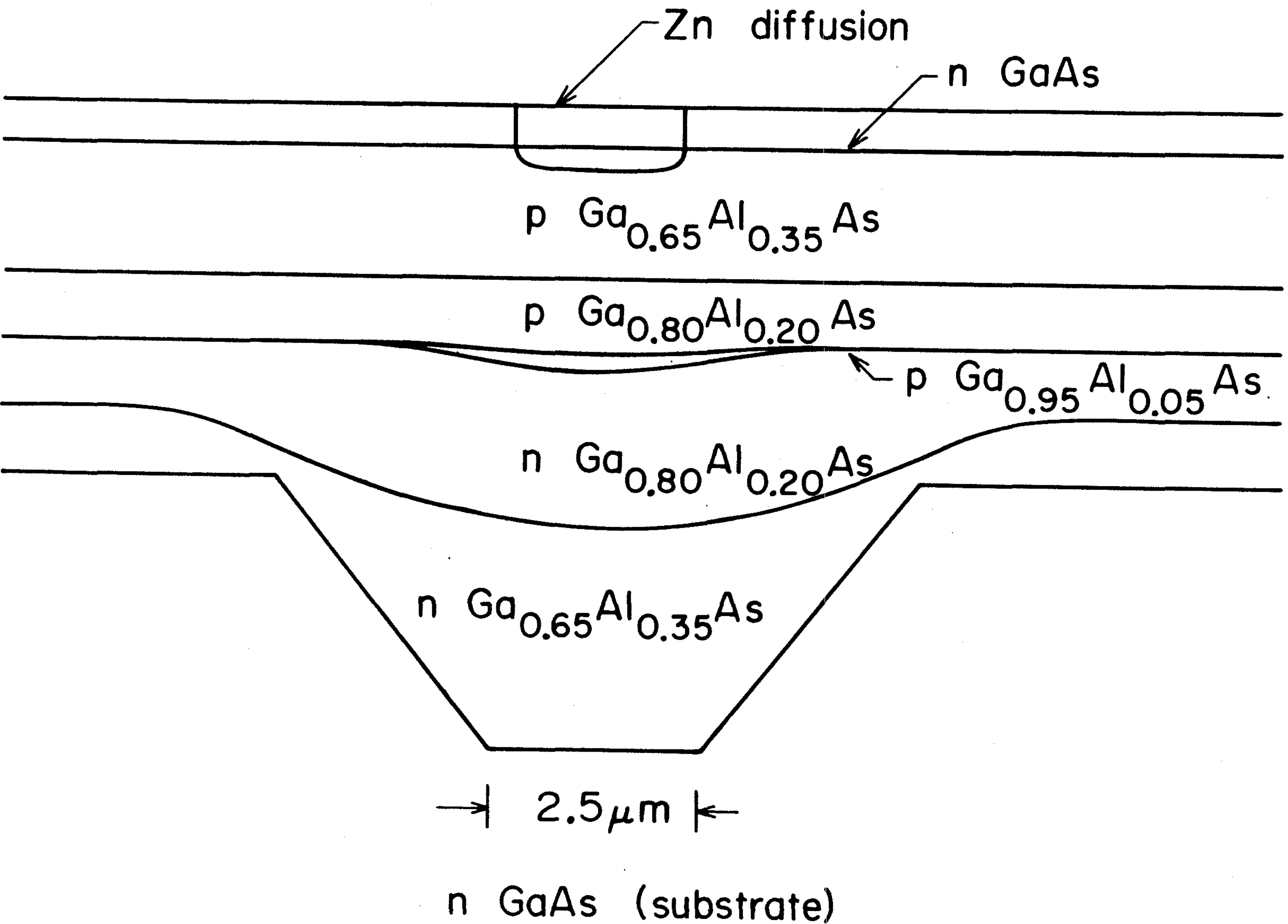

Figure 4.3 Lateral cross section of the example device treated. This type of device is characterized as a nonplanar large-optical-cavity laser.

Table 4.1 Material parameters used in the modelling program.

Parameter	Value
N_c	$4.7 \cdot 10^{17}$ cm^{-3}
N_v	$7 \cdot 10^{18}$ cm^{-3}
$N_a^- - N_d^+$	$3 \cdot 10^{17}$ cm^{-3}
τ_n , τ_p	$1 \cdot 10^{-7}$ s
B	$0.9 \cdot 10^{-10}$ $\frac{cm^3}{s}$
μ_n	4000 $\frac{cm^2}{Vs}$
μ_p	300 $\frac{cm^2}{Vs}$
g_0	-180 cm^{-1}
g_{1p} , g_{1n}	0
g_{2pn}	$7 \cdot 10^{-35}$ cm^5
α	12 cm^{-1}
E_g , $\hbar\omega$	1.43 eV
L	$2.5 \cdot 10^{-2}$ cm
R	0.32

Table 4.2 Structural parameters used in the modelling program.

Layer	Conductivity	Refractive Index
n GaAs substrate	1000 ohm^{-1} cm^{-1}	3.64−0.0528i
n $Ga_{0.65}$ $Al_{0.35}$ As	200	3.39
n $Ga_{0.80}$ $Al_{0.20}$ As	200	3.50
p $Ga_{0.95}$ $Al_{0.05}$ As	–	3.64 + $dn_{carriers}$
n $Ga_{0.80}$ $Al_{0.20}$ As	8	3.50
n $Ga_{0.65}$ $Al_{0.35}$ As	8	3.39
n GaAs isolation	–	3.64−0.0528i

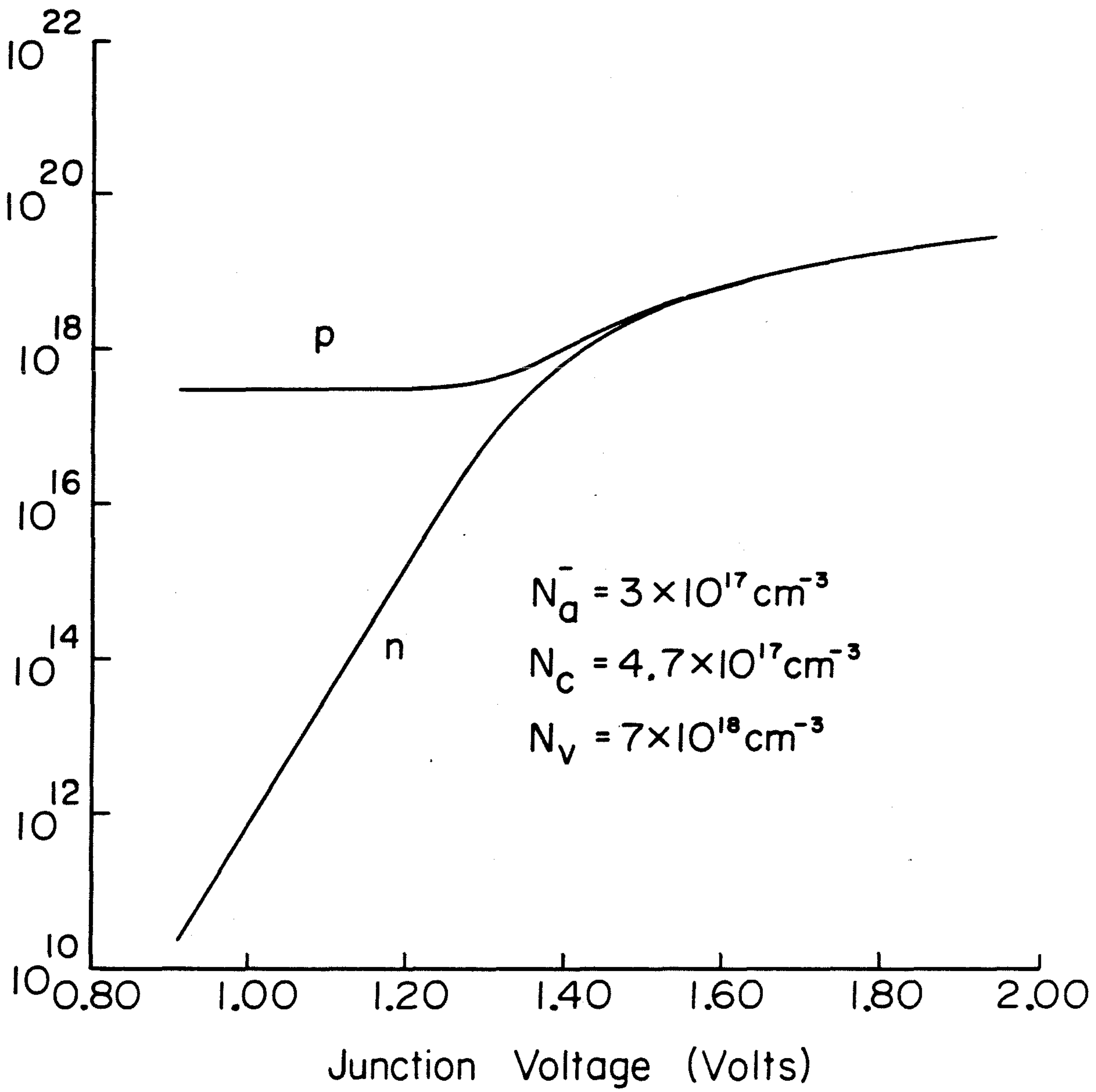

Figure 4.4 The electron and hole densities in the active layer as a function of the voltage across the heterojunction.

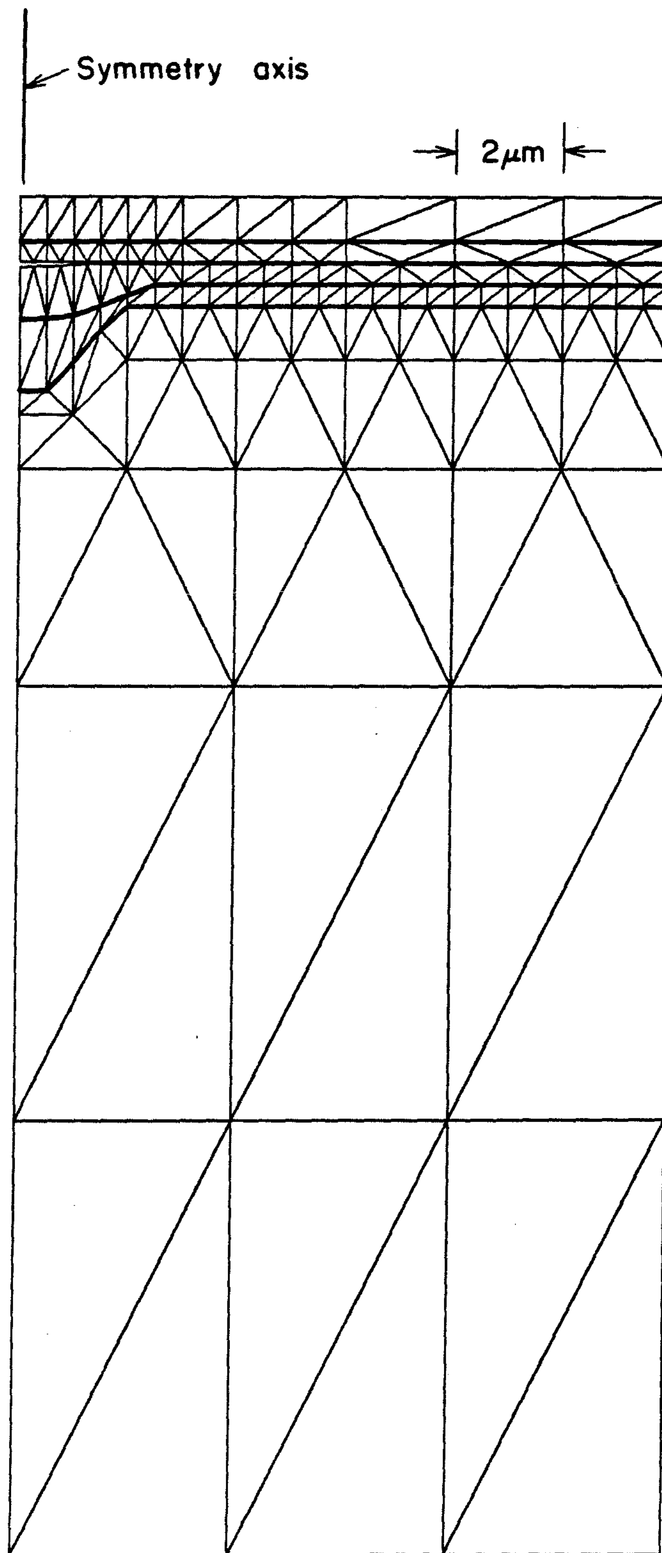

Figure 4.5 The finite element model constructed for the ohmic conduction problems. Use has been made of the device symmetry.

The geometric model of the device, Figure 4.3, is used for the calculation of the effective permittivity and the lowest four lateral optical modes (Y) are calculated as described earlier. The active layer thickness is assumed to vary as

$$t_{act} = 0.08 + 0.12\, e^{-0.0732\, y^2} \tag{4.64}$$

where t_{act} is the active layer thickness and y is the lateral distance measured from the center of the stripe, both measured in μm. The effective permittivity profile for the device is shown in Figure 4.6, and the lowest four lateral modes and their corresponding far field patterns are shown in Figure 4.7. Since the waveguiding properties are geometrically determined, equation (4.54) is used to determine modal gains for the device.

The solutions for the steady state device behavior with pump current as a parameter are shown in Figures 4.8 through 4.11. Figure 4.8 shows the current versus voltage characteristics of the diode, and clearly shows the saturation of junction voltage associated with lasing threshold, which can be seen to occur at approximately 31 mA of total device current. Above threshold, further increases in device voltage are due to the finite device resistance, here approximately 2.4 Ω. The carrier profiles for the device with pump current as a parameter are shown in Figure 4.9. The total device current varies in this figure at 4 mA per step from 4 to 100 mA. The saturation of the carrier populations at lasing threshold and the effects of spatial holeburning can be seen. This is a different effect from the "diffusion focussing" described by Streifer et al. [16,17]. The light versus current characteristics of the device are shown in Figure 4.10, where stimulated power output to each mode as well as modal gains are plotted as a function of pump current. The total power output as a function of pump current is shown in Figure 4.11. The effect of spatial holeburning in this device can be seen to eventually let higher order lateral modes of the structure emit

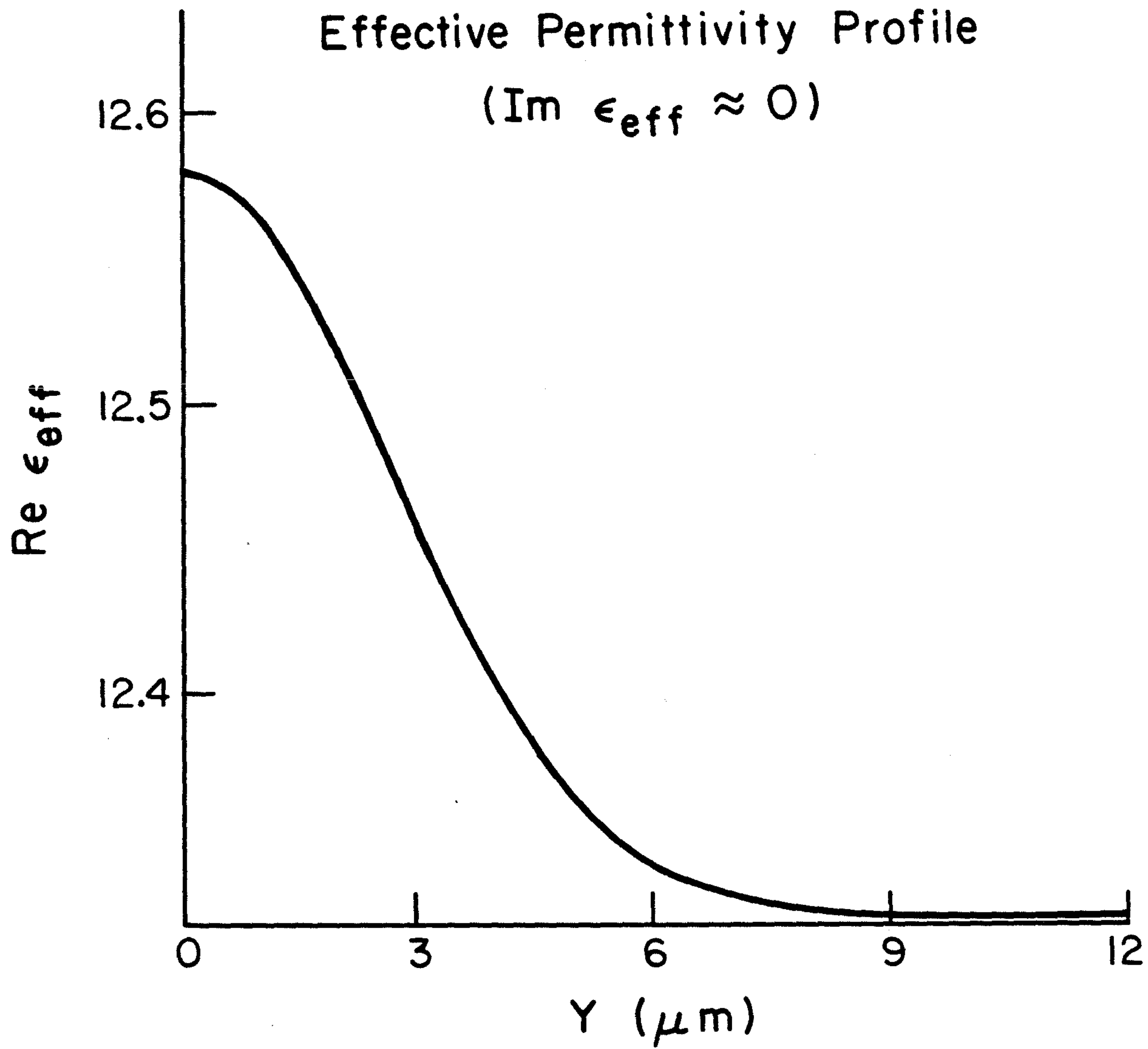

Figure 4.6 The effective permittivity profile for the device. Use has been made of the device symmetry.

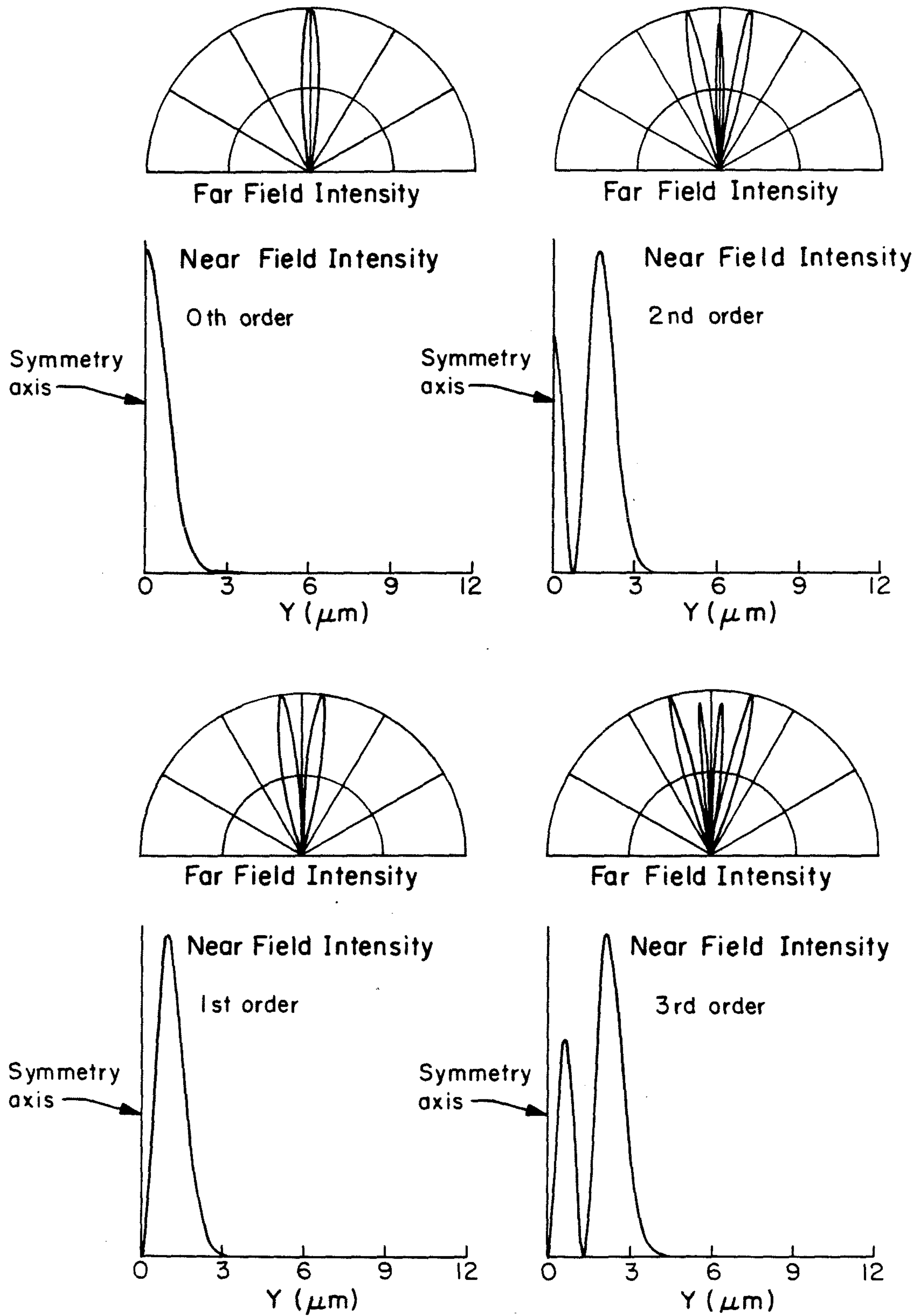

Figure 4.7 The four lowest lateral modes (Y) of the device and their corresponding far field patterns. Use has been made of the device symmetry.

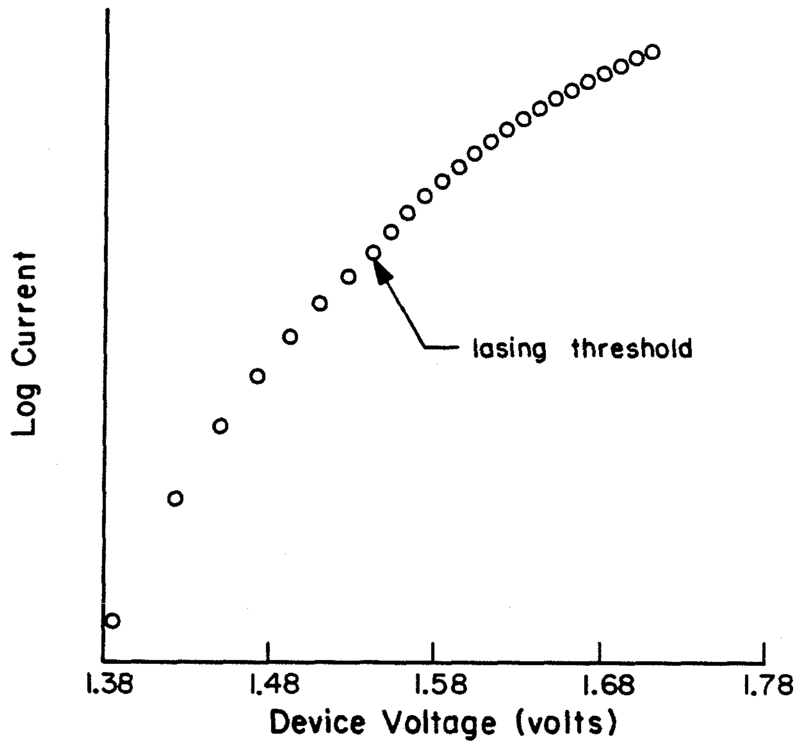

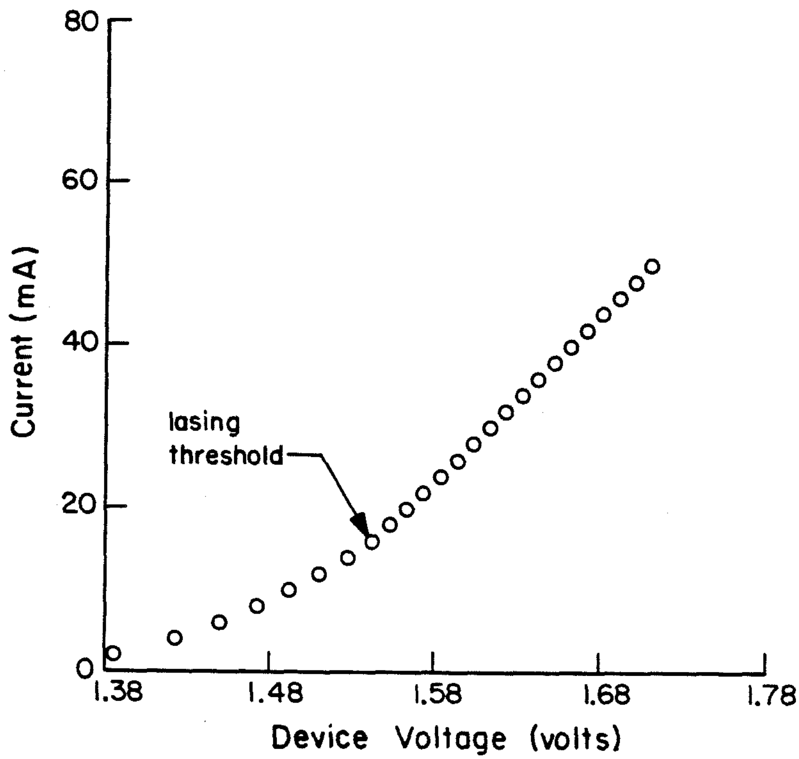

Figure 4.8 The current-voltage characteristics of the device. To obtain total device current, the scale should be doubled.

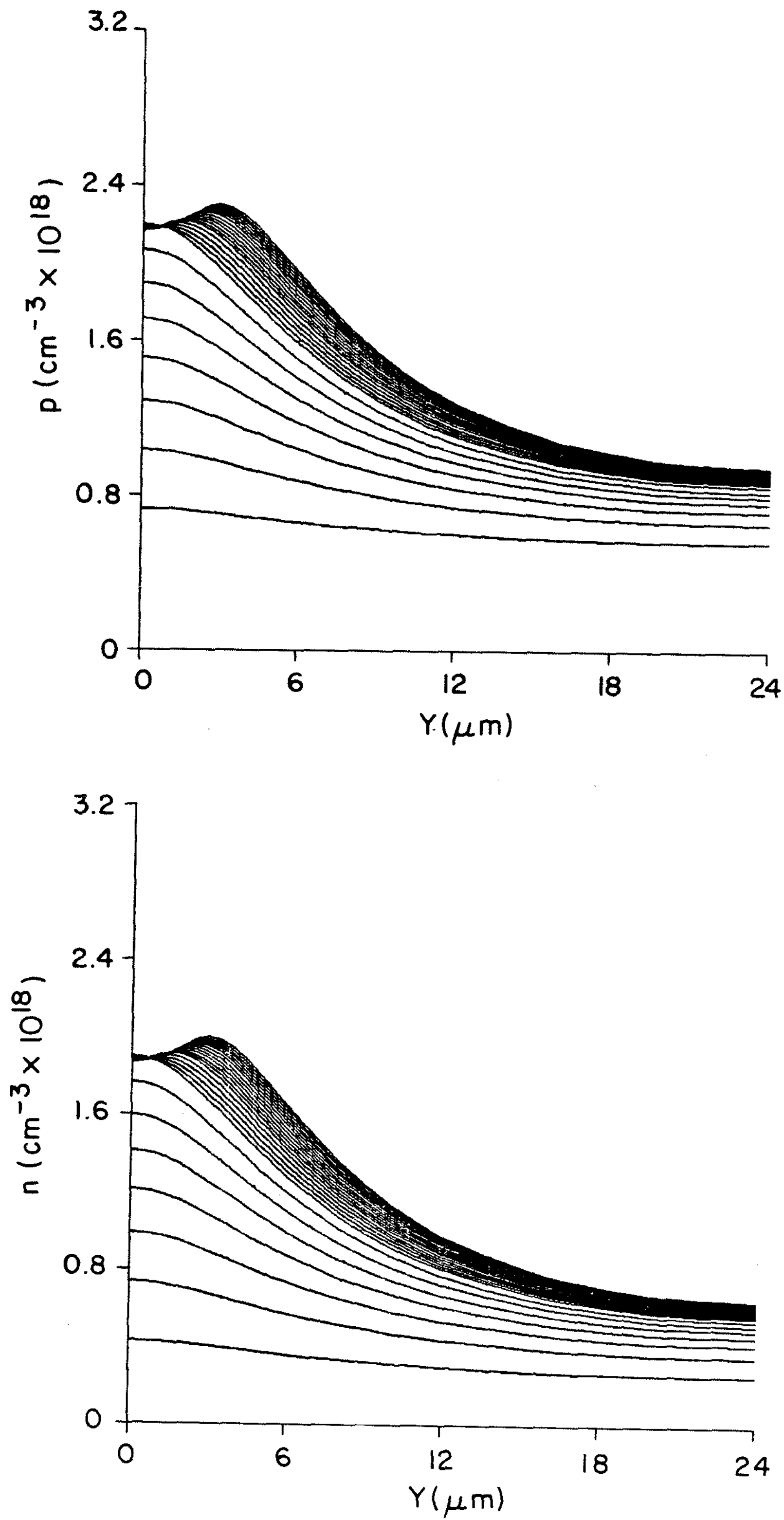

Figure 4.9 The lateral carrier density profiles for the device in operation. Total device current is varied as a parameter from 4 to 100 mA with a step of 4 mA.

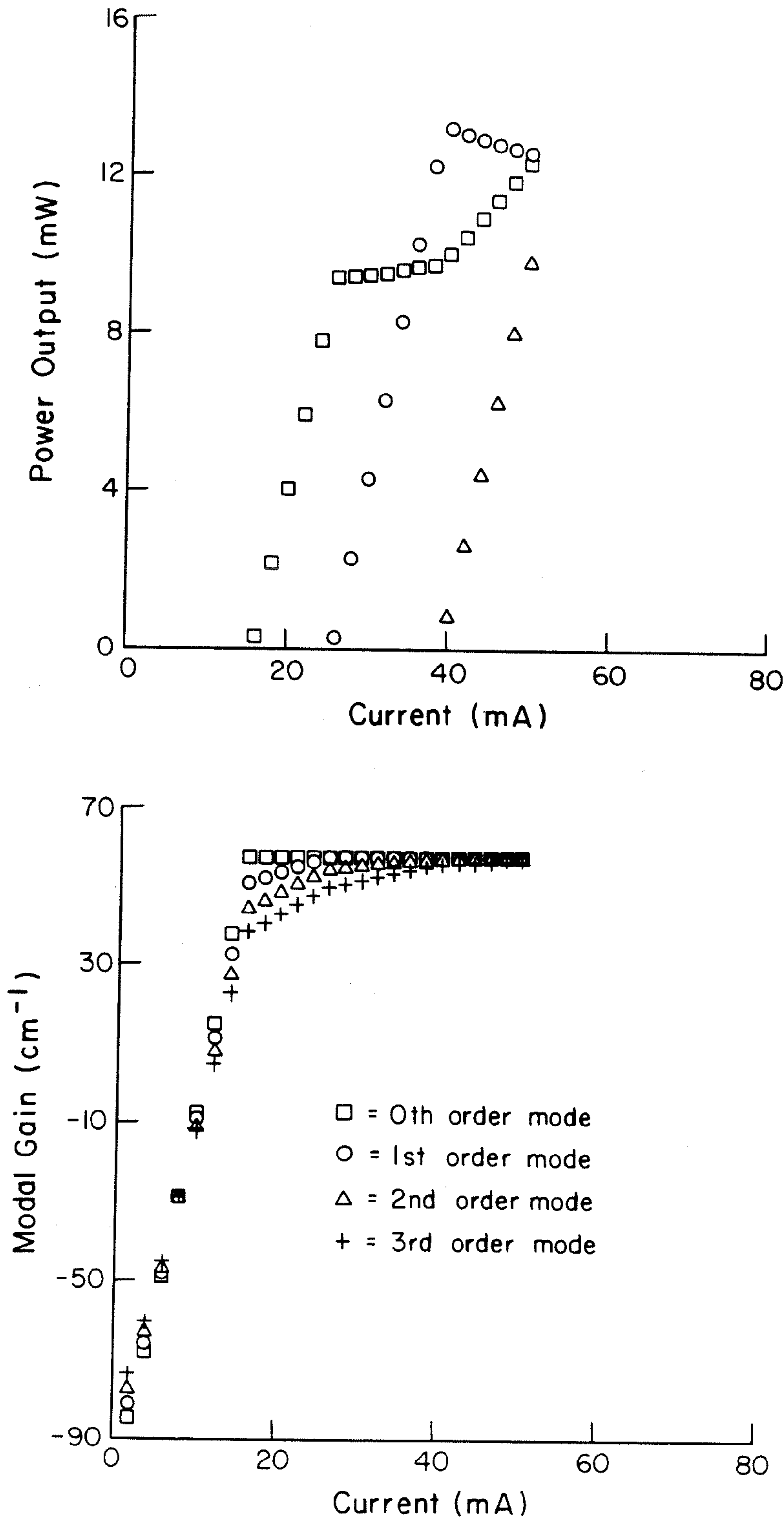

Figure 4.10 The light versus current characteristics and modal gains for the device. Each lateral mode is plotted separately. To obtain total device current and power, the scales should be doubled.

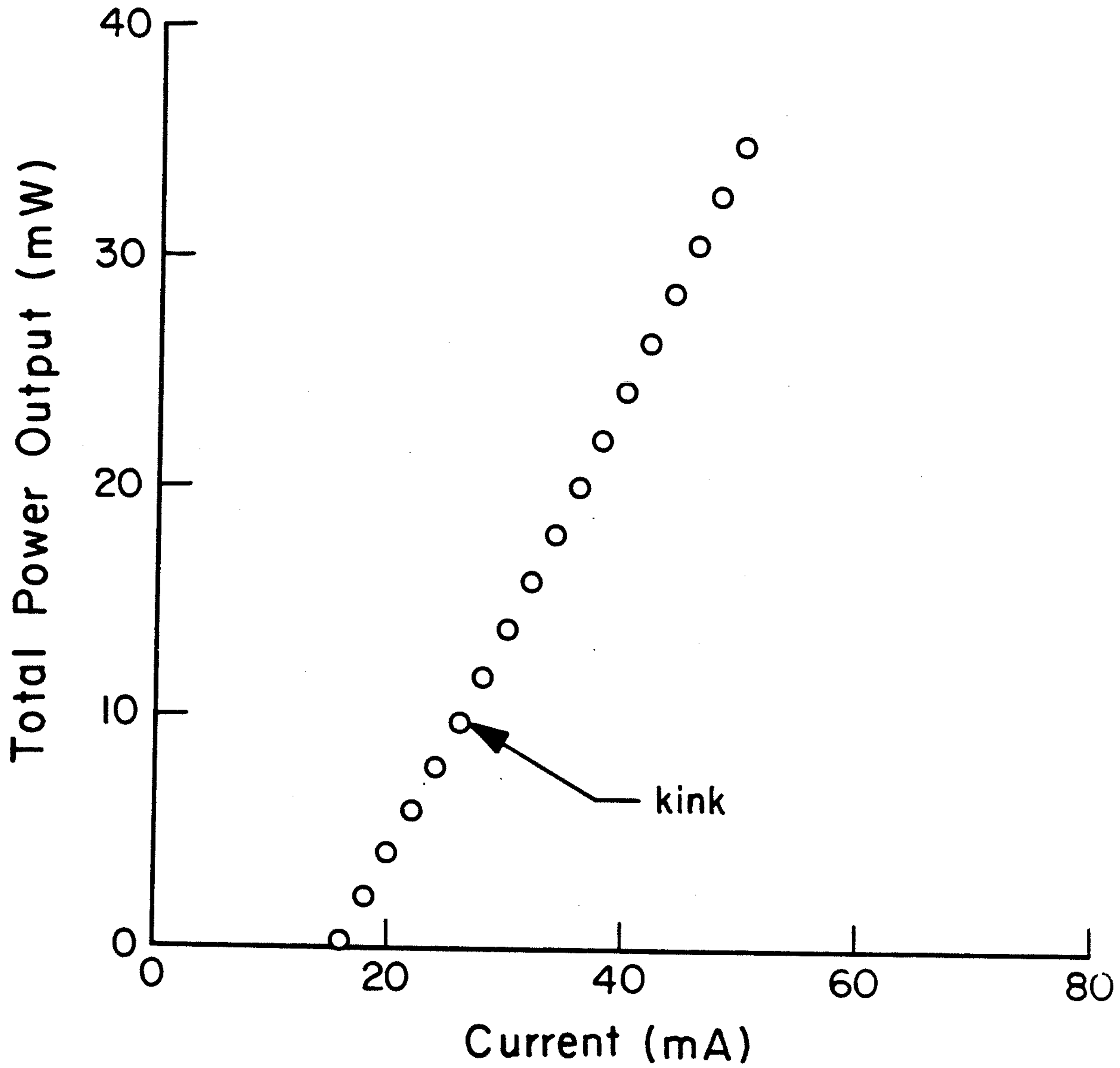

Figure 4.11 The light versus current characteristics for the device, with output powers in the lateral modes summed. To obtain total device current and power, the scales should be doubled.

stimulated power. The kink associated with the onset of oscillation of the first order mode at approximately 52 mA of total current and 20 mW of total power output is clearly visible. These results are in agreement with the experimental results for this device, which claim threshold currents as low as 32 mA and output powers into the lowest mode of up to 25 mW.

To compare with the results presented in the references (16) and (17), the sheet resistance for the p layers assumed here is approximately 500 Ω. The calculated threshold current in reference (16) for this sheet resistance and a 2 μm wide stripe contact is 53.7 mA. In this model, the injected carrier profile at threshold falls to half of its value at the center of the stripe at a lateral distance of 10 μm. In comparison, reference (16) yields 6 μm for this distance. In addition, the above threshold analysis in reference (17), although for a different structure, shows a different type of spatial holeburning than this model. In that calculation, spatial holeburning was found to significantly lower the carrier population at the center of the stripe under lasing conditions. In this model, the carrier population at the center of the stripe is nearly constant above threshold, and lateral mode switching results from the increase in the carrier population outside the lasing mode. This difference can be attributed directly to the p-n junction boundary conditions applied in the two models.

IV.7 Summary and Conclusions

A model of the double heterostructure laser has been presented which correctly treats the diode junction of this device. It is valid above lasing threshold and is capable of treating a large number of the device geometries in popular use. With this model, the quantitative behavior of devices can be investigated independently of experimental variations and compared and possibly optimized. The channelled substrate structure of Burnham et al.[10] has been treated as an

example, and the experimental and theoretical results are in good agreement.

IV.8 References for Chapter IV

1. For some examples and more references, see:
H. C. Casey, Jr. and M. B. Panish, **Heterostructure Lasers: Part B, Materials and Operating Characteristics,** Academic Press, New York (1978).

2. J. Buus, "A Model for the Static Properties of DH Lasers," IEEE J. Quant. Elect. **QE-15,** 734 (1979).

3. K. A. Shore, T. E. Rozzi, and G. H. in't Veld, "Semiconductor Laser Analysis: General Method for Characterising Devices of Various Cross Sectional Geometries," IEE Proc. pt. I **127,** 221 (1980).

4. T. L. Paoli and P. A. Barnes, "Saturation of the Junction Voltage in Stripe Geometry (AlGa)As Double-Heterostructure Junction Lasers," Appl. Phys. Lett. **28,** 714 (1976).

5. P. M. Asbeck, D. A. Cammack, J. J. Daniele, and V. Klebanoff, "Lateral Mode Behavior in Narrow Stripe Lasers," IEEE J. Quant. Elect. **QE-15,** 727 (1979).

6. D. Wilt and A. Yariv, submitted for publication.

7. S. M. Sze, **Physics of Semiconductor Devices,** Wiley-Interscience, New York (1969).

8. T. Tsukada, "GaAs$-$Ga$_x$Al$_{1-x}$As Buried Heterostructure Injection Lasers," J. Appl. Phys. **45,** 4899 (1974).

9. K. Aiki, M. Nakamura, T. Kuroda, and J. Umeda, "Channelled-Substrate Planar Structure (AlGa)As Injection Lasers," Appl. Phys. Lett. **30,** 649 (1977).

10. R. D. Burnham, D. R. Scifres, W. Streifer, and S. Peled, "Nonplanar Large Optical Cavity GaAs/GaAlAs Semiconductor Laser," Appl. Phys. Lett. **35,** 734 (1979).

11. N. Bar-Chaim, M. Lanir, S. Margalit, I. Ury, D. Wilt, M. Yust, and A. Yariv, "Be

Implanted (GaAl)As Stripe Geometry Lasers," Appl. Phys. Lett. **36**, 233 (1980).

12. H. Yonezu, I. Sakuma, K. Kobayashi, T. Kamejima, M. Ueno, and Y. Nannichi, "A GaAs–$Al_xGa_{1-x}As$ Double Heterostructure Planar Stripe Laser," Jpn. J. Appl. Phys. **12**, 1585 (1973).

13. D. Botez, "CW High-Power Single-Mode Lasers Using Constricted Double Heterostructures with a Large Optical Cavity (CDH-LOC)," Topical Meeting on Integrated and Guided Wave Optics, paper MC2, Incline Village, Nevada, January 1980.

14. S. B. Dong, J. A. Wolf, Jr., and F. E. Peterson, "On a Direct-Iterative Eigensolution Technique," International J. for Numerical Methods in Engineering **4**, 155 (1972).

15. J. Katz, S. Margalit, D. Wilt, P. C. Chen, and A. Yariv, "Single Growth Embedded Epitaxy AlGaAs Injection Lasers with Extremely Low Threshold Currents," Appl. Phys. Lett. **37**, 987 (1980).

16. W. Streifer, R. D. Burnham, and D. R. Scifres, "Analysis of Diode Lasers with Lateral Spatial Variations in Thickness," Appl. Phys. Lett. **37**, 121 (1980).

17. W. Streifer, D. R. Scifres, and R. D. Burnham, "Above Threshold Analysis of Double-Heterostructure Lasers with Laterally Tapered Active Regions," Appl. Phys. Lett. **37**, 877 (1980).

Chapter V

The Effect of Lateral Carrier Diffusion on the Modulation Response of a Semiconductor Laser

V.1 Introduction

Semiconductor lasers are potentially devices of great use in optical communications systems. Part of their attractiveness for this application stems from their high efficiency and high upper modulation frequency limit. Compared with conventional light emitting diodes, the laser offers much more in terms of both of these criteria, due to the presence in the laser of high densities of stimulated photons which have very short lifetimes (on the order of picoseconds). These affect very strongly the behavior of the laser diode.

The modulation response of the laser diode at present still leaves something to be desired. The upper modulation frequency limit, now approximately 2 GHz, is still unacceptable for some applications. In addition, most laser diodes have a strong resonance peak in the range of 1-2 GHz in their small signal response which proves to be a considerable impediment to their use in communications systems. This resonance manifests itself in the time domain as damped oscillations in the light output of the device when driven with a step input current. Many lasers exhibit this type of behavior, which results from the exchange of energy between the inverted medium and the photons in the resonant cavity of the device.

As a result of these problems, methods for improving the modulation response of these devices such as damping of this relaxation resonance are topics of active current interest.

Several authors have investigated the effect of lateral carrier diffusion upon the modulation response of the semiconductor laser [1-5]. These investigations have centered mainly upon the time domain response of the laser to a step

change in input current [2,3], or the small signal frequency response [1,4,5], and have indicated that the transverse diffusion of carriers can improve considerably the modulation response of the laser. This improvement comes mainly in the damping of the relaxation oscillations of the laser which usually occur within a time scale of nanoseconds after the current step, or in the damping of the resonance peak in the small signal frequency response at approximately 1-2 GHz.

The purpose of this chapter is to present a simple, self consistent model of the effect of lateral carrier diffusion upon the semiconductor laser to illustrate both its theoretical and practical limits for improving the modulation response of these devices [6]. This model is formulated in the frequency regime so that the analog small signal response of the device is made available. The general model developed is applied to the case of the TJS (transverse junction stripe) laser [7] as an example, and the effect of both the carrier diffusion and the spontaneous emission factor in the damping of the relaxation resonance of this device are compared with experiment. The TJS laser is chosen as an example since its injection can be modelled by a δ - function spatial dependence, eliminating the question of the lateral distribution of injected current and clarifying the contribution of lateral carrier diffusion to the device.

V.2 The Spatially Dependent Rate Equations

The starting point of this analysis is the spatially dependent rate equations, using the assumption that only a single carrier need be considered (for example, holes). We also assume that the active layer in the laser is thin so that all the physical variables are averaged over this dimension. In addition, the laser is assumed to oscillate in a single lateral mode.

$$\frac{\partial n}{\partial t} = -\frac{n}{\tau_s} + D\frac{\partial^2 n}{\partial x^2} - \frac{S}{\hbar\omega}\frac{\Gamma}{d} F a (n - n_t) + \frac{j}{e d} \tag{5.1}$$

$$\frac{dS}{dt} = v S \Gamma \int_{-\infty}^{\infty} F a (n - n_t) \, dx - \frac{S}{\tau_p} + \beta v \hbar\omega d \int_{-\infty}^{\infty} \frac{n}{\tau_s} dx \tag{5.2}$$

In these equations, n is the inversion density, τ_s is the spontaneous lifetime, D is the lateral diffusion constant, S is the power in the single lasing mode, $\hbar\omega$ is the photon energy, a is the gain coefficient and n_t is the inversion required for transparency, so that the optical gain is $a(n - n_t)$. F is the lateral intensity profile of the optical mode, assumed normalized, Γ is the intensity confinement factor normal to the active region, j is the injected current density, e is the electronic charge, d is the active layer thickness, v is the group velocity of the optical mode, τ_p is the photon lifetime, and β is a coupling coefficient for spontaneous emission into the optical mode.

The spontaneous emission factor is treated in a very simple manner here. To treat spontaneous emission into the lasing mode properly would involve a much more complex treatment which is unnecessary for this calculation. This is because the major contribution of spontaneous emission to the modulation characteristics comes from the background it adds to the optical power. Spontaneous emission could also be considered by adding a constant term $\frac{S_{spont}}{\tau_p}$ to equation (5.2).

These equations are normalized in the following manner. Time is normalized to τ_s, distance is normalized to the diffusion length, $\sqrt{D\tau_s}$, n is normalized to n_t. S is normalized to $\frac{\hbar\omega d\sqrt{D\tau_s}}{a\Gamma\tau_s}$, and j is normalized to $\frac{e d n_t}{\tau_s}$. With this choice of normalization, the rate equations appear as

$$\frac{\partial n}{\partial t} = - n + \frac{\partial^2 n}{\partial x^2} - S F (n - 1) + j \tag{5.3}$$

$$\frac{dS}{dt} = a_1 a_2 S \int_{-\infty}^{\infty} F (n - 1) dx - a_1 S + \beta a_1 a_2 \int_{-\infty}^{\infty} n \, dx \tag{5.4}$$

The two parameters a_1 and a_2 are

$$a_1 = \frac{\tau_s}{\tau_p} \tag{5.5}$$

$$a_2 = \Gamma a n_t v \tau_p \tag{5.6}$$

With reasonable values of the various parameters, $\tau_s = 3$ ns, $D = 10 \frac{cm^2}{s}$, $\hbar\omega = 1.43$ eV, $\Gamma = 0.5$, $d = 0.2$ μm, $a = 10^{-16}$ cm^2, $n_t = 2 \cdot 10^{18}$ cm^{-3}, $v = 10^{10} \frac{cm}{sec}$, $\tau_p = 2$ ps, the values for these parameters are approximately $1.5 \cdot 10^3$ for a_1 and 2 for a_2. In addition we have the condition

$$v \tau_p = \frac{L}{\alpha L + \ln(\frac{1}{R})} \tag{5.7}$$

where L is the diode length, α is a distributed loss, and R is the mirror reflectivity of the device.

V.3 Analytic Treatment of Lateral Carrier Diffusion Effects

In a qualitative sense, one might argue that lateral carrier diffusion in a device with a narrow optical mode and a very restricted current injection would increase the maximum modulation speed of the laser. This argument claims that the effective carrier lifetime in the device is shortened by the fact that carriers that diffuse away from the optical mode region are lost to stimulated emission. This, and the fact that the maximum modulation rate depends upon carrier lifetime, would seem to indicate that such a diffusion dominated laser would be a faster device. In addition, one might expect that lateral carrier diffusion

serves to damp the relaxation oscillations in the laser diode, since the exchange of energy between the photons and inverted carriers responsible for these oscillations is damped strongly by the gain and loss of carriers that diffuse into and out of the optical mode region.

An analytic result can be derived from the rate equations that indicates to what extent these qualitative arguments are true. One simple limiting case is that where the optical mode and current injection have no spatial dependence. Another limiting case, the one of most interest here, is that where the current injection and optical mode are both δ functions in the lateral direction. In either case, we will derive small signal modulation transfer functions, and a comparison reveals the extent to which the above assertions are true. To simplify the analytic results and to clarify the contribution of diffusion, we will assume the spontaneous emission coupling, β, to be zero.

The steady state solution to the spatially uniform case is then

$$(n_0 - 1) = \frac{1}{a_2} \tag{5.8}$$

$$S_0 F = a_2 (j_0 - j_{th}) \tag{5.9}$$

$$j_{th} = 1 + \frac{1}{a_2} \tag{5.10}$$

where zero subscripts indicate steady state values. Note that a power density, $S_0 F$, is given, where F is a constant, and the threshold current is defined as j_{th}. The small signal equations for the spatially uniform case are, assuming $n = n_0 + n_1 e^{i\omega t}$, $S = S_0 + S_1 e^{i\omega t}$, and $j = j_0 + j_1 e^{i\omega t}$,

$$i \omega n_1 = - n_1 - S_0 F n_1 - S_1 F (n_0 - 1) + j_1 \tag{5.11}$$

$$i \omega S_1 = a_1 a_2 S_0 n_1 + a_1 a_2 S_1 (n_0 - 1) - a_1 S_1 \tag{5.12}$$

Using the steady state relationships, equations (5.8) through (5.10), these simplify to

$$n_1 \, (\, i \, \omega + 1 + S_0 \, F \,) + S_1 \, F \, (\, \frac{1}{a_2} \,) = j_1 \tag{5.13}$$

$$i \, \omega \, S_1 \, F = a_1 \, a_2 \, S_0 \, F \, n_1 \tag{5.14}$$

Solving these relationships yields

$$S_1 \, F = a_2 \, j_1 \, \frac{1}{1 + \frac{i \, \omega}{a_1} \, (\, 1 + \frac{1 + i \, \omega}{S_0 \, F} \,)} \tag{5.15}$$

This transfer function represents a two pole lowpass response, with a characteristic frequency of

$$\omega_r = \sqrt{a_1 \, S_0 \, F} \tag{5.16}$$

With reasonable values of a_1, a_2, and the power density S_0 F, this resonance lies in the microwave range of 1-2 GHz. However, the resonance also has a typical amplitude of 10 dB over the dc value. This represents a considerable problem to the use of this device in a high speed communications system. This response is plotted as a function of frequency in Figure 5.1 for the values of the parameters as specified above. S_0F takes the values of 0.1, 0.3, 1, and 3 $\frac{mW}{\mu m}$ in these curves.

In the case where the current injection and the optical mode have δ function profiles,

$$j(x) = A \, \delta(\, x \,) \tag{5.17}$$

$$F(x) = \delta(\, x - x_0 \,) \tag{5.18}$$

the steady state solution to the equations above, neglecting spontaneous emission, is

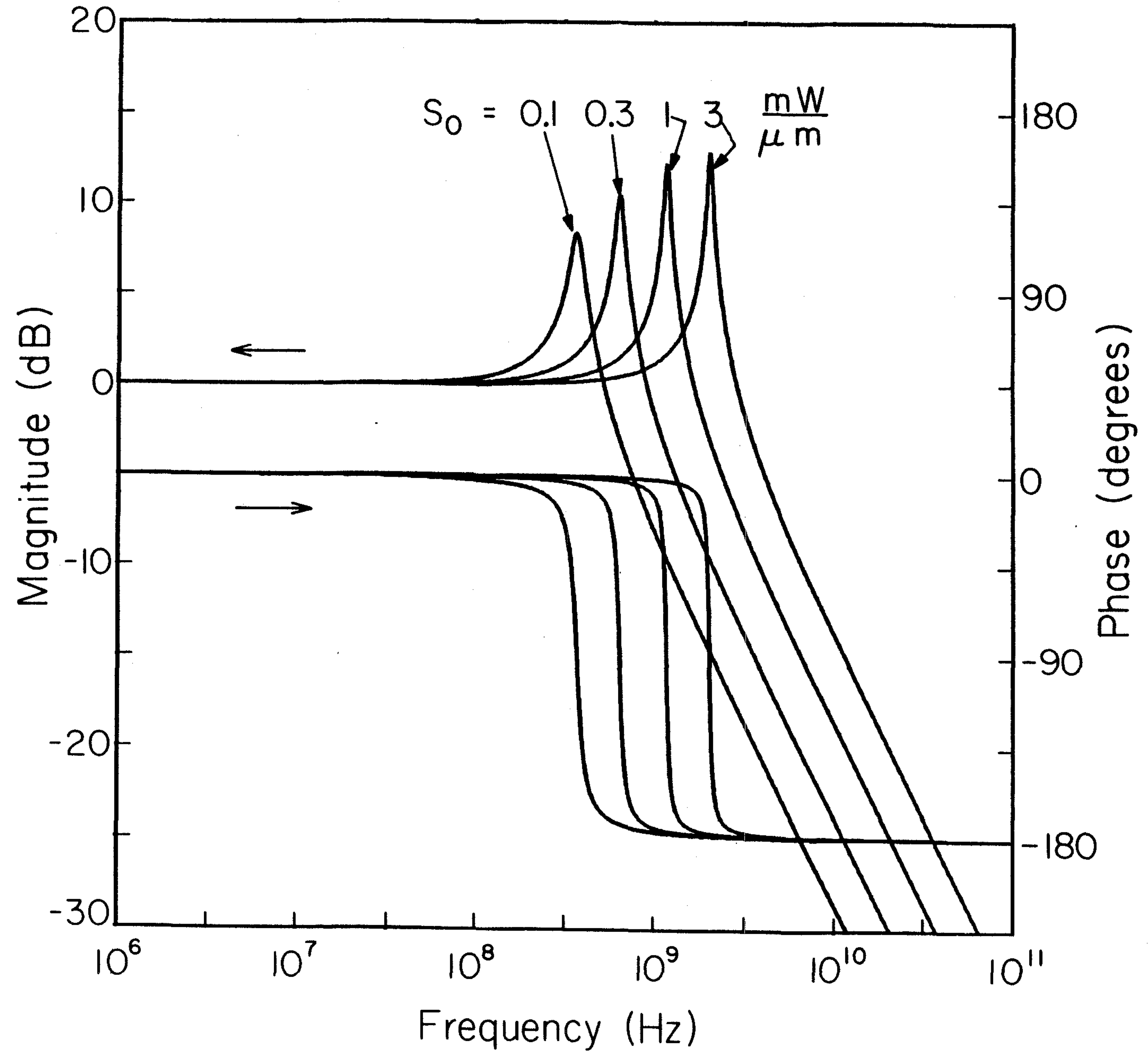

Figure 5.1 Small signal transfer function for the spatially uniform laser.

$$n_0(x_0) = 1 + \frac{1}{a_2} \tag{5.19}$$

$$n_0(x) = \frac{A_0}{2} e^{-|x|} - \frac{S_0}{2 a_2} e^{-|x - x_0|} \tag{5.20}$$

$$S_0 = a_2 e^{-|x_0|} (A_0 - A_{th}) \tag{5.21}$$

$$A_{th} = 2 e^{|x_0|} (1 + \frac{1}{a_2}) \tag{5.22}$$

where the lasing threshold A_{th} has been defined. Note that this threshold is just $e^{|x_0|}$ times the threshold for a two - diffusion - length wide uniform laser. The small signal equations for this case are then

$$i \omega n_1 = - n_1 + \frac{d^2 n_1}{dx^2} - S_1 (n_0 - 1) \delta(x - x_0) \tag{5.23}$$

$$- S_0 n_1 \delta(x - x_0) + A_1 \delta(x)$$

$$i \omega S_1 = a_1 a_2 S_1 (n_0(x_0) - 1) + a_1 a_2 S_0 n_1(x_0) - a_1 S_1 \tag{5.24}$$

Again, using the steady state relationships, equations (5.19) through (5.22), we can reduce these relationships to

$$i \omega S_1 = a_1 a_2 S_0 n_1(x_0) \tag{5.25}$$

$$\frac{d^2 n_1}{dx^2} - n_1 (1 + i \omega) = A_1 \delta(x) - S_0 (1 + \frac{a_1}{i \omega}) n_1(x_0) \delta(x - x_0) \tag{5.26}$$

A solution to these equations which must be made self consistent is

$$n_1(x) = \frac{A_1}{2\sqrt{1+i\omega}} e^{-|x|\sqrt{1+i\omega}} \tag{5.27}$$

$$- \frac{S_0 \left(1 + \frac{a_1}{i\omega}\right)}{2\sqrt{1+i\omega}} n_1(x_0)\, e^{-|x-x_0|\sqrt{1+i\omega}}$$

The requirement of self consistency yields

$$n_1(x_0) = \frac{A_1}{2} e^{-|x_0|\sqrt{1+i\omega}} \frac{1}{\sqrt{1+i\omega} + \frac{S_0}{2}\left(1 + \frac{a_1}{i\omega}\right)} \tag{5.28}$$

With some simplification and the substitution of equation (5.25) this gives

$$S_1 = a_2 A_1 \frac{e^{-|x_0|\sqrt{1+i\omega}}}{1 + \frac{i\omega}{a_1}\left(1 + \frac{\sqrt{1+i\omega}}{\frac{S_0}{2}}\right)} \tag{5.29}$$

The resemblance between equation (5.29) and equation (5.15) is remarkable. The behavior of this transfer function is plotted in Figure 5.2, again for the parameters chosen earlier, and with the offset x_0 chosen to be zero. The parameter S_0 takes on the values 0.1, 0.3, 1, and 3 mW. This transfer function has slightly improved frequency response over the uniform case, manifested mostly in the reduced resonance peaks. This is achieved, however, at the price of slightly worse phase response in the region near the resonance.

This transfer function represents the maximum contribution of diffusion to the modulation behavior of the semiconductor laser. Any other case should lie in the intermediate region between the spatially uniform case and this δ - function laser. It is most interesting to note that this limiting case has an analytic solution which does not show pathological behavior such as an infinite frequency response. In fact, even with the infinite power density represented by the δ function optical mode, this laser has an upper limit on modulation frequency

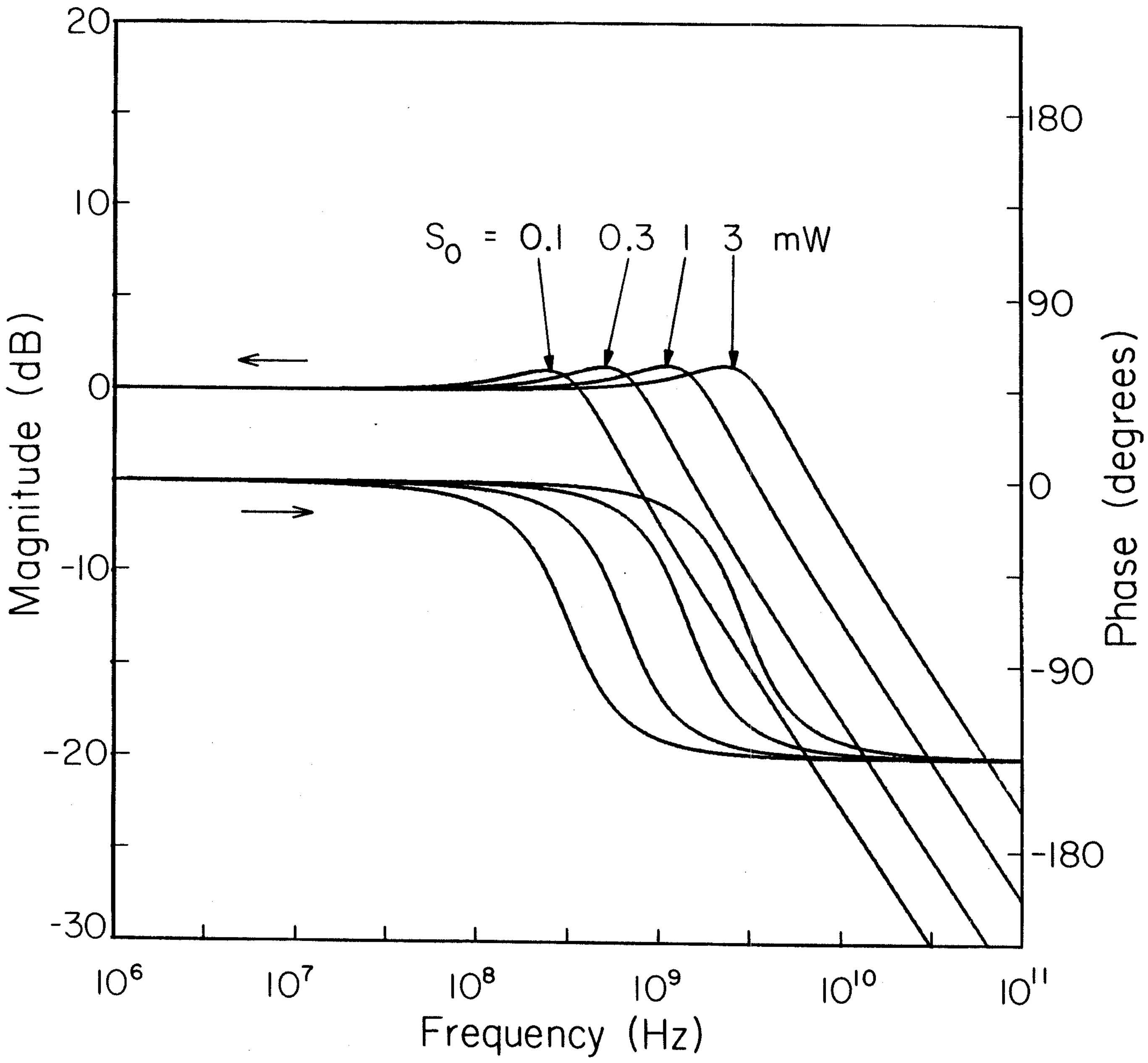

Figure 5.2 **Small signal transfer function for the δ - function laser.**

which is quite similar to the spatially uniform case. Thus it appears that while lateral carrier diffusion may be expected to improve the damping of the relaxation resonance, it cannot be expected to greatly improve the upper modulation frequency limit of the semiconductor laser.

V.4 Modulation Response of the TJS Laser

To analyze the case where the injected current and the optical mode are allowed to assume arbitrary profiles, numerical analysis of the rate equations (5.3) and (5.4) is required. First, the steady state solution of these equations is found, and using this solution, small signal equations for the system are derived. Since the steady state equations are nonlinear, their solution can be quite tedious. However, if we assume the optical mode profile F to be fixed and the profile of the injected current j to be fixed so that $j = A\,G(x)$ where G is a fixed function and A is a scalar, this calculation can be reduced to the solution of a linear system.

With the output power S_0 assumed, the equations to be solved for the steady state solution are

$$-n + \frac{\partial^2 n}{\partial x^2} - S_0 F(n-1) + A G = 0 \qquad (5.30)$$

$$a_1 a_2 S_0 \int_{-\infty}^{\infty} F(n-1)\,dx - a_1 S_0 + \beta a_1 a_2 \int_{-\infty}^{\infty} n\,dx = 0 \qquad (5.31)$$

These equations are both linear in the unknowns, n and A. With the assumption of a finite element variational form for n involving a one dimensional grid where the values of n at the nodes are the variational parameters and using linear interpolation between nodes, these two equations are transformed into a linear algebraic system which may be solved quite simply to yield both the nodal values of n and the scalar current A.

In the small signal analysis, the equations are already linear in all the unknowns, and we simply assume a value for the small signal output power S_1, assume a finite element form for the small signal carrier distribution n_1, and solve the resulting linear algebraic system for the nodal values of n_1 and the small signal scalar current A_1.

This calculation has been performed for the TJS laser, and the results are shown in Figures 5.3 through 5.6. The TJS laser was taken as the test device because of its simple electrical and optical structure. Since it is a lateral homojunction device, the current injection profile G can be taken to have a δ function form. This eliminates the problem of determining how the current distribution varies with steady state optical power output or modulation frequency. In addition, this device has a built in index profile in the lateral dimension that defines the lateral optical mode profile F. In the calculation, the parameters for the device were taken to be $\alpha = 50\ \text{cm}^{-1}$, $R = 0.3$, $\Gamma = 0.6$, $\hbar\omega = 1.43\ \text{eV}$, $a = 10^{-16}\ \text{cm}^2$, $d = 0.2\ \mu\text{m}$, $L = 250\ \mu\text{m}$, $n_t = 2 \cdot 10^{18}\ \text{cm}^{-3}$, $\sqrt{D\,\tau_s} = 3\ \mu\text{m}$, $\tau_s = 3\ \text{ns}$, and $v = 0.83 \cdot 10^{10}\ \frac{\text{cm}}{\text{sec}}$. This gives for the parameters $a_1 = 2500$ and $a_2 = 1.2$. The lateral mode intensity profile assumed for this device is

$$F(x) = \frac{1}{\sqrt{2\pi}\ w} e^{-\frac{(x - x_{off})^2}{2w^2}} \tag{5.32}$$

where x_{off} is the offset between the center of the optical mode and the diode junction, and w is the width of the lasing mode, both assumed to be 0.6 μm. The origin is taken to lie at the diode junction. The small signal modulation transfer functions calculated for these parameters, a power output from the device of 1 mW, and various values of the spontaneous emission coupling factor are shown in Figures 5.3 and 5.4. The interesting feature of these curves is the suppression of the relaxation oscillation resonance caused by the lateral diffusion of carriers in the device. Compared with the spatially uniform case, the height of the

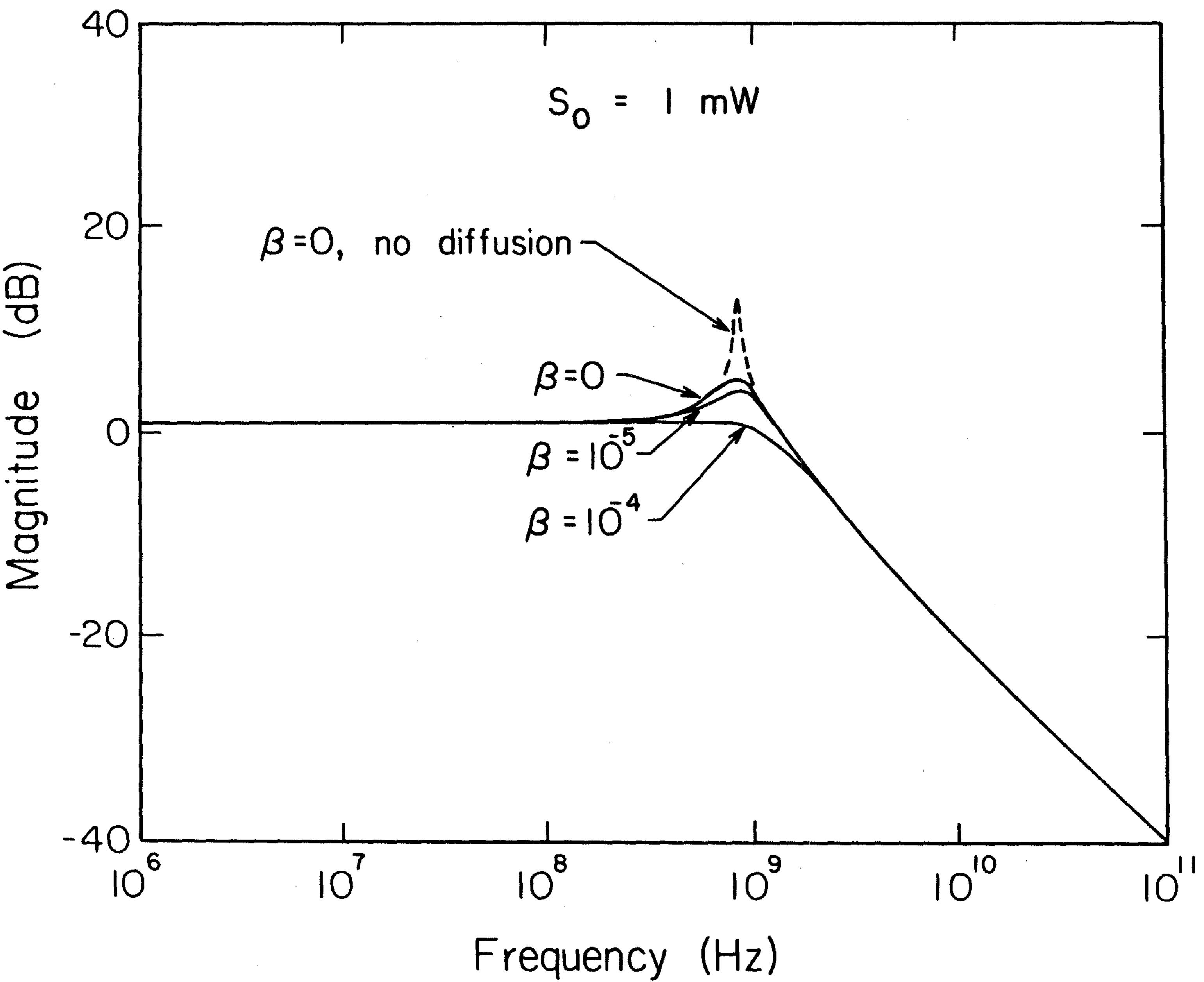

Figure 5.3 Magnitude of small signal transfer function for TJS laser, showing dependence upon the spontaneous emission coupling factor.

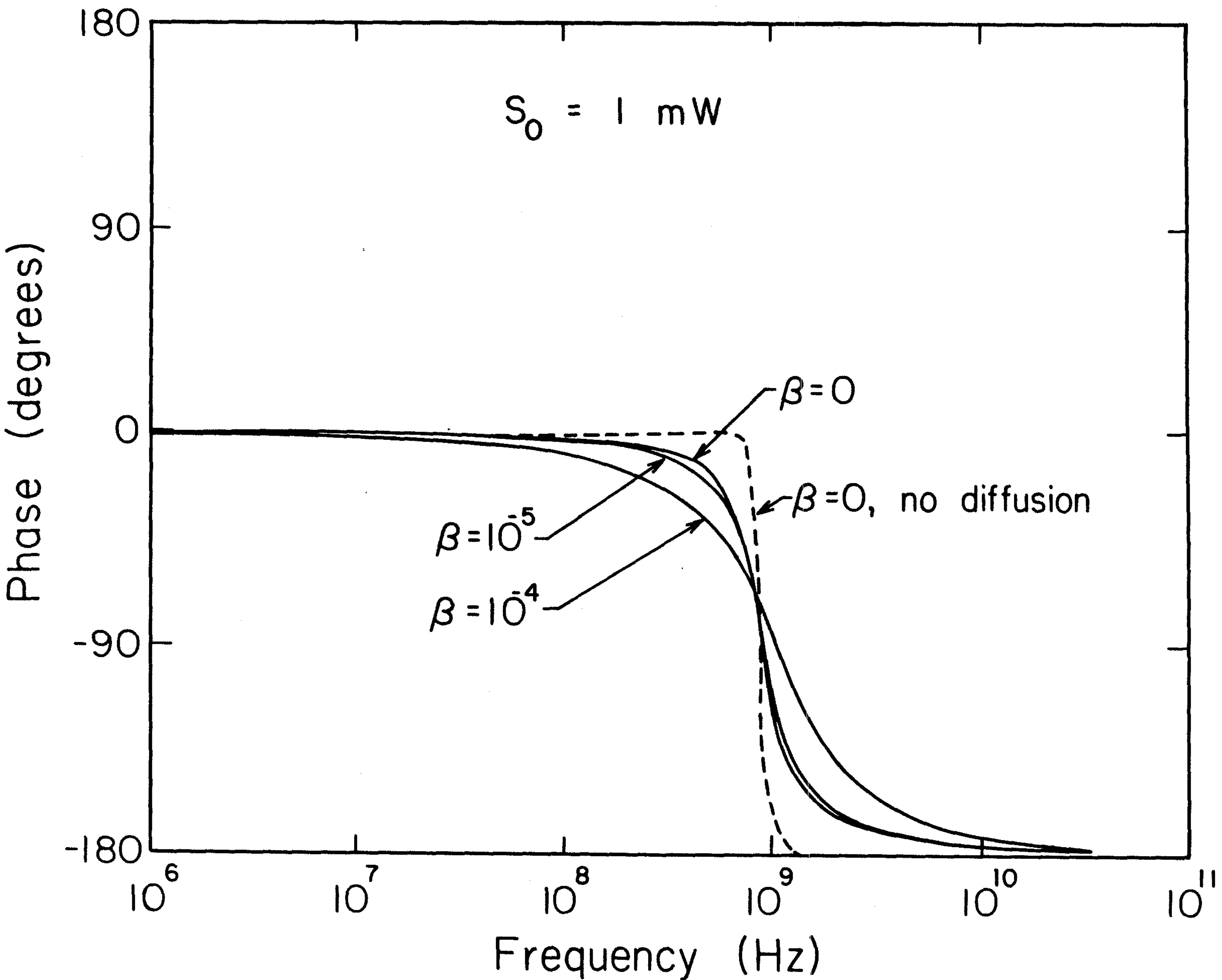

Figure 5.4 Phase of small signal transfer function for TJS laser, showing dependence upon the spontaneous emission coupling factor.

resonance is lowered by approximately 9 dB by the action of lateral diffusion. The additional contribution of spontaneous emission into the lasing mode can be seen to be appreciable only for relatively large spontaneous emission coupling factors of 10^{-4}. In Figures 5.5 and 5.6, the behavior of the transfer function as a function of optical output power is calculated for a spontaneous emission coupling of zero. The optical output powers are 0.1 mW for the lowest curve, 1 mW for the center curve, and 10 mW for the upper curve.

Figure 5.7 shows the measured small signal transfer function for a TJS laser. It should be noted that the vertical scale in this measurement is twice as large as in the theoretical calculations. This is due to the fact that the measurement was done with a square law detector, a silicon avalanche photodiode (APD). The resonance peak in the amplitude response of this device has a magnitude of approximately 5 dB on this scale, or 2.5 dB on the scale of the theoretical curves. This corresponds well with the calculations if a spontaneous emission factor of approximately $3 \cdot 10^{-5}$ is assumed. This is a reasonable value to assume for spontaneous emission coupling in this type of device. It is quite difficult to draw any more information from this experimental measurement as it contains also the frequency response of the measurement system, including the APD response which has a 3 dB cutoff frequency of approximately 1.8 GHz.

The measured phase response of the system also supports the diffusion damped model of the laser, since it displays a gradual rolloff rather than the sharp transition of the spatially uniform laser.

The model of the TJS laser, then, as a diffusion damped device can be seen to be verified quite well. This device should be quite useful in both analog and digital information transmission systems where its well damped resonance would cause minimal interference with modulated information.

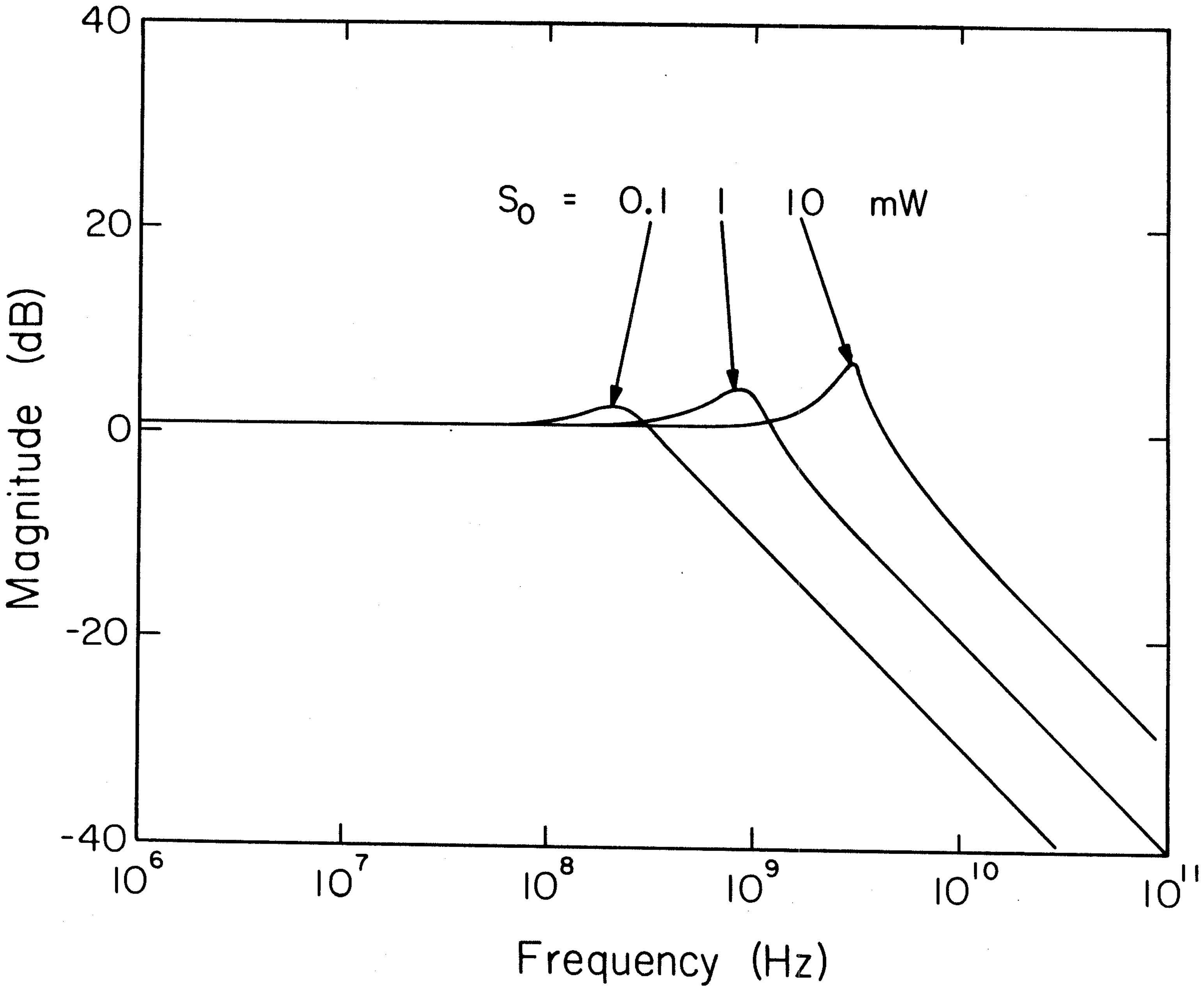

Figure 5.5 Magnitude of small signal transfer function for TJS laser, showing dependence upon the steady state output power.

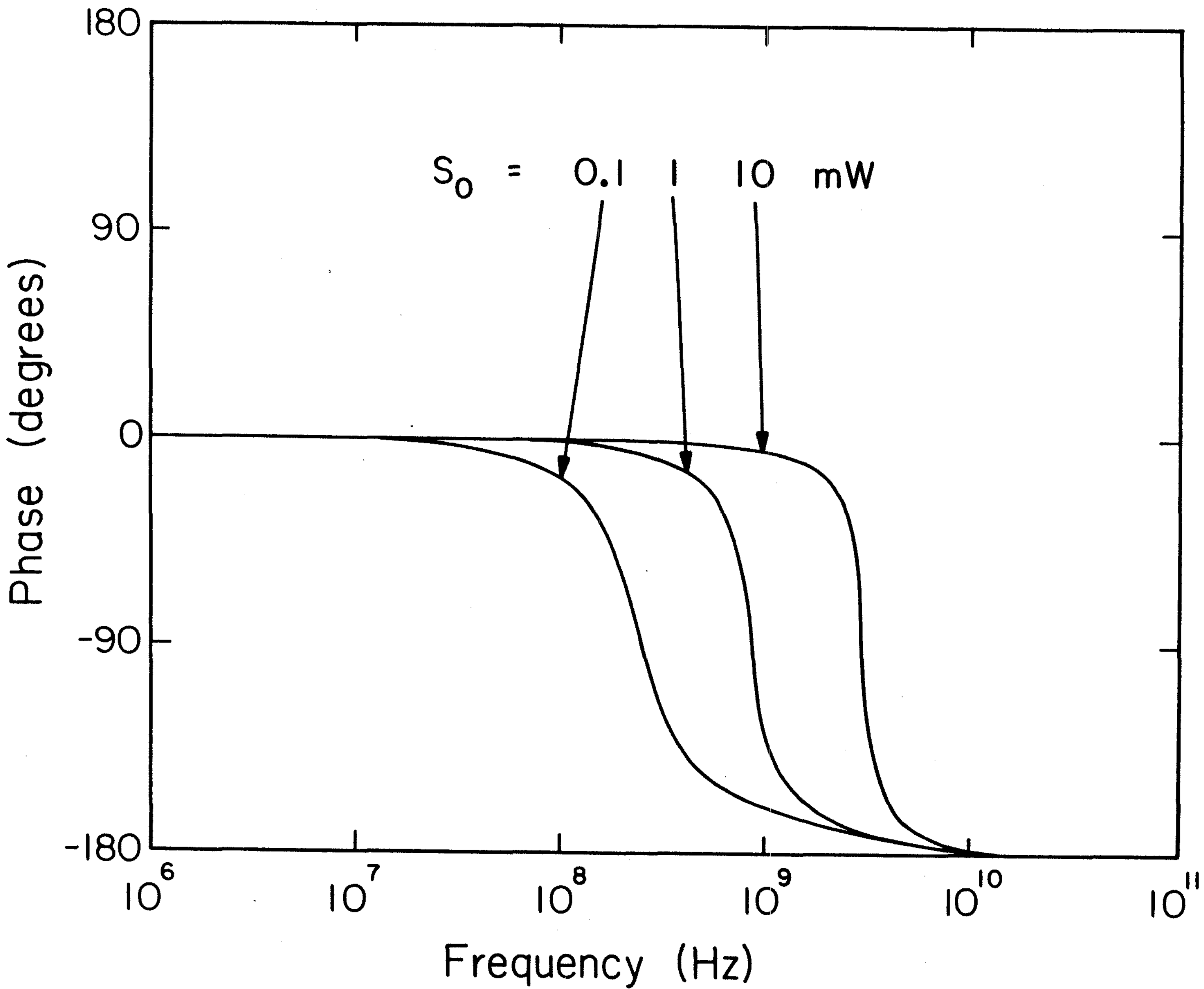

Figure 5.6 Phase of small signal transfer function for TJS laser, showing dependence upon the steady state output power.

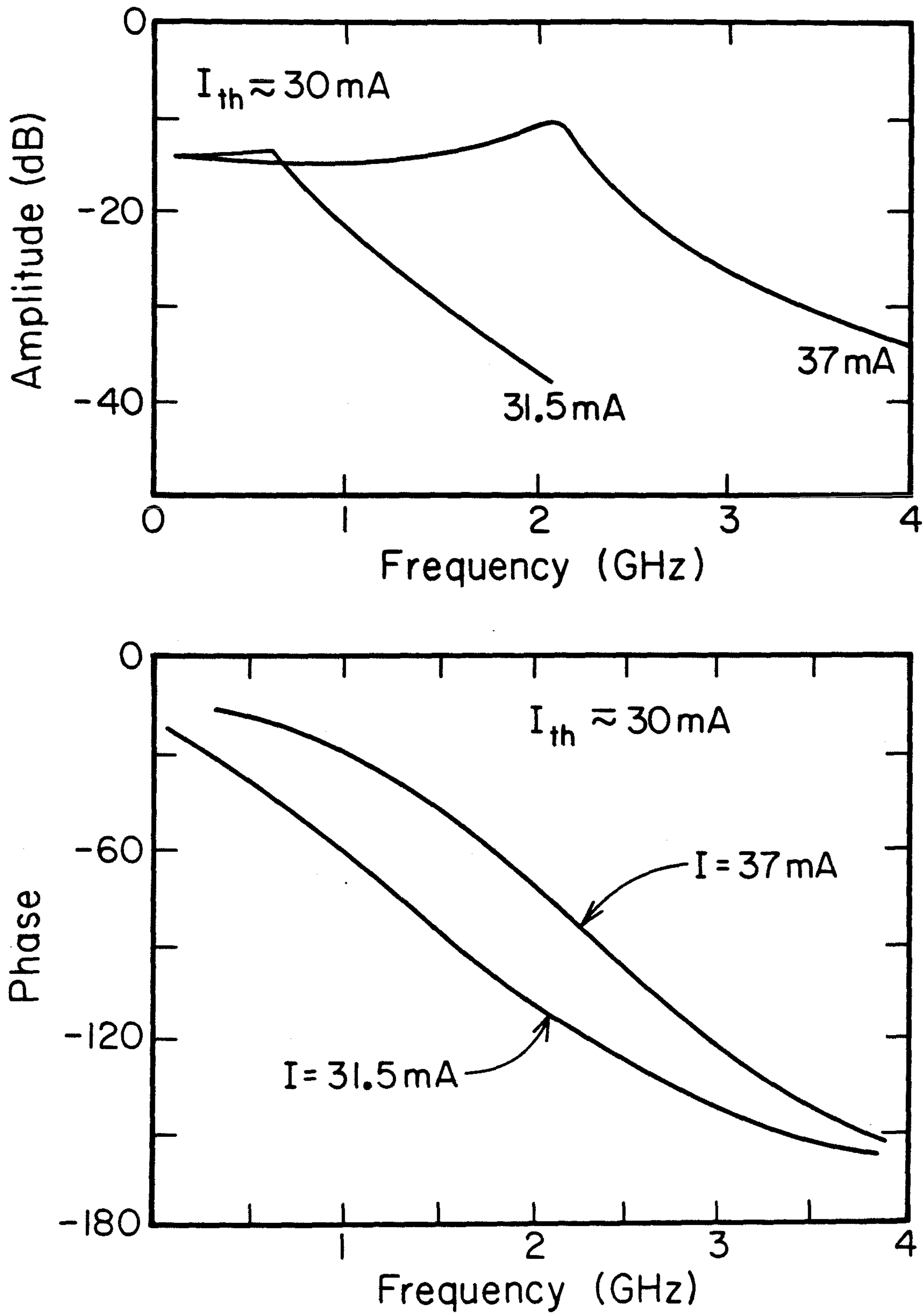

Figure 5.7 Measured amplitude and phase response of a TJS laser.

In conclusion, a model of diffusion effects on the small signal modulation characteristics of the semiconductor laser has been presented which shows both the theoretical limits and practical behavior of the diffusion dominated laser. It can be seen that lateral carrier diffusion is a useful mechanism for the control of the relaxation resonance in this device. It has also been shown that the use of lateral carrier diffusion to improve the upper limit on modulation frequency is not practical. In addition, the model of the TJS laser as a diffusion damped laser has been shown to account for the experimental small signal modulation function of this device.

V.5 References for Chapter V

1. T. Ikegami, "Spectrum Broadening and Tailing Effect in Directly Modulated Injection Lasers," First European Conference on Optical Fibre Communication, IEE London, September, 1975.

2. J. Buus and M. Danielsen, "Carrier Diffusion and Higher Order Transversal Modes in Spectral Dynamics of the Semiconductor Laser," IEEE J. Quant. Electron. **QE-13**, 669 (1977).

3. N. Chinone, K. Aiki, M. Nakamura, and R. Ito, "Effects of Lateral Mode and Carrier Density Profile on Dynamic Behaviors of Semiconductor Lasers," IEEE J. Quant. Electron. **QE-14**, 625 (1978).

4. K. Furuya, Y. Suematsu, and T. Hong, "Reduction of Resonance - Like Peak in Direct Modulation due to Carrier Diffusion in Injection Lasers," Appl. Opt. **17**, 1949 (1978).

5. G. H. B. Thompson, **Physics of Semiconductor Laser Devices**, Section 7.3.4, John Wiley & Sons, Inc., New York, (1980).

6. D. Wilt, K. Y. Lau, and A. Yariv, submitted for publication.

7. H. Namizaki, H. Kau, M. Ishii, and A. Ito, "Transverse-Junction-Stripe-Geometry Double Heterostructure Lasers with Very Low Threshold Current," J. Appl. Phys. **45**, 2785 (1974).

Chapter VI

Effective Permittivity Formalism and the Design of Buried Heterostructure Lasers

VI.1 Introduction

One of the most important aspects in the design and understanding of the semiconductor laser is the waveguiding that defines its optical modes, since this impacts strongly upon the modal behavior of the lasing device. Well behaved semiconductor lasers oscillate in a single spatial mode, and this phenomenon is based upon gain discrimination between the optical modes of the waveguide structure.

The optical guiding in these devices has often been treated theoretically by a technique known as the effective permittivity formalism [1-7]. This technique is usually presented as an approximate solution method for the eigenvalue equation defining the optical modes of the laser. This approximation takes note of the fact that the waveguide in a typical semiconductor laser resembles quite closely that in a uniform planar waveguide. The active region in the laser is usually quite thin and is sandwiched between two cladding layers of considerably lower permittivity, so that the optical mode in the direction normal to the active layer is quite strongly confined. In the lateral dimension, the variations in permittivity are usually much smaller, so that one can make the approximation that the optical mode in the laser has a separable form with the profile in the direction normal to the active layer unperturbed from the mode shape for the uniform planar guide. One then uses this mode shape to define an effective permittivity in the lateral dimension by forming an average of the permittivities in the normal direction. This approach to the definition of effective permittivity formalism leaves open the question of what weighting form to use for the effective permittivity.

A more sophisticated approach to the problem includes error criteria which aid in the choice of this weighting function[7]. The best choice is to choose a weight which minimizes the correction to the lateral modal field in a perturbation analysis of the original waveguide equation. This criterion leads to the choice of the intensity profile as a weighting function, and prefers to weight the relative permittivity (as opposed, for instance, to the refractive index).

This paper presents an even more general approach to the treatment of effective permittivity formalism which treats this technique as a variational approximation, and allows considerably more freedom in the choice of the modal profiles used in the approximation. With this approach, one is no longer limited to the use of simple planar waveguide profiles in the direction normal to the active region, and one can even use a normal profile which is not an eigensolution in this direction. This may be a wise choice in certain types of lasers such as the buried heterostructure laser. In this case, the choice of a mode profile in the direction normal to the active layer which is an eigensolution leads to the use of plane wave modes in the regions of regrown cladding. This is clearly a poor approximation to the true modal profile in this device. A much better approximation would be to use the same modal profile normal to the active layer in the regrown clad as is used inside the buried mesa. The value of the effective permittivity thus obtained is quite different from that resulting from the usual technique, and shows that the guiding in this device is much stronger than might be suspected from the usual effective permittivity formalism.

VI.2 Effective Permittivity Formalism

The starting point in this analysis is the vector wave equation,

$$(\nabla^2 + k^2 \varepsilon) \vec{E} = 0 \tag{6.1}$$

here k is the wavenumber for the frequency of interest ($k = \frac{\omega}{c}$) and ε is the

complex permittivity of the medium. This wave equation is derived with the assumption that the scale of variation for ε is much larger than a wavelength so that a term involving the gradient of ε can be dropped. $\vec{E}$ is the electric field, assumed to vary as $e^{i\omega t}$.

With the assumption that we are interested in a waveguide mode which varies as $e^{i\beta z}$ where the z axis is chosen to be parallel to the guide, we get

$$(\nabla_t^2 + k^2 \varepsilon - \beta^2) \vec{E} = 0 \tag{6.2}$$

where ∇_t is the transverse gradient operator ($\nabla_t = \vec{e}_x \frac{\partial}{\partial x} + \vec{e}_y \frac{\partial}{\partial y}$).

Semiconductor lasers are most often fabricated with a waveguide that is strongly confining in one transverse direction and weakly confining in the other. In the strongly confined direction, normal to the active layer, the waveguiding is dominated by the discontinuity in permittivity between the active layer and the larger bandgap cladding layers. In order to achieve modal control in this direction, the active layer is made quite thin (on the order of 0.2 μm) so that the low order modes are much more tightly confined than the higher modes. In the lateral direction, parallel to the active layer, the waveguiding is usually weak. Thus, the waveguide modes split, in a manner similar to that in the uniform planar waveguide, into pseudo-TE and pseudo-TM modes. The pseudo-TE modes are known to dominate the behavior of the semiconductor laser. This is because they are more tightly confined to the gain region (the active layer) and also have higher reflectivities from the cleaved mirrors. For this reason, we will assume a TE mode for the laser and solve a scalar modal eigenequation

$$(\nabla_t^2 + k^2 \varepsilon - \beta^2) u = 0 \tag{6.3}$$

where u represents the TE electric field, E_y. We have taken the y coordinate to be parallel to the active layer, and the x coordinate normal to the active layer.

This eigenequation can be cast in a variational form as

$$\delta \beta^2 = \delta \left(\frac{\int_{-\infty}^{\infty} \int_{-\infty}^{\infty} dx\, dy \left(-(\nabla_t u)^2 + k^2 \varepsilon u^2 \right)}{\int_{-\infty}^{\infty} \int_{-\infty}^{\infty} dx\, dy\, u^2} \right) = 0 \tag{6.4}$$

Keeping in mind the situation that the mode is tightly confined in one dimension (normal to the active layer) and weakly confined in the other, we will assume a variational form for u with a fixed mode profile in the direction normal to the active layer and allow the lateral mode profile to vary. The resulting Euler equation for the lateral mode profile contains the effective permittivity. One choice for the variation in the direction normal to the active layer is to solve an eigenmode equation in this direction, ignoring the partial derivative in the y direction.

$$\left(\frac{\partial^2}{\partial x^2} + k^2 \varepsilon(x,y) - \gamma_1^2(y) \right) X(x,y) = 0 \tag{6.5}$$

The lateral coordinate y is considered here to be a parameter, and we choose the solution with the largest eigenvalue (the lowest mode). This eigenvalue, γ_1, is not the propagation constant for the mode, but is related to the effective permittivity. Alternatively, any functional form X(x,y) desired can be used to represent the variation in the normal direction, if for some reason the eigenmode solution above is felt to be a poor approximation. Consistent with the use of complex permittivities, the normalization condition on this field is taken to be

$$\int_{-\infty}^{\infty} dx\, X^2 = 1 \tag{6.6}$$

We next need to find the best possible approximation to the true modal field using the field X to represent the variation in the perpendicular (x) direction. To

this end, we assume a variational form to substitute into the variational equation (6.4)

$$u(x,y) = X(x,y)\, Y(y) \tag{6.7}$$

where Y(y) is the function we will allow to vary. Since the variation in the x direction has been determined, we may integrate over x in the variational equation and get as a result

$$\delta \left(\frac{\int_{-\infty}^{\infty} dy \left(- \left(\frac{dY}{dy} \right)^2 + \left(k^2 \varepsilon_{eff} \right) Y^2 \right)}{\int_{-\infty}^{\infty} dy\, Y^2} \right) = 0 \tag{6.8}$$

where

$$k^2 \varepsilon_{eff}(y) = \int_{-\infty}^{\infty} dx \left(- \left(\nabla_t X \right)^2 + k^2 \varepsilon X^2 \right) \tag{6.9}$$

The normalization condition (6.6) has been used in the simplification of the expression (6.8). This effective permittivity can be simplified in the case where X is a solution of the eigenmode equation (6.5) to

$$k^2 \varepsilon_{eff}(y) = \gamma_1^2(y) - \int_{-\infty}^{\infty} dx \left(\frac{\partial X}{\partial y} \right)^2 \tag{6.10}$$

where $\gamma_1^2(y)$ is the eigenvalue of the equation (6.5). Apart from the second term involving $\frac{\partial X}{\partial y}$, this is the same result as that of the conventional effective index formalism. In many cases, this extra term is small enough to neglect. However, it represents an important consideration in some cases, especially those where the variational form assumed for X has an abrupt variation in the lateral direction. This is the case, for instance, in the conventional analysis of the buried heterostructure laser [11].

The Euler equation for this variational expression is then

$$\left(\frac{d^2}{dy^2} + k^2 \varepsilon_{eff}(y) - \beta^2 \right) Y = 0 \tag{6.11}$$

If the normalization is taken as

$$\int_{-\infty}^{\infty} dy\, Y^2 = 1 \tag{6.12}$$

then the normalization of the field u is

$$\int_{-\infty}^{\infty} \int_{-\infty}^{\infty} dx\, dy\, u^2 = 1 \tag{6.13}$$

The advantage of approaching the effective permittivity problem from the standpoint of the variational principle is that it assures in some sense that the best possible approximation to the true modal field has been obtained. This statement can be quantified further if the profile taken for X is an eigensolution of the equation (6.5). In this case, if first order perturbation theory is applied to the modal profiles found, all corrections to the modal field u involving overlap integrals of X with itself are zero. The lowest nonzero terms involve overlap integrals of X with higher order modes in the x direction. However, it is important to keep in mind that the choice of eigensolutions for X may not necessarily be the optimal one from the standpoint of approximating the field u.

VI.3 Design of the Buried Heterostructure Laser

The design of the buried heterostructure laser[8,9] and its optimization represent an interesting and illustrative example of the use of this effective permittivity formalism. The typical buried heterostructure laser is illustrated in Figure 6.1. Its fabrication involves the growth of a double heterostructure wafer, the subsequent etching of narrow mesas, and the regrowth of cladding on the sides of these mesas. This device has a waveguide that consists of the

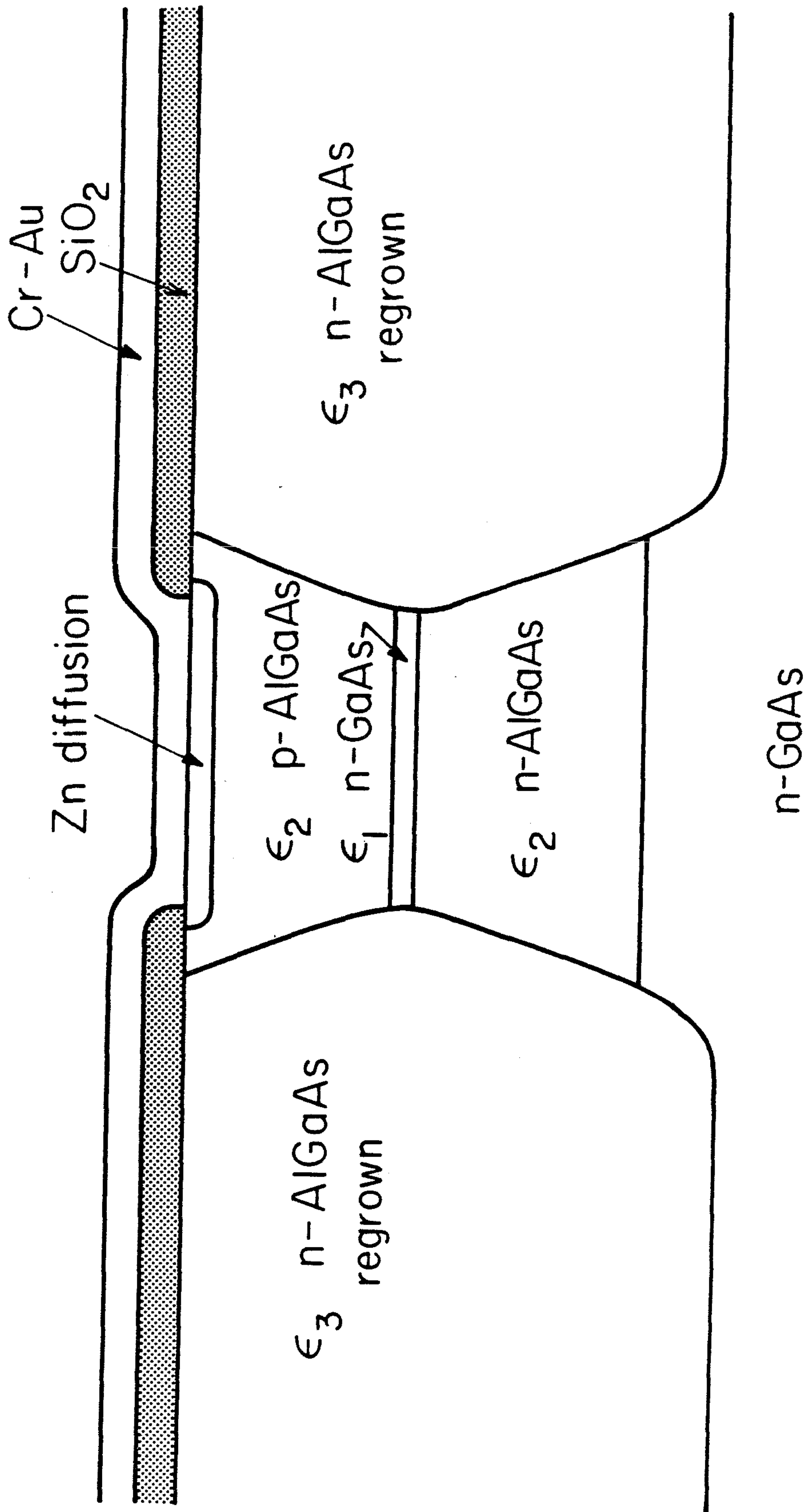

Figure 8.1 Lateral cross section of a typical buried heterostructure laser.

rectangular active layer and surrounding lower permittivity cladding layers.

The smallness of the lateral dimension of the active layer, typically less than 2 μm, greatly simplifies the electrical characteristics of this device. Uneven current injection, spatial holeburning, and other considerations of paramount importance in other laser structures are of minor importance in this device since the lateral carrier diffusion tends to smear out any nonuniformities along the active layer. A self consistent analysis [10] of this type of laser yields the result that nonuniformities in pumping rarely exceed 5 percent of the total, and this occurs only at high levels of stimulated emission.

Thus, the design criteria for the buried heterostructure laser center upon the optical mode design of the device. Clearly, to achieve single lateral mode operation in such a laser, one must include a gain discrimination between lateral modes that exceeds the expected nonuniformity in pumping. A design value of 5 percent represents a reasonable choice. A good way to achieve this gain discrimination is the use of mode confinement. To do this, the waveguide in the device is constructed in such a manner as to be near cutoff, so that the fundamental mode (TE_{00}) has an appreciably larger confinement to the high permittivity gain region (the active layer) than higher order modes.

Another important design consideration involves scattering from the dominant lasing mode. In a real laser, there is considerable scattering from nonuniformities in the guide of the device. The scattered radiation may be lost (coupled into radiation modes) or may continue to travel down the guide in a higher order confined but nonlasing mode. This confined scattered radiation is emitted from the laser mirror facets in the same manner as the radiation in the lasing mode, and the interference of these fields causes the far field of this device to display undesirable speckle-type patterns. This effect can be reduced consider-

ably by cutting off as many of the lateral modes in the device as possible, and making the confinement of any remaining modes other than the lowest (lasing) mode as small as possible.

Thus, the design criteria for the buried heterostructure laser may be stated as the design of an optical waveguide with the largest possible confinement of the lowest lateral mode (for low threshold current) and the lowest possible confinement of any higher order lateral modes, consistent with electrical and fabrication considerations.

For the purpose of this paper, we will analyze the structure shown in Figure 1. We will employ two approximations, first the popular one that uses plane wave modes in the regrown cladding of the device, and second what is felt to be a more accurate approximation that uses the same normal mode profile in the regrown cladding as in the mesa region of the device. The first approach resembles the one taken by Saito and Ito [11].

Inside the mesa, we solve the one dimensional eigenmode equation (6.5). This is just the familiar symmetric three layer slab waveguide problem. With the definition of the dimensionless parameter

$$a = \frac{k\,t}{2}\sqrt{\varepsilon_1 - \varepsilon_2} \tag{6.14}$$

where k is the wavevector, $k = \frac{\omega}{c}$, t is the active layer thickness, ε_1 is the permittivity of the active layer, and ε_2 is the permittivity of the upper and lower cladding material (assumed identical), the eigenequations for the normal mode profile reduce to

$$a_o = \begin{matrix} a_i \tan a_i & \text{(even modes)} \\ -\,a_i \cot a_i & \text{(odd modes)} \end{matrix} \tag{6.15}$$

$$a_i^2 + a_o^2 = a^2 \tag{6.16}$$

where we look for solutions with positive a_i and a_o, which are defined by

$$a_i = \frac{k\,t}{2} \sqrt{\varepsilon_1 - \frac{\gamma_1^2}{k^2}} \tag{6.17}$$

$$a_o = \frac{k\,t}{2} \sqrt{\frac{\gamma_1^2}{k^2} - \varepsilon_2} \tag{6.18}$$

The solution of equations (6.15) through (6.18) yields the effective permittivity inside the mesa region. In addition, we have the following interesting relationships

$$k^2\, \varepsilon_{eff,in} = \gamma_1^2 = b\, k^2\, \varepsilon_1 + (\, 1 - b\,)\, k^2\, \varepsilon_2 \tag{6.19}$$

where the factor b is

$$b = \begin{array}{ll} \sin^2 a_i & \text{(even modes)} \\ \cos^2 a_i & \text{(odd modes)} \end{array} \tag{6.20}$$

For the even modes, we also have

$$b = \frac{\int_{\text{active layer}} dx\, X}{\int_{-\infty}^{\infty} dx\, X} \qquad \text{(even modes)} \tag{6.21}$$

In addition, we define the intensity confinement factor

$$\Gamma = \frac{\int_{\text{active layer}} dx\, X^2}{\int_{-\infty}^{\infty} dx\, X^2} = \begin{array}{ll} \dfrac{|\sin a_i|\,(\,a + |\sin a_i|\,)}{1 + a\,|\sin a_i|} & \text{(even modes)} \\ \dfrac{|\cos a_i|\,(\,a + |\cos a_i|\,)}{1 + a\,|\cos a_i|} & \text{(odd modes)} \end{array} \tag{6.22}$$

In the popular approximation, the eigensolutions for X outside the mesa are

plane waves. However, we should note that the normal field profiles inside the mesa and outside the mesa do not match. This introduces a singularity in the effective permittivity at the interface between the two regions, according to equation (6.9). This singularity represents a considerable problem if it is included in the lateral waveguiding, as it demands that the lateral field Y be zero at the interface. In previous treatments of the waveguiding in buried heterostructure lasers [11], this singularity has been ignored, and the lateral waveguiding treated as a slab waveguide problem. The effective permittivity in the regrown cladding is then

$$k^2\, \varepsilon_{\mathrm{eff,out}} = k^2\, \varepsilon_3 \tag{6.23}$$

and thus the dimensionless parameter for lateral waveguiding is

$$a_{\mathrm{lateral}} = \frac{k\,w}{2}\sqrt{b\,\varepsilon_1 + (\,1 - b\,)\,\varepsilon_2 - \varepsilon_3} \tag{6.24}$$

where w is the lateral width of the buried mesa. However, it should be pointed out that this approach to the problem no longer makes use of the variational principle. By ignoring the singularity at the interface between the two modal profiles used, the benefits and advantages to the use of the variational principle are lost. One possible means of fixing this problem is to smear out the interface between the two regions. This approach leads to an effective permittivity without singularities and well behaved solutions. In some situations, this fix represents a minor correction to the modal profiles found by ignoring the singularity. A good example of this is the channelled substrate structure [12] where a smearing on the order of a fraction of a micron will give a smooth effective permittivity variation and nearly identical profiles to those obtained by ignoring the singularity. On the other hand, the large changes in permittivity and small dimensions associated with the buried heterostructure laser make the smearing approach a poor one. It is for this reason we adopt the following approximation using the

same X modal profile in the regrown cladding as in the laser mesa. An additional incentive to the use of this type of profile for the variational form is that it matches more closely the true modal pattern of this device. For this choice of a variational mode profile, we are using a non - eigensolution profile in the regrown cladding. However, we avoid the singularity in effective permittivity associated with the previous approximation.

For this profile we must resort to the expression (6.9) to calculate the effective index in the regrown cladding

$$k^2 \varepsilon_{eff,out} = \int_{-\infty}^{\infty} dx \left(- (\nabla_t X)^2 + k^2 \varepsilon X^2 \right) \tag{6.25}$$

This expression can be simplified by using the fact that the profile X is an eigensolution of the slab waveguide inside the mesa,

$$k^2 \varepsilon_{eff,out} = k^2 \varepsilon_3 - (\Gamma - b) (k^2 \varepsilon_1 - k^2 \varepsilon_2) \tag{6.26}$$

In the lateral direction we again solve a slab waveguide problem, but with a different effective permittivity for the regrown cladding layer than for the previous approximation. This effective permittivity in the regrown clad is always less than that in the previous approximation. In this case, the dimensionless parameter for lateral waveguiding is

$$a_{lateral} = \frac{k\,w}{2} \sqrt{\Gamma\, \varepsilon_1 + (1 - \Gamma)\, \varepsilon_2 - \varepsilon_3} \tag{6.27}$$

where w is again the lateral width of the buried mesa.

To decide which of the two approximations is the more accurate, we will make use of the variational principle, equation (6.4). This variational principle always yields a β for the lowest mode that is lower than the true β in the case of a bound, real index guided mode. Thus, approximations can be judged simply by which gives the largest β for the lowest mode. If we keep the singularity

associated with the first approximation, the resulting lateral eigenmodes are sinusoidal inside the mesa, zero at the interfaces, and zero outside the mesa. The lowest mode in this case can be shown rigorously to posess a β which is smaller than that produced by the second approximation. On the other hand, if the singularity in effective permittivity is ignored, negating the effect of the variational principle, the β resulting from the lateral eigenmode equation (6.11) and the β resulting from the variational principle (6.4) are no longer in agreement. In fact, the β from the variational principle, which we compare with, is $\beta = -\infty$. The approximation which results from ignoring the singularity is not actually as poor as this indicates, but it cannot be compared in a reasonable manner through the use of the variational principle. Another comparison that can be made, however, is to point out that when the a variational approximation yields a bound mode to the scalar eigenequation, such a bound mode must exist, based upon the fact that the true β for the mode must be larger than that from the variational approximation. Noting that the dimensionless parameter $a_{lateral}$ for lateral guiding in the second case is always larger than that for the first case where the singularity in the effective permittivity is ignored, and that it can yield bound modes when the first approximation does not, leads us to the conclusion that the second case is the better approximation.

In the design of the buried heterostructure laser, we need only concern ourselves, then, with solutions of the three layer symmetric slab waveguide. These can be presented in convenient form as graphs of the parameters b and Γ as functions of the dimensionless parameter a for the various mode orders. These graphs are shown in Figures 6.2 and 6.3.

To design a buried heterostructure laser, one could proceed by first choosing an upper and lower cladding layer aluminum content and an active layer thickness. Then the effective permittivity inside the mesa can be calculated. The aluminum content of the regrown cladding can then be chosen to get the

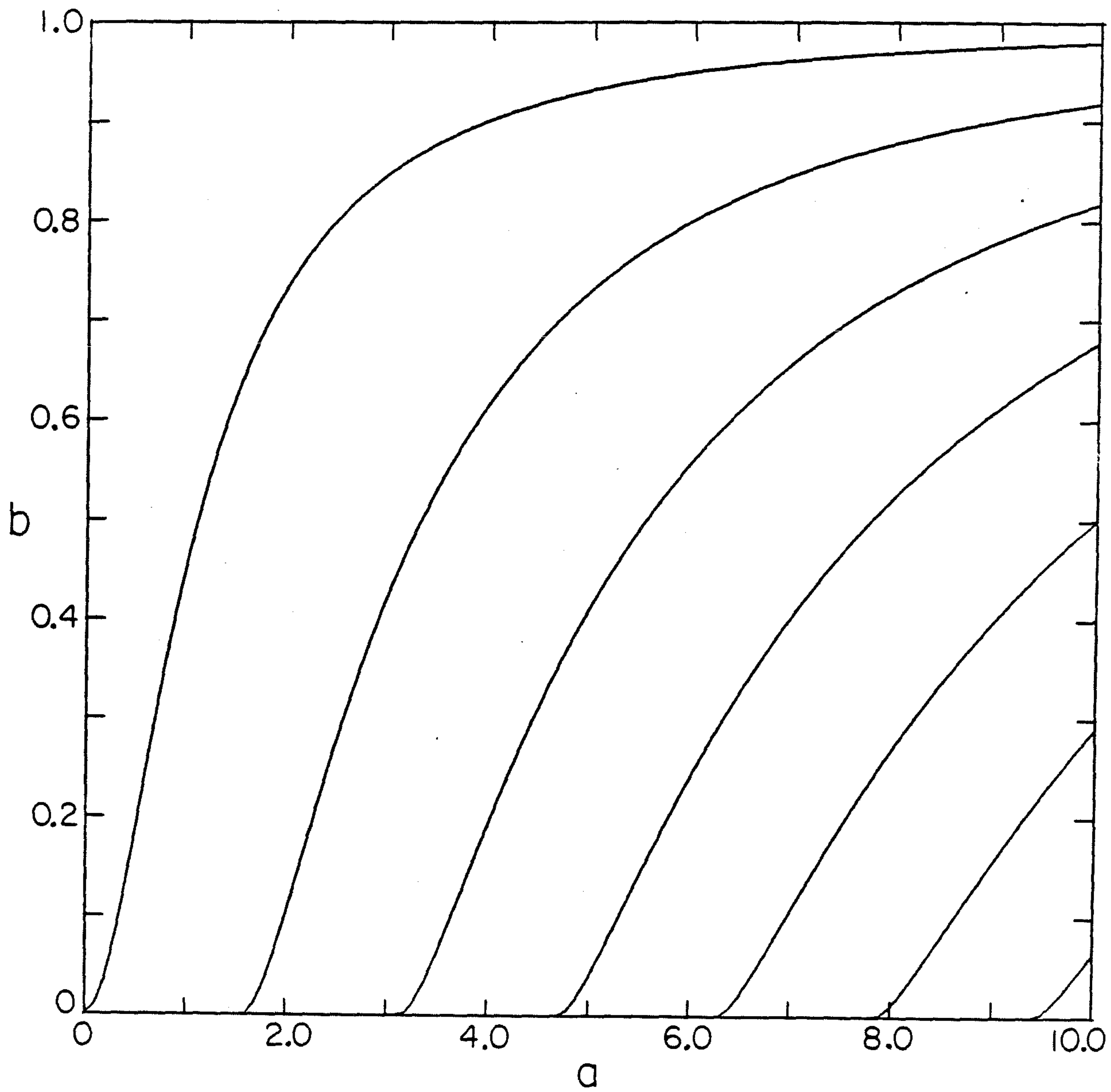

Figure 6.2 The parameter b as a function of the dimensionless parameter a, for various mode orders.

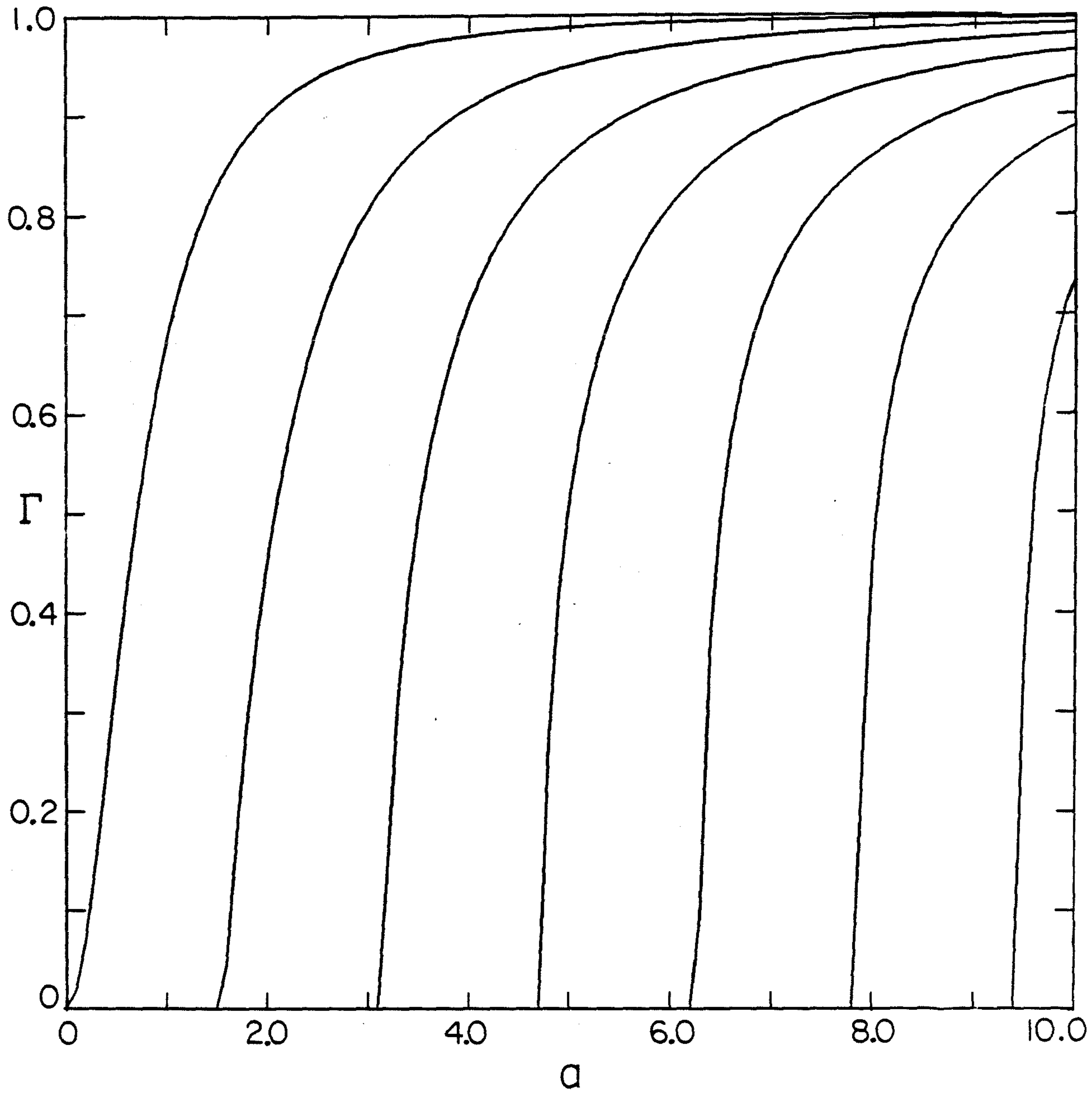

Figure 6.3 The parameter Γ as a function of the dimensionless parameter a, for various mode orders.

highest possible lateral mode confinement (Γ) for the lowest mode and cut off as many of the higher order lateral modes as possible.

As an example of this procedure we choose a GaAs active layer with $Al_{0.4}Ga_{0.6}As$ cladding. The optimum active layer thickness in terms of threshold current density for this choice is approximately 0.15 μm. The lasing wavelength is taken to be $\lambda = 0.883\ \mu$ m, and we also assume the values $\varepsilon_1 = 3.64^2 = 13.25$ and $\varepsilon_2 = 3.32^2 = 11.02$. This gives for the direction normal to the active layer $\Gamma = 0.563$ and $b = 0.356$. Thus inside the laser mesa we have $\varepsilon_{eff,in} = 3.44^2 = 11.83$. If $Al_{0.4}Ga_{0.6}As$ material is regrown as cladding, we have $\varepsilon_{eff,out} = 3.25^2 = 10.56$ for the second approximation. This corresponds to a strongly guided case in the lateral dimension. To have $a_{lateral}$ less than 5, as would be required for reliable single lateral mode operation, requires the lateral width of the guide to be less than 1.25 μm. Considerable advantage can be had, however, by the regrowth of much lower index cladding. If one were to choose $Al_{0.2}Ga_{0.8}As$ as the regrown cladding material ($\varepsilon_3 = 3.45^2 = 11.90$) the effective permittivity in the regrown cladding would be $\varepsilon_{eff,out} = 3.38^2 = 11.42$, again using the second approximation, corresponding to a laser with weak lateral guiding. To get $a_{lateral}$ less than 5, the lateral width must be less than 2.30 μm, a much less stringent requirement on device processing. Of course, there is an advantage to reduce $a_{lateral}$ even more, down to a lower limit of approximately 1. Below this value, the confinement of the lowest mode becomes objectionably small. When $a_{lateral}$ is less than $\frac{\pi}{2}$, the lateral waveguide has only one bound mode.

To illustrate the difference between the two approximations to the design of buried heterostructure laser waveguides, the curves in Figures 6.4 through 6.7 are presented. These curves show the relationship between refractive index of the regrown aluminum cladding and the mesa width of laser for different active

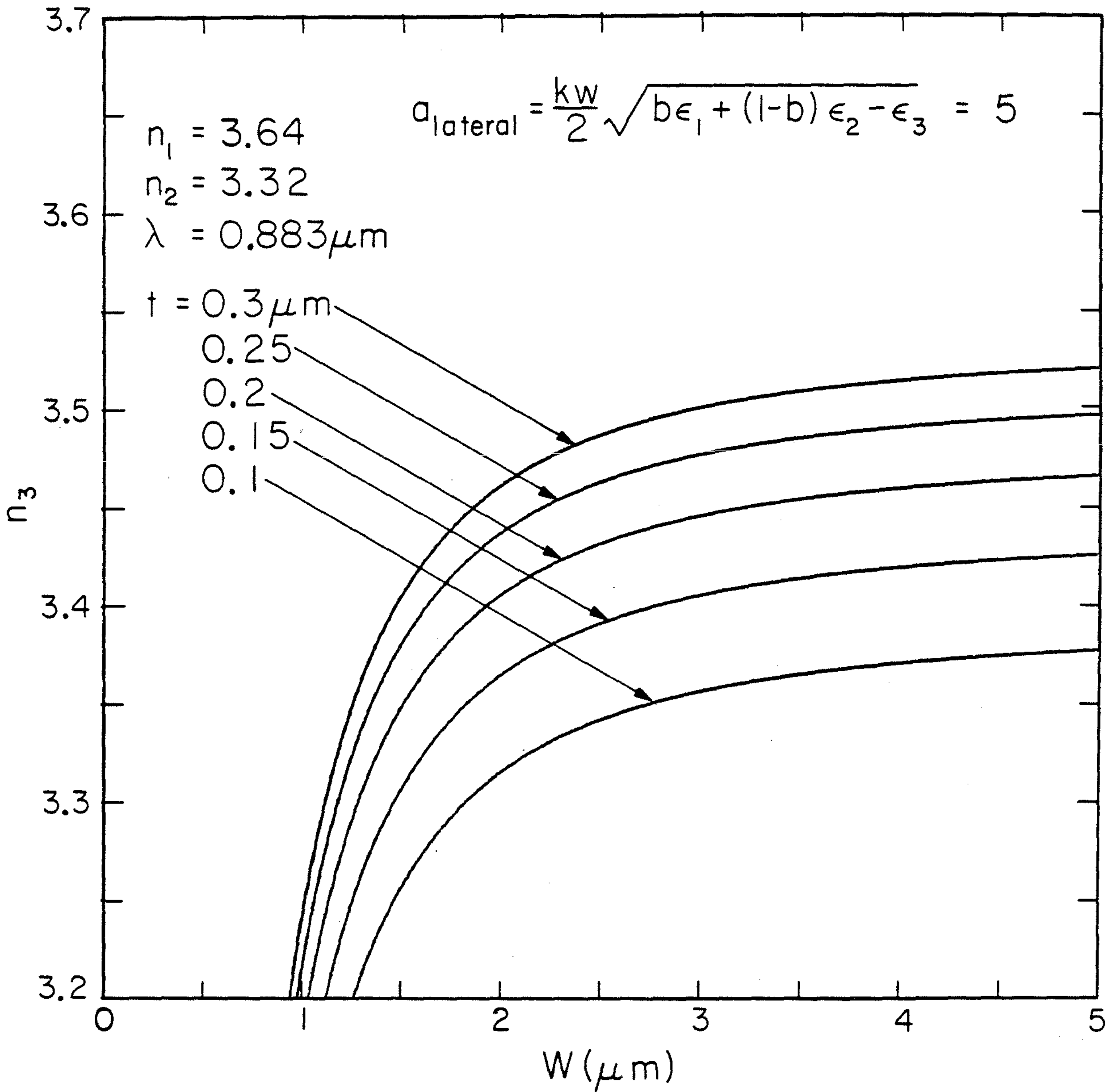

Figure 6.4 The relationship between refractive index of the regrown cladding and lateral width of the buried mesa, using the first approximation (singularity ignored) and a lateral waveguiding parameter of 5, corresponding to 5 percent gain discrimination between the zeroth and first order lateral modes.

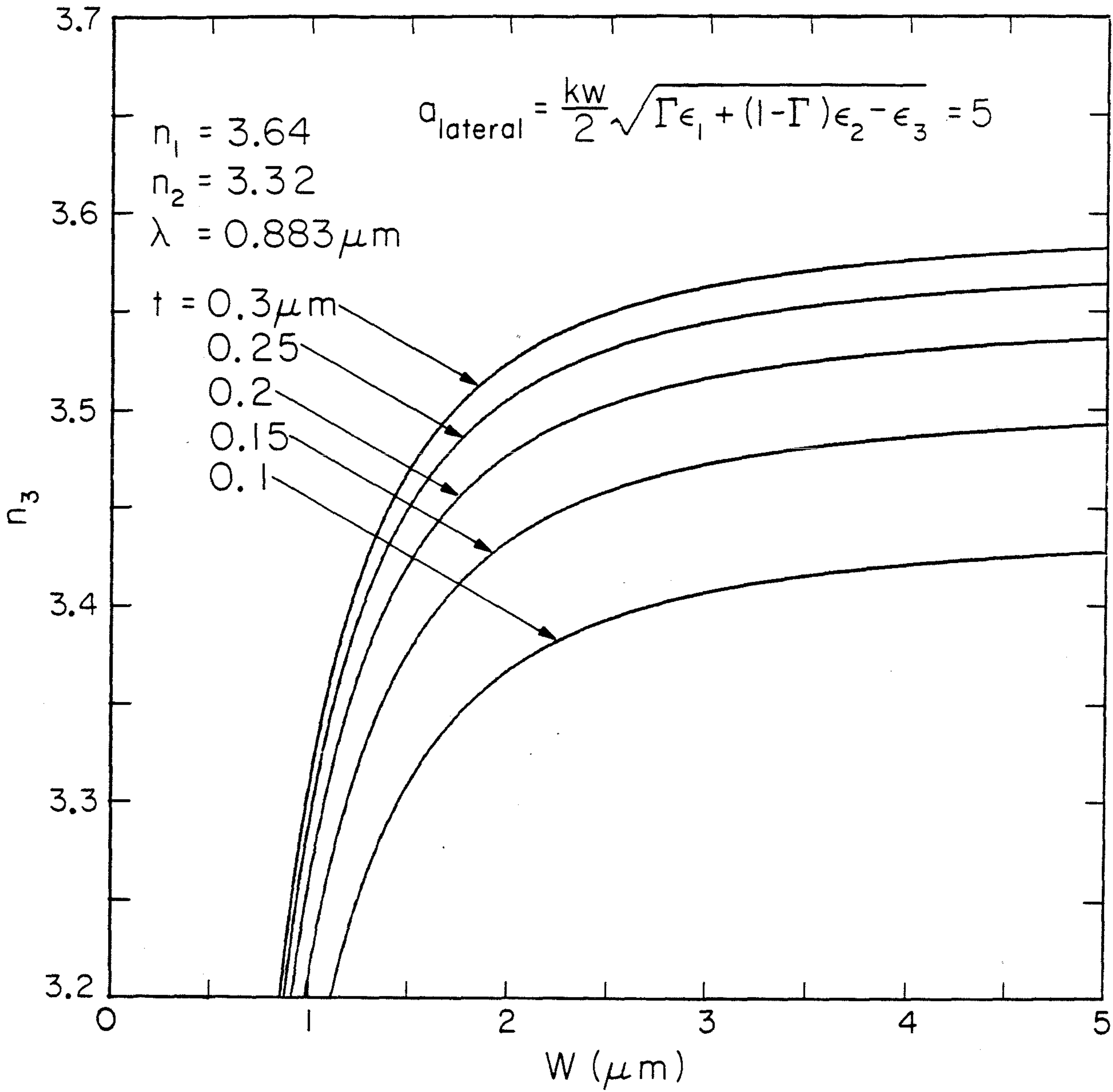

Figure 6.5 The relationship between refractive index of the regrown cladding and lateral width of the buried mesa, using the second approximation and a lateral waveguiding parameter of 5, corresponding to 5 percent gain discrimination between the zeroth and first order lateral modes.

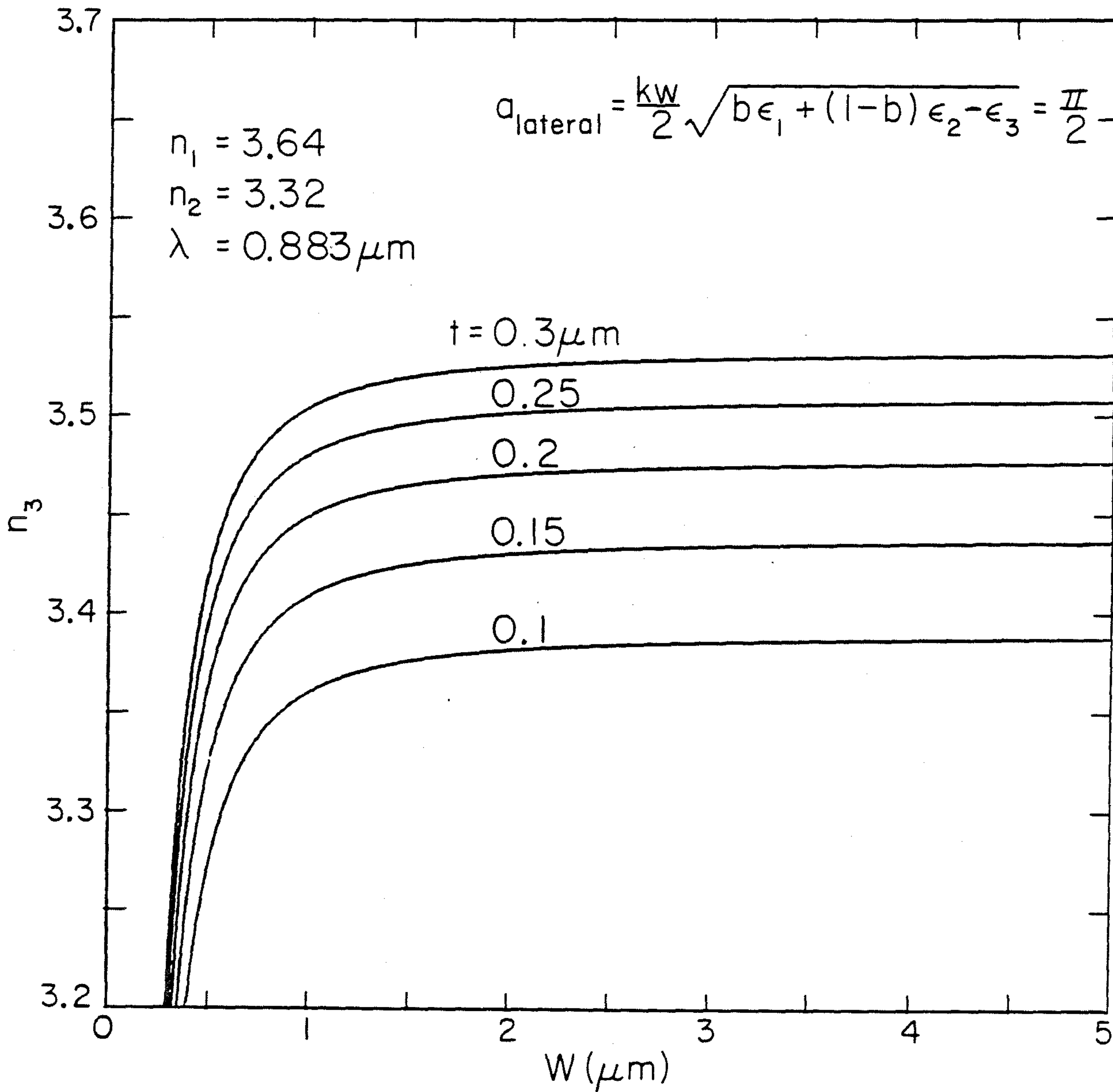

Figure 6.6 The relationship between refractive index of the regrown cladding and lateral width of the buried mesa, using the first approximation (singularity ignored) and a lateral waveguiding parameter of $\frac{\pi}{2}$, corresponding to cutoff of the first order lateral mode.

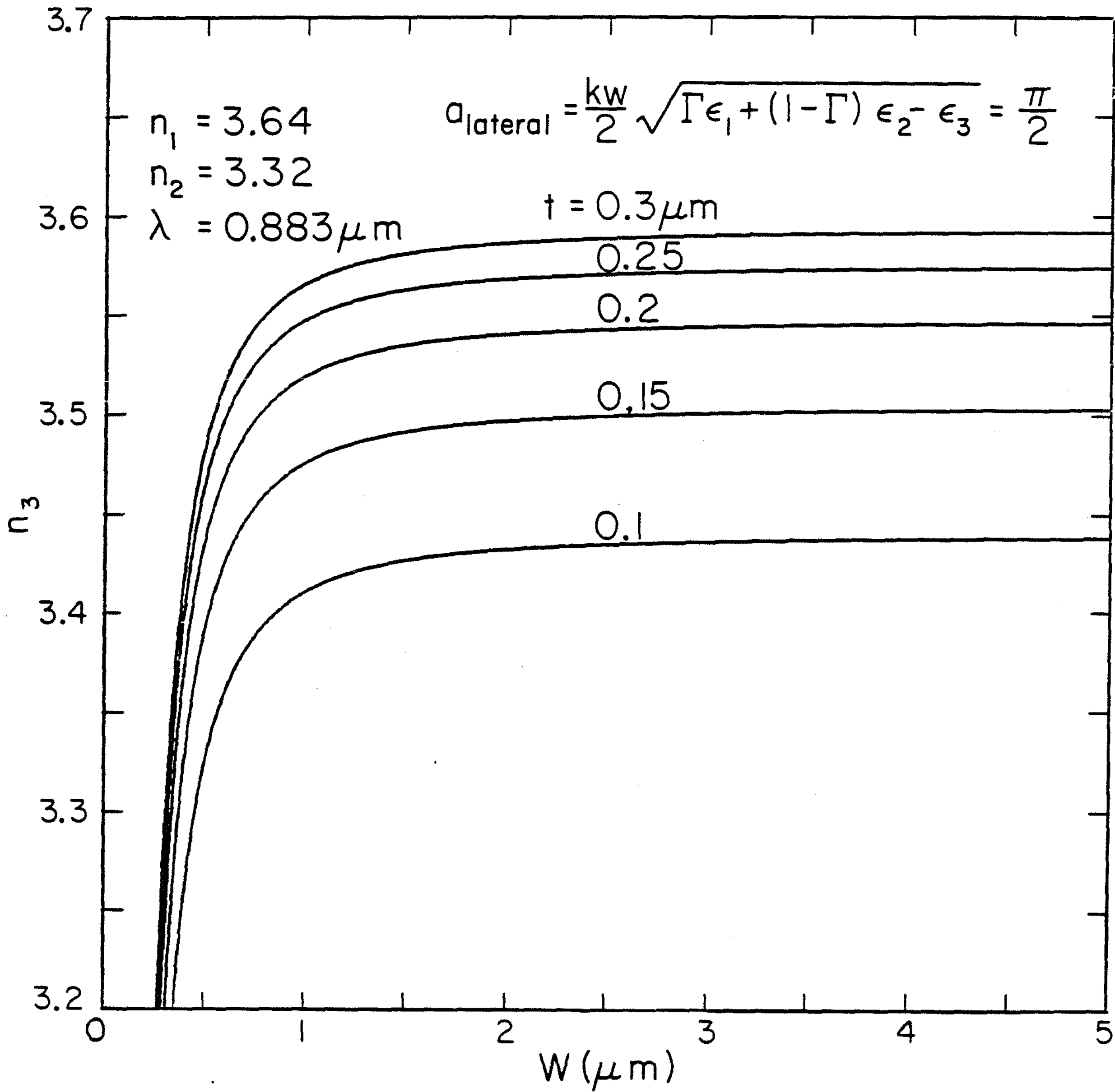

Figure 6.7 The relationship between refractive index of the regrown cladding and lateral width of the buried mesa, using the second approximation and a lateral waveguiding parameter of $\frac{\pi}{2}$, corresponding to cutoff of the first order lateral mode.

layer thicknesses and lateral waveguiding parameters. The lateral waveguiding parameters in these curves are 5, corresponding to approximately 5 percent gain discrimination between the zeroth and first order lateral modes, and $\frac{\pi}{2}$, corresponding to the cutoff of the first order lateral mode. In these curves the active layer is assumed to be GaAs, the upper and lower cladding layers are assumed to be $Al_{0.4}Ga_{0.6}As$, and the emission wavelength is assumed to be 0.883 μm. The difference between the two approximations can be seen to be considerable, with the second approximation yielding much stronger confinement for the modes.

In conclusion, a new form of effective permittivity formalism has been derived, which illustrates clearly both the nature of the approximation and its limits. The technique has been extended to cases where it may be desirable to use non - eigensolution profiles for the variation in the strongly guided direction, and this technique has been applied to the buried heterostructure laser as an example. This technique should be extremely useful with new types of laser structures which depend upon strong geometric effects for waveguiding in the lateral direction.

VI.4 References for Chapter VI

1. W. V. McLevige, T. Itoh, and R. Mittra, "New Waveguide Structures for Millimeter-Wave and Optical Integrated Circuits," IEEE Trans. Microwave Theory Tech. **MTT-23**, 788 (1975).

2. P. A. Kirkby and G. H. B. Thompson, "Channeled Substrate Buried Heterostructure GaAs-(GaAl)As Injection Lasers," J. Appl. Phys. **47**, 4578 (1976).

3. T. Itoh, "Inverted Strip Dielectric Waveguide for Millimeter Wave Integrated Circuits," IEEE Trans. Microwave Theory Tech. **MTT-24** 821 (1976).

4. T. Rozzi, T. Itoh, and L. Grun, "Two Dimensional Analysis of the GaAs Double Hetero Stripe Geometry Laser," Radio Science **12**, 543 (1977).

5. G. B. Hocker and W. K. Burns, "Mode Dispersion in Diffused Channel Waveguides by the Effective Index Method," Appl. Opt. **16**, 113 (1977).

6. J. Buus, "A Model for the Static Properties of DH Lasers," IEEE J. Quant. Electron. **QE-15**, 734 (1979).

7. W. Streifer and E. Kapon, "Application of the Equivalent-Index Method to DH Diode Lasers," Appl. Opt. **18**, 3724 (1979).

8. T. Tsukada, "GaAs$-$Ga$_{1-x}$Al$_x$As Buried-Heterostructure Injection Lasers," J. Appl. Phys. **45**, 4899 (1974).

9. T. Kajimura, K. Saito, N. Shige, and R. Ito, "Leaky-Mode Buried-Heterostructure AlGaAs Injection Lasers," Appl. Phys. Lett. **30**, 590 (1977).

10. D. Wilt and A. Yariv, submitted for publication.

11. K. Saito and R. Ito, "Buried-Heterostructure AlGaAs Injection Lasers," IEEE J. Quant. Electron. **QE-16**, 205 (1980).

12. K. Aiki, M. Nakamura, T. Kuroda, J. Umeda, R. Ito, N. Chinone, and M. Maeda, "Transverse Mode Stabilized Al$_x$Ga$_{1-x}$As Injection Lasers with Channeled-

Substrate-Planar Structure," IEEE J. Quant. Electron. **QE-14**, 89 (1978).